Sequential Electron Acceptor Model of Intrinsic Bioremediation at a BTEX Contaminated LUST Site in Laurel Bay, South Carolina

by

Nancy A. Lade

Thesis submitted to the Faculty of the
Virginia Polytechnic Institute and State University
in partial fulfillment of the requirements for the degree of

Master of Science
in
Civil Engineering

Dr. Mark A. Widdowson, Chair
Dr. John T. Novak
Dr. Panos Diplas

September 9, 1999
Blacksburg, Virginia

Sequential Electron Acceptor Model of Intrinsic Bioremediation at a BTEX Contaminated LUST Site in Laurel Bay, South Carolina

by

Nancy A. Lade

ABSTRACT

Contaminant transport modeling is being used with increasing frequency at petroleum hydrocarbon contaminated sites in an attempt to aid engineers in evaluating the feasibility of natural attenuation as a remediation alternative in groundwater systems. In this research, a three-dimensional sequential electron acceptor computer model, SEAM3D, developed by Waddill and Widdowson (1997) was used to simulate contaminant transport at a leaking underground storage tank site in Beaufort, South Carolina. Gasoline containing benzene, toluene, ethylbenzene, and xylene (BTEX) as well as methyl tertiary butyl ether (MTBE) leaked into the subsurface at the site late in 1990, and monitoring of the water table elevations and contaminant concentrations began in 1993. Using the field data, the groundwater flow model MODFLOW was used to develop and calibrate a flow model for the Laurel Bay site using GMS (Groundwater Modeling System) v2.1. MODFLOW was coupled with the SEAM3D contaminant transport model, and the available concentration levels were used to calibrate, verify, and validate the site model. The results indicated that SEAM3D simulated complex, interconnected processes including biodegradation, and the transport of multiple hydrocarbon compounds, electron acceptors, and end products over time and space at a specific petroleum hydrocarbon contaminated site. Once the model was calibrated and verified, the model output was used to study the changes in contaminant mass distribution, contaminant mass loss, and mass loss rates for each terminal electron accepting process (TEAP) over time. It was found that the natural attenuation capacity of the aquifer was insufficient to stabilize the plume and prevent it from reaching the defined point of contact (POC). Contamination was shown to have reached the POC by 1994, just four years into the simulation. Results indicated that despite oxygen limitation within the BTEX plume, aerobic biodegradation was responsible for the greatest amount of mass loss, close to 70 %, relative to the sum of the anaerobic processes after 20 years.

Acknowledgements

I would like to begin by thanking my advisor, Dr. Mark Widdowson, for the opportunity to work with him on this project. His guidance, patience, and support have contributed significantly to this project's completion as well as to my growth as an engineer. I would also like to thank the other members of my committee, Dr. John Novak and Dr. Panayiotis Diplas, for their contributions during my time here at Virginia Tech. Without the fellowship provided by the Via family through the Civil Engineering Department, I would not have been able to pursue graduate studies at Virginia Tech, so to them I am deeply appreciative.

Additional funding for this project came from the U.S. Army Engineers Waterways Experiment Station Vicksburg, Mississippi, so I want to say thank you to them. I would like to thank Jim Landmeyer of the USGS for all of the data that he provided from the site that was critical to the successful completion of the project. I am grateful to Alan Lemon at Brigham Young University for the assistance that he gave me with various versions of GMS.

I wish to thank Dan Waddill and Steve Brauner because without their aid this project would have taken twice as long. Their assistance in understanding the computer code and various other aspects of the project is deeply appreciated. I would also like to thank Marc Killingstad whose help at various times throughout the project proved to be invaluable and whose humor helped to keep me motivated during the final stages of my work.

To my friends from my time here at Tech, I want to say thank you from the bottom of my heart. Your friendships have been a method of support during times when my work as well as other aspects of my life were not going very well. A special thanks to all of my roommates from the last 2 years for putting up with me when things were moving slowly, or not moving at all, as well as for the countless rides that you provided me with. To my friends from home, I want to thank you for the motivation and support you have given me, inspiring me to want to succeed in all that I do.

To my fellow students in the hydrosystems department, I also say thank you. Thanks for challenging me academically, for providing a fun place to come to work, and for your friendships. To Eric, thank you for your patience, support, and encouragement over the last 10 months. Most importantly, thank you for helping me to see what is truly important in life.

Finally I would like to thank my family, and most specifically, my parents. The knowledge they have instilled in me along with the love and encouragement they have given me have made me who I am today. Thank you.

Table of Contents

List of Figures

List of Tables

1.0 Introduction

1.1 Background

Groundwater is one of the most important resources in this country with close to half of the population of the United States receiving their drinking water supply from groundwater sources (Hall and Johnson, 1992). Chemicals from leaking underground storage tanks, the improper disposal of waste, and hazardous waste spills are a continuing source of contamination to the nation's groundwater. Leaking petroleum filled underground storage tanks are described as a serious and widespread environmental problem (Kao and Borden, 1997). The number of reported releases is increasing more quickly than the number of completed cleanups (Small, 1998). As the distance between these two values increases, it has become necessary for regulatory agencies to alter the way in which they deal with subsurface contamination.

Many methods are used to clean up these sites including pump and treat, enhanced bioremediation, soil vapor extraction, air sparging, and contaminant excavation. These technologies can restore some of the contaminated sites to meet regulatory standards, but total clean up at most sites is not possible due to the diversity of the contamination and the complexities in the subsurface environment (Swett and Rapaport, 1998). There is evidence showing natural processes resulting in a more rapid decrease in contaminant concentrations at a petroleum contaminated site than engineered solutions (Borden et al., 1986). As the limitations regarding the effectiveness of remediation technologies becomes more apparent and the number of sites needing remediation increases, the need for new clean up alternatives is emerging.

The U.S. EPA reports that there is not enough money or resources to clean up all of the contaminated sites to nondetect concentrations (Small, 1998). For that reason, regulators are shifting towards a more risk-based approach when dealing with contaminated sites. Previously, the clean up goal for every contaminated site was the reduction of concentrations to the lowest levels achievable without assessing the exposure risks. The new approach involves measuring the potential risk to human health and the environment against the site characteristics and selecting site management and remediation alternatives that correspond to the perceived risk.

Natural attenuation is emerging as a preferred method of remediation at the lower risk petroleum contaminated sites. It is estimated that 80%-85% of fuel-contaminated sites may be manageable using just natural attenuation (Swett and Rapaport, 1998). Natural attenuation, or intrinsic bioremediation, involves letting nature become the environmental cleaner. Processes such as biodegradation, dilution, dispersion, adsorption, and volatilization combine to result in a reduction in contaminant mass, mobility, toxicity, or all three.

When evaluating natural attenuation as a potential remedial alternative at a site, it is necessary to have historical site-specific data and evidence that attenuation mechanisms such as biodegradation are occurring. Demonstrating the effectiveness of natural attenuation at a site can be a significant task for an engineer. It is necessary to show that the original source of the contamination has been stopped, the plume has been stabilized, and there is no additional threat of contamination (Swett and Rapaport, 1998). To do these things, detailed knowledge of the hydrogeology and geochemistry of the site is needed (Chapelle, et al., 1996). This information can be obtained through a site investigation as well as data on the historical soil and groundwater conditions. This data along with what was learned through the site investigation can be used in modeling efforts designed to evaluate the effect that attenuation will have on the contaminant fate and transport and plume management at a particular site.

Several contaminant transport models have been used at petroleum hydrocarbon contaminated sites in an attempt to aid engineers in evaluating the feasibility of natural attenuation as a remediation alternative. These models include BIOPLUME (I, II, and III), BIO1D, Hydrocarbon Spill Screening Model (HSMM), BIOSCREEN, and MT3D (Bedient and Rifai, 1992; Chiang et al., 1989; Klecka et al., 1990; Charbeneau and Weaver, 1992). The earlier versions of BIOPLUME (I and II) are two-dimensional models that have been used to simulate the transport of hydrocarbon contaminants in the subsurface under the influence of oxygen (Bedient and Rifai, 1992; Chiang et al., 1989). BIOPLUME III is a 2-D model with features that permit the modeling of additional electron acceptors including NO_3^-, Fe(III), SO_4^{-2}, and CO_2 (Clement et al., 1998). Within the model, aerobic biodegradation and nitrate reduction are simulated as instantaneous reactions while iron reduction, sulfate reduction, and methanogenesis are simulated as zero or first order reactions. BIO1D is a one-dimensional solute transport model that has the ability to simulate both adsorption and first order biodegradation (Klecka et al., 1990). Both BIOSCREEN and HSMM are screening models used to estimate the effects hydrocarbon contamination will have on a homogeneous aquifer (Charbenau and Weaver, 1992; Widdowson, 1998). BIOSCREEN has the ability to simulate both aerobic and anaerobic biodecay as well as sorption. MT3D is a solute transport modeling tool within the Department of Defense's Groundwater Modeling System. It has the ability to simulate both sorption and first order decay in three dimensions. A more recent version of MT3D, MT3DMS, has the ability to simulate multi-species transport.

As natural attenuation is being looked at as a remedial alternative at a growing number of hydrocarbon contaminated sites, the need for a contaminant transport model that can accurately simulate complex subsurface processes in heterogeneous environments has increased. SEAM3D

(sequential electron acceptor model, 3 dimensional) is a model that has the ability to depict subsurface transport of multiple solutes in a three-dimensional, anisotropic, heterogeneous domain under the influence of advection, dispersion, adsorption, and biodegradation (Waddill and Widdowson, 1997). Solutes that can be simulated include biodegradable substrates, nutrients, electron acceptors, biodegradation products, daughter products of the substrates, and non-biodegradable tracers. Biodegradation is simulated with the available electron acceptors utilized in the following sequence: O_2, NO_3^-, Mn(IV), Fe(III), SO_4^{-2}, and CO_2 (Waddill and Widdowson, 1998). Before SEAM3D, or any model, can be applied to contaminated sites, it is necessary to demonstrate that model simulations accurately depict what is occurring in the subsurface over time.

1.2 Research Objectives

The goal of this research is to develop and execute a site transport model using SEAM3D to accurately simulate contaminant transport at a gasoline-contaminated leaking underground storage tank (LUST) site. A LUST site located in Beaufort, South Carolina has been monitored since 1993, documenting water table elevations, contaminant concentrations, and geochemical indicator concentrations nearly every year since monitoring began. The available data can be used to calibrate, verify, and validate the site model to determine if SEAM3D is capable of matching complex, interconnected processes over time and space. These processes include the simulation of biodegradation and the transport of multiple hydrocarbon compounds, electron acceptors, and end products. Once the site model developed using SEAM3D is calibrated and verified at Laurel Bay, the model can then be used to interpret data. From this data, information can be learned about natural attenuation occurring at the site.

1.3 Approach

The first step in this research project was to use the groundwater flow model MODFLOW to develop and calibrate a flow model for the Laurel Bay site using GMS (Groundwater Modeling System) v2.1. The input parameters for the model were based on site characterization data, groundwater flow equations, and other literature values (ABB Environmental Services, 1993; Anderson and Woessner, 1992; Fetter 1994; and Landmeyer et al., 1996). Model calibration was achieved by matching water table elevations and hydraulic gradients simulated by the model with those observed in the field.

A site contaminant transport model using SEAM3D was developed following calibration of the groundwater model. The initial input values for the SEAM3D model were taken from those

values used by Waddill and Widdowson (1997) in their study of the Laurel Bay site. The model was calibrated to the 1994 data from the site by varying certain parameters in an effort to match concentration values along a transect through the center of the plume. Comparisons were made for each of the contaminants as well as the geochemical indicators and end products simulated by the model. Once the model was calibrated, it was verified using field data from 1996 and 1997.

The final step in the research was data interpretation. SEAM3D calculates mass balances and losses on all species simulated by the model. This data includes information on the mass distribution of each hydrocarbon between the aqueous, adsorbed, and NAPL phases. The masses of substrate lost due to each terminal electron accepting process (TEAP) are also contained in the model output. The data was used to study the changes in contaminant mass distribution, contaminant mass loss, and mass loss rates for each TEAP over time. These results were used to learn more about natural attenuation and its feasibility as a remedial strategy at the Laurel Bay site.

1.4 Site History

The site used in this research is the Laurel Bay Marine Corps Exchange Station (MCEX) located in Laurel Bay, South Carolina. MCEX is located at the Marine Corps Air Station (MCAS) housing development in Laurel Bay. It has been estimated that petroleum began leaking from three underground storage tanks in December 1990. Gasoline containing benzene, toluene, ethylbenzene, and xylene (BTEX) as well as methyl tertiary butyl ether (MTBE) was not discovered until November 1991 when the presence of free product was observed in an on site monitoring well. At that time, one leaking tank was found responsible. The tank was emptied and taken out of service to prevent further contamination of the aquifer. The free product already present in the subsurface acted as a continual source of contamination, and it was not until 1993 that the remaining two tanks and contaminated soil were removed (ABB Environmental Services, 1993).

The service station is located in the center of a large housing development and a concrete swail carrying water to the Broad River is around 200 meters downgradient from the source area (ABB Environmental Services, 1993). The BTEX compounds that have leaked into the groundwater are on the Hazardous Substance List for the regulation of underground storage tanks due to their potential risk to human health and the environment (Federal Register, 1989). Since the contaminants presented a risk and there was the opportunity for exposure, the transport of the contaminant plume at the site was a major concern. A contamination assessment was performed in 1993 to determine the exact extent of the plume. Using a combination of soil borings and

groundwater monitoring wells, it was determined that the contamination had remained in the upper unconfined aquifer, and it extended horizontally around 100 meters from the source (ABB Environmental Services, 1993).

Two modeling studies have been performed on the Laurel Bay site. In the first, Landmeyer et al. (1996) presented exploratory model simulations designed to determine if intrinsic bioremediation could attenuate the contaminant plume. Model simulations were performed using a range of input parameters, which were designed to exhibit the inherent uncertainty associated with model results. Transport was modeled for a range of hydraulic gradients, hydraulic conductivities, adsorption isotherms, and microbial degradation rates for both benzene and toluene. Toluene simulations were run out to 2011 and benzene simulations were run out to 2050 (Landmeyer et al., 1996).

Landmeyer et al. (1996) showed that the only conditions under which contamination had the potential to negatively impact human health of the environment was when neither adsorption nor biodegradation was simulated. The contamination was said to be effectively isolated to the Laurel Bay site in 1994, and there was no cause for concern that the contamination may affect any adjacent surface water bodies. An additional site study was published by Landmeyer et al. in 1998, and it contradicted the results found in the 1996 study. Using field data, the fate of MTBE and benzene within the contaminated aquifer was investigated. The data showed benzene contamination reaching the concrete swail by July 1997. Within the swail, the contamination could be transported to the Broad River. These results indicate that the modeling study performed in 1996 failed to predict the contaminant fate and transport.

A second study of the Laurel Bay site was presented in Waddill and Widdowson (1997). A three-dimensional model grid was constructed and input parameters were selected based on site data or literature values (ABB Environmental Services, 1993; Borden et al., 1995; Chen et al., 1992; Landmeyer et al., 1996; and Parker et al., 1994). The model was calibrated to the 1993, 1994, and the 1996 site data, and the 1997 data was used to test its predictive capabilities. The model predicted contaminant concentrations similar to those that had been observed in the field. The actual and simulated travel distances were also compared, and they were in general agreement as well. This indicated that the estimates made of groundwater velocity, retardation coefficients, and the start date of the leak were all relatively accurate.

Once the model was calibrated to field data sets, it was used to predict future contaminant transport. The results indicated that the contamination would not reach the concrete swail, 200 meters downgradient from the source area, until around 10 years from its release in 1990. The 1998 publication by Landmeyer et al. indicated that the contamination had reached the swail by

1997 indicating the SEAM3D model was not accurately simulating the contaminant fate and transport at the Laurel Bay site. A major flaw in the study by Widdowson and Waddill (1997) was in the groundwater flow model used to generate the flow field for contaminant transport. The groundwater model was not calibrated to site data, and if it is desired to accurately depict contaminant transport, the groundwater flow model must simulate flow conditions as close as possible to those observed in the field.

1.5 Thesis Organization

This chapter has presented an overview of natural attenuation and the use of contaminant transport modeling to simulate natural attenuation at petroleum hydrocarbon contaminated sites. The accurate simulation of contaminant transport at the Laurel Bay site has been defined as the goal of this research. The history of the site has been discussed including the failure of previous attempts to model contaminant transport at Laurel Bay.

Chapter 2 presents a review of the literature pertaining to hydrocarbon contamination, biodegradation of BTEX compounds, contaminant transport modeling studies, and the Laurel Bay site. Chapter 3 provides a description of the groundwater flow model conceptualization and calibration. The contaminant transport model design, calibration, and verification are also discussed in Chapter 3. Chapter 4 presents and discusses the results of the calibration and verification of the contaminant transport model. A more detailed interpretation of the biodegradation trends shown by the contaminant transport model is found in Chapter 5. The conclusions made based on the research are presented in Chapter 6.

2.0 Literature Review

Leaking underground storage tanks containing gasoline and other fuels have been a major source of groundwater contamination for many years. Since a single fuel spill can contain hundreds of hydrocarbon components, it is important to be able to determine which cause the greatest risk with respect to human health and the environment. These risks are based on the properties of the various hydrocarbons, and once they have been assessed, it is possible to select a remediation alternative for the contaminated site. There has been a movement towards the use of natural attenuation to clean up contaminated aquifers. Monitored natural attenuation is only used if it can be shown that it can effectively limit the travel distance and concentration of petroleum hydrocarbons in groundwater thus preventing them from reaching potential receptors. One way to determine the feasibility of natural attenuation as a remediation alternative is using contaminant transport modeling.

This literature review is divided up into two parts. Sections 2.1 through 2.3 comprise the first part, which begins by discussing the sources of hydrocarbon contamination and reviewing the properties of the compounds that pose the greatest risks. A broad discussion of natural attenuation follows with particular focus on its recent emergence as an approved means of meeting regulatory standards at hydrocarbon contaminated sites. Biodegradation of BTEX compounds is reviewed briefly in Section 2.2. The final part of the first section discusses previous contaminant transport modeling studies designed to simulate natural attenuation.

Section 2.4 makes up the second part of the literature review. This section reviews the background information about the Laurel Bay site used in this research. It summarizes the previous research performed on the site as well as the results of that research.

2.1 Hydrocarbon Contamination

2.1.1 Sources

Petroleum hydrocarbon contamination of shallow water table aquifers has been a significant environmental problem since the early 1980s (Chapelle, 1999). Petroleum filled LUST sites are one of the most common sources of contamination of these aquifers. It has been estimated that between 100,000 and 400,000 gasoline containing storage tanks are leaking into the soil or directly into the groundwater in the United States (Atlas and Cerniglia, 1995).

In 1989 and 1990, there were 90,000 confirmed releases from gasoline containing underground storage tanks (Borden et al., 1995). In 1993, it was reported that each year tens of millions of gallons of gasoline were released from storage tanks into the ground (Sulfita, 1993).

There were over 350,000 confirmed releases of petroleum products or leaking underground storage tanks in 1998 (Small, 1998). It can be seen from the above statistics that the problem involving leaking underground storage tanks has not improved over the last decade. Consequently, large volumes of potentially toxic compounds have been released into groundwater systems throughout the country. This is a major concern because UST sites are often located near heavily populated areas (Landmeyer et al., 1998), and the contamination of groundwater by these compounds represents the potential for serious public health problems.

2.1.2 Properties

Contamination caused by petroleum leaks and spills can be harmful to both human health and the environment. For this reason, risks along with remediation alternatives are often quickly investigated at contaminated sites. In order to properly assess the risk and design a remediation system, it is important to know the properties of the contaminants. A single commercial gasoline could have over two hundred hydrocarbon contaminants, and each of those contaminants can have a wide range of physical and chemical properties. The properties that are of highest importance include the solubility, the bioavailibility, the degradability, and the toxicity of the various components of the contaminant spill (Munoz and Irarrazaval, 1998).

In terms of petroleum contamination, the monoaromatics are the compounds of greatest concern. These include benzene, toluene, and three xylene isomers, m-, p-, and o-xylene. Monoaromatics make up a significant percent of gasoline, have high aqueous solubilities, and a high estimated toxicity. These compounds are also highly volatile, able to biodegrade, have low tendencies for adsorption, and a high mobility (Murarka et al., 1992).

Contaminants can range from being extremely soluble such as methyl-tertiary butyl ether, or MTBE, to being essentially insoluble such as the aliphatic components of a hydrocarbon spill. There is an order of magnitude difference between the most and least soluble BTEX compounds. The solubility of benzene is 1780 mg/L, of toluene is 515 mg/L, of ethylbenzene is 152 mg/L, of xylene is 198 mg/L (LaGrega et al., 1994), and of MTBE is 51,200 mg/L.

Both the solubility of a compound and its propensity to be absorbed to aquifer material have significant impacts on the potential of the contaminant to reach a point-of-contact (POC). A compound with a relatively high solubility and low adsorption potential, such as benzene, has the chance to quickly reach a downgradient receptor where it can impact both human health and the environment. On the other hand, compounds with higher solubilities and lower adsorption potential are also more bioavailable to the microbial populations in the subsurface, so there is more of an opportunity for contaminant mass loss.

It has been shown that the molecular structure of a compound is important when determining if that chemical can be biodegraded. Gasoline contains mostly low to moderate molecular weight compounds (Borden et al., 1995). These moderate to lower molecular weight hydrocarbons, including C_{10} to C_{24} alkanes and single-ring aromatics, appear to biodegrade most easily (Atlas, 1988). For aromatic compounds, it has been observed that biodegradability is enhanced by methyl substitutions on the benzene ring such as is seen in toluene and xylene (Gibson and Subramanian, 1984). Compounds that have many branches such as MTBE are more resistant to biodegradation than other compounds of similar size with fewer branches (Sulfita, 1993).

Certain compounds in gasoline have been found to be hazardous to human health. Benzene has been classified as a human carcinogen by the National Cancer Institute (Burmaster and Harris, 1982). Toluene, ethylbenzene, and xylene have all been classified by the EPA as Class D which indicates that is "not classifiable as to human carcinogenicity" (LaGrega, 1994). The Resource Conservation and Recovery Act of 1976 has classified both toluene and xylene as hazardous (Corapcioglu and Baehr, 1987). Since evidence exists supporting an association between benzene and cancer, it often drives the regulatory concern regarding hydrocarbon contaminated groundwater containing BTEX compounds (Chapelle, 1999).

2.1.3 Natural Attenuation

Experience has shown that all groundwater systems have the ability to limit contaminant migration to some degree (Chapelle, 1999). Processes including biodegradation, dispersion, dilution, volatilization and sorption are responsible for what has become known as natural attenuation (Small, 1998). Natural attenuation involves reducing the mass, mobility, or toxicity of contaminants in soils, sediments, or groundwater using the natural processes listed above.

In some instances, the natural processes occurring in the subsurface are often adequate avoiding the need for additional source removal or plume clean up activities (Clement et al., 1998). It has been shown that natural attenuation can effectively limit the travel distance and concentration of petroleum hydrocarbons in groundwater at many leaking underground storage tank sites (Rice et al., 1995). Natural attenuation has also been shown to result in contaminant dissipation rates similar to those produced using engineered remediation methods (Swett and Rapaport, 1998).

As of 1995, there were few well-documented demonstrations of natural attenuation at hydrocarbon contaminated sites (Borden et al., 1995). Recent studies have indicated that the natural attenuation should be considered as a remediation strategy at all petroleum hydrocarbon

contaminated sites. This was a result of a leaking underground fuel tanks (LUFTs) study performed in California. The study suggested that leaking underground fuel tank, LUFT, plumes are generally no more than 250 meters in length and either stabilize or shrink over time (Rice et al., 1995). One of the final recommendations of the study was to "utilize passive bioremediation as a remediation alternative whenever possible".

The U.S. EPA has given the name "monitored natural attenuation" (MNA) to the process of intentionally using natural processes to achieve remediation objectives. The goal of MNA is to achieve remediation objectives that are fully protective of human health and the environment (Swett and Rapaport, 1998). Natural attenuation as a remedial alternative is not a hands off approach. Before MNA can be used as a remediation alternative, sufficient site investigation and characterization must occur in order to establish a clean up objective as well as a time frame for clean up (Swett and Rapaport, 1998; and Small 1998). Once the monitored natural attenuation process has been implemented, it must be demonstrated that natural attenuation is in fact occurring and monitoring must be used to compare results with expectations (Chapelle, 1999; and Swett and Rapaport, 1998).

Using natural attenuation as a remediation method at petroleum hydrocarbon contaminated sites has led to changes in the clean up process of leaking underground storage tanks sites in many parts of the country (Small, 1998). Rather than using the previously established concentration based goals to assess if a site has been sufficiently cleaned up, performance based goals are being used. The clean up goals at a site are now being defined using plume containment or the achievement of a risk based concentration at some downgradient POC instead of achieving a specified concentration at every point at a site (Small, 1998).

Several advantages to MNA exist. Since it is an in situ process, it is relatively non-intrusive and there are low volumes of waste generated resulting in a lower risk for human exposure to the contaminated material. Another advantage of monitored natural attenuation is that the costs associated with it are low (Swett and Rapaport, 1998). If it can be shown that natural attenuation is working to remediate a contaminated site, more resources can be used to clean up an alternative site where natural attenuation is not feasible. The one major disadvantage to MNA is that the time to remediation is generally long and difficult to predict.

According to Chapelle (1999), intrinsic bioremediation is most effective when it is applied to plumes of BTEX compounds. Natural attenuation has been shown to remove BTEX compounds in shallow sandy aquifers (Lahvis et al., 1999). Barker et al. (1987) showed in a controlled experiment that naturally occurring degradation processes were able to remove benzene, toluene, and three xylene isomers from solution in around one year.

Before natural attenuation can be selected as a remedial solution, it is important to understand the "natural contaminant destruction potential" or "natural attenuation capacity" of the contaminated aquifer (Chapelle and Bradley, 1998; and Clement et al., 1998). Three factors that contribute heavily to an aquifer's ability to naturally attenuate contamination are its hydrogeology, geochemistry, and microbiology. All three of these factors and their overall impact on the contamination can be investigated using a solute transport model (Chapelle, 1999). Modeling can also be used to obtain better estimates of the time to remediation (Swett and Rapaport, 1998).

2.2 BTEX Biodegradation

The major mechanism contributing to the natural attenuation of petroleum hydrocarbon contaminated sites is biodegradation (Baedecker et al., 1993). McAllister and Chiang (1994) reported that biodegradation by indigenous microbes appeared to be the mechanism most responsible for natural attenuation at many BTEX contaminated sites. Biodegradation has been described by Kennedy et al. (1998) as an important mechanism capable of destroying organic contaminants in the subsurface. Lahvis et al. (1999) found that aerobic biodegradation and volatilization near the water table contribute significantly to the natural attenuation of hydrocarbons at gasoline contaminated sites. Biodegradation is the only natural attenuation process that is able to transform the contaminants into harmless byproducts thus removing actual contaminant mass (Wiedemeier, et al., 1996).

Microbial populations indigenous to the sediments at contaminated sites have the ability to use multiple electron acceptors commonly found in the subsurface. These include oxygen (O_2), nitrate (NO_3^-), ferric iron (Fe(III)), manganese (Mn^{+4}), and sulfate (SO_4^{-2}) (Kennedy et al., 1998). When contamination is introduced to a groundwater system, a biodegradation order develops with the electron acceptors being preferentially selected in the following order: $O_2 > NO_3^- > Mn^{+4} > Fe(III) > SO_4^{-2} >$ methanogenesis (Kennedy et al., 1998). This order is established by the microbes based on the amount of free energy that can be generated for each of the processes with aerobic biodegradation providing the largest amount of free energy (Kennedy et al., 1998). An electron acceptor further down in the sequence will only be utilized significantly if the higher energy electron acceptors have become depleted.

Microbes have been shown to biodegrade petroleum hydrocarbons in both aerobic and anaerobic environments (Davis et al., 1994). Due to the high amount of energy microbes receive from aerobic biodegradation, dissolved oxygen is the preferred electron acceptor at contaminated sites. Most petroleum hydrocarbons are biodegradable under aerobic conditions (Borden et al.,

1995), and the biodegradation rates for the BTEX compounds are high in these conditions (Kao and Borden, 1997). For hydrocarbons subject to limited retardation, oxygen availability was found to be the dominant control on the persistence of the contaminants in the subsurface environment (Barker et al., 1987; and Borden et al., 1995).

The major disadvantage to aerobic biodegradation is the low availability of O_2 in the contaminated groundwater. O_2 is a dissolved gas and is limited to a maximum saturation of 8 to 9 mg/L (Ray, 1995). That, in combination with the fact that oxygen is rapidly consumed by microbes, can cause the conditions in contaminated aquifers to quickly become anaerobic resulting in the need for alternative forms of biodegradation. It has been shown that BTEX compounds can biodegrade anaerobically provided there are alternative electron acceptors present. BTEX biodegradation has been demonstrated to occur in nitrate reducing conditions (Hutchins et al., 1991; Kao and Borden, 1995) as well as in iron reducing conditions (Lovley et al., 1989). Biodegradation of BTEX has also been observed in sulfate reducing conditions (Edwards et al., 1991; and Haag et al., 1991) as well as in conditions supporting methanogenesis (Wilson et al., 1986; and Grbic-Galic and Vogel, 1987). It has been reported by many researchers that one of the BTEX compounds, benzene, is resistant to microbial biodegradation in anaerobic conditions (Acton and Barker, 1992; Barker et al., 1987; Hutchins et al., 1991; Weiner et al., 1998).

Studies can be performed at sites to assess the role that bioremediation is playing in natural attenuation. Generally, this involves examining the depletion of electron acceptors present at the site as well as the production of biodegradation end products including ferrous iron (Fe(II)), sulfide (HS^-), and methane (CH_4). There are some instances when quantitative measurements may not accurately reflect the processes occurring in the subsurface. Studies have shown that once ferrous iron (Fe(II)) is produced, it has a tendency to precipitate through several reactions including some with sulfide (Kennedy et al., 1998). Since ferrous iron and sulfide in the groundwater can react forming precipitated iron sulfide mineral forms, measuring the concentrations of these compounds in the groundwater may not verify the presence of iron and sulfate reduction. Sulfate concentrations can be used to determine the presence of sulfate reduction, but solid mineral analysis may be necessary to verify the presence of iron reduction (Kennedy et al., 1998).

Since biodegradation is such an important part of the natural attenuation process, estimating the biodegradation rates is an important first step in determining the potential for natural attenuation at a contaminated site (Chapelle et al., 1996). Biodegradation rates can be measured using both field and laboratory methods that track the consumption of electron donors,

the consumption of electron acceptors, and the production of final products of microbial metabolism with time (Chapelle et al., 1996). If the predominant TEAP at a site changes, there can be a significant change in the biodegradation rates (Vroblesky and Chapelle, 1994). Consequently, biodegradation is probably not as efficient in conditions favoring methanogenesis as it is in iron or sulfate reducing conditions.

2.3 Modeling Studies

A protocol presented by Wiedemeier et al. (1995) emphasized the role that computer-modeling studies can have in assessing the natural attenuation potential of petroleum hydrocarbon plumes. Numerical models have been used to simulate contaminant transport for many years. Model predictions can be used to determine whether potential receptors will be impacted by the contaminant, the expected concentration levels and associated risks, and how long it will take for the contaminant plume to completely degrade.

Predictive modeling is used to determine the viability of natural attenuation as a remediation alternative at contaminated sites. Provided sufficient site characterization data is available, detailed numerical modeling of ground water flow and contaminant transport can be performed to help demonstrate natural attenuation. One, two, and three-dimensional contaminant transport models have all been used in studying the effects of both sorption and biodegradation on the movement of hydrocarbon contaminants in the subsurface.

Early contaminant transport models were relatively basic simulating a single hydrocarbon substrate undergoing first order decay, or, in some instances, biodegradation was modeled as an instantaneous reaction. Models of this type included the Hydrocarbon Spill Screening Model (HSSM) (Charbeneau and Weaver, 1992), MT3D (Widdowson, 1998), BIOSCREEN (Widdowson, 1998), and BIO1D (Davis et al., 1994; and Klecka et al., 1990). These models were often used as screening tools in an effort to obtain approximations of contaminant concentrations and travel distances.

Regulators now require evidence that natural attenuation will prevent contaminants from reaching potential receptors at concentrations higher than regulatory standards. Consequently, contaminant transport models have become more detailed. Most of the increased detail can be seen in the way the models deal with biodegradation in the subsurface. Now several models have the ability to simulate aerobic biodegradation, anaerobic biodegradation, or both as well as multiple hydrocarbon substrates and electron acceptors.

BIOPLUME II is a two-dimensional numerical biodegradation model that has the ability to simulate the transport of oxygen and contaminants in the subsurface (Bedient and Rifai, 1992).

Biodegradation is approximated by an instantaneous reaction. A modeling study was conducted at a BTEX contaminated site in Traverse City, Michigan to understand and aid in the evaluation of natural biodegradation at the site (Bedient and Rifai, 1992). One of the major goals of the study was to aid in the calibration, formulation and understanding of modeling overall bioremediation at the site. The general trend in the results indicated that the model overpredicted contaminant concentrations, and this was more pronounced as the time from the beginning of the simulation increased (Bedient and Rifai, 1992). BIOPLUME II only simulates aerobic biodegradation, and it is possible that anaerobic biodegradation in the field was contributing to the observed contaminant loss thus explaining the high concentrations predicted by the model.

Modeling studies were performed on a BTX contaminated aquifer in Michigan also using BIOPLUME II. The study was intended to aid in understanding the natural biodegradation processes that were at work at the site. Similarly to the previous study by Bedient and Rifai (1992), this study simulated the transport of the soluble BTX and dissolved oxygen. The results of this modeling study showed good correlations between the simulated and observed BTX concentrations, but the measured and simulated concentrations of DO were not similar. BIOPLUME II assumes that 3 ppm of DO is required to biodegrade 1 ppm of aromatic hydrocarbons. The results of this study indicated that the actual DO concentrations required for BTX biodegradation may be less than the model assumes (Chiang et al., 1989).

RT3D is a general purpose, multispecies, reactive transport code (Clement et al., 1998). RT3D can simulate simultaneously the reactive transport of microbes, substrates, and contaminants within the subsurface as well as aerobic and anaerobic biodegradation and microbial growth. Little information is available regarding the use of RT3D at actual contaminated field sites.

There are many models available to simulate the transport and attenuation of hydrocarbon contamination. There are limitations associated with each of the models, and these include the ability to simulate only one contaminant, the inability to simulate three dimensions, as well as the inability to simulate anaerobic biodegradation. SEAM3D is a model that is not limited by any of the factors just described. It is a three-dimensional model that can more accurately simulate what is occurring in the subsurface at a contaminated site using multiple substrates undergoing both aerobic and anaerobic biodegradation.

2.4 Laurel Bay Research

A research project as a part of a regulatory assessment has been ongoing since 1993 at the Laurel Bay site in Beaufort, South Carolina on the fate of petroleum hydrocarbon contamination

of the soil and groundwater. Leaking underground storage tanks led to the contamination of an aquifer immediately underlying the ground surface. The major contaminants being investigated are the BTEX compounds along with MTBE. All of the material presented in this section is from Landmeyer et al. (1996) and Landmeyer et al. (1998).

2.4.1 Study Area

The Laurel Bay Exchange, Marine Corps Air Station is located in Beaufort, South Carolina. The location of the site can be seen in Figure 2.1. Underground storage tanks at a service station on the site leaked gasoline containing fuel oxygenates into the aquifer, and it was first detected in the aquifer in late 1991. A contamination assessment performed in 1993 indicated concentrations of BTEX compounds above U.S. Environmental Protection Agency maximum contaminant levels (MCLs). The tanks and surrounding sediments were removed from the ground in late 1993.

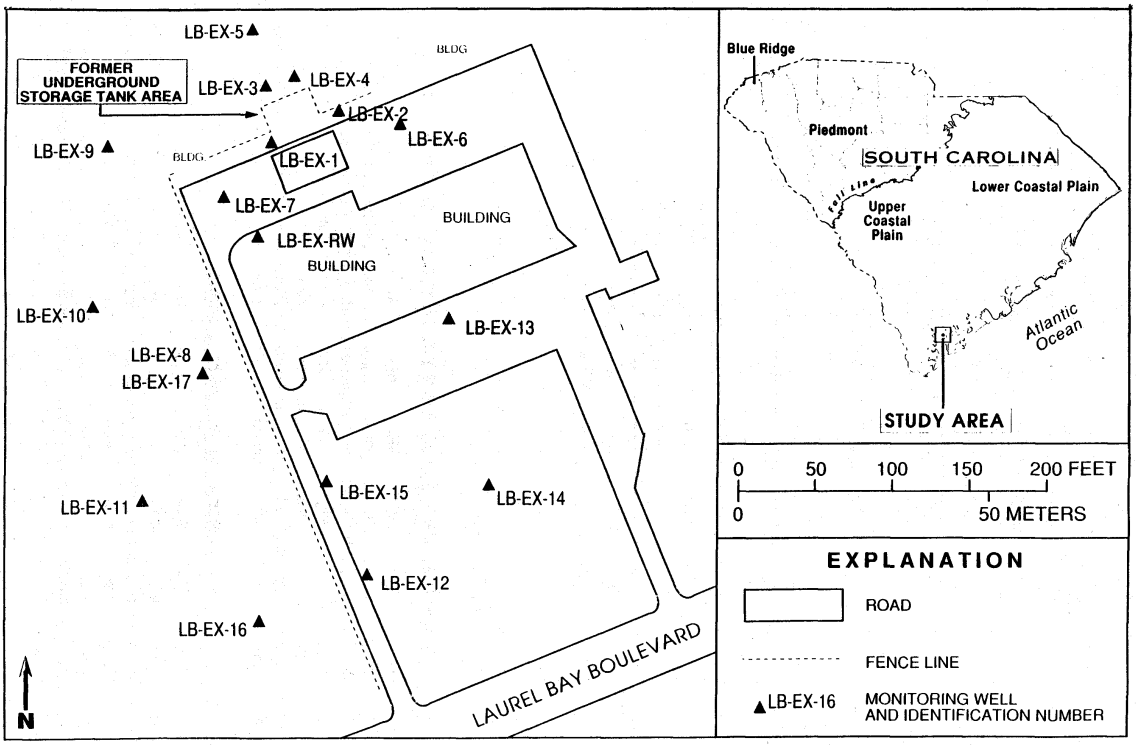

Figure 2.1 Location of Laurel Bay Exchange study area (Landmeyer et al., 1996)

The contamination is confined to a shallow, unconfined water table aquifer comprised mainly of silty sand sediments that reach to depths of around 40 feet below the land surface. No clays or clay lenses have been detected in the aquifer. The depth to groundwater is around 13 feet

near the source and between 2 and 9 feet closer to the concrete swail, approximately 200 meters downgradient from the source area.

The general direction of groundwater flow at the site is from north to south, or from the source area towards the concrete swail. The average hydraulic conductivity of the aquifer material is 11 ft/day (3.4 m/day). This results in an average groundwater velocity of 70 ft/yr (21 m/yr) near the source area and 500 ft/yr (153 m/yr) closer to the swail. Sloping topographic conditions near the swail account for the significant increase in groundwater velocity.

All recharge to the aquifer results from rainwater infiltration. The estimates for recharge at the site are 20 to 25 inches/year. Since research was begun at the site in 1993, the general flow direction and hydraulic gradients across the site have remained consistent. This has been explained by the fact that any changes in the water levels due to varying rainfall events have been uniform across the entire site resulting in little change to the flow direction and gradients. The ground water levels in the aquifer have varied significantly over the 6 year study period. Fluctuations as high as 2 to 3 feet (0.6 to 0.9 meters) have been seen in some of the monitoring wells at Laurel Bay. Rainfall events have had a large impact on the groundwater levels because the aquifer is shallow.

Rainfall also has been shown to have a direct influence on the vertical flow of the contaminant plume. By examining the water table levels between wells LB-EX-8 and LB-EX-17, it can be seen that there is a vertical downward flow gradient in the aquifer. This downward gradient is increased by recharge events at the site. Heavy rain events have been used as the explanation for a definite downward dip of the BTEX/MTBE plume. Recharge events deflected the originally horizontal flow lines, pushing the plume vertically downward. Following the rainfall, flow predominantly in the horizontal direction resumed.

2.4.2 Field Sampling and Data Collection

From 1993 to 1998, ground water samples were collected from both monitoring wells and multilevel sampling wells to provide vertical and horizontal distributions of MTBE and BTEX. Concentrations of dissolved oxygen, H_2, Fe(II), sulfide, sulfate, and CH_4 were also measured in March 1994, June 1996, January 1997, July 1997, and January 1998. Results from these sampling events can be seen in Appendix C. This was done to determine if changes in the concentrations of the contaminants resulted from microbial processes. Wells were sampled for BTEX and MTBE in April 1993 as well as the five dates of testing previously listed.

In March 1994, the shallow ground water was aerobic and low in sulfide concentrations in areas that were free of hydrocarbon contamination. In the wells containing contamination, low

dissolved oxygen concentrations and higher dissolved Fe(II) concentrations were measured. The low concentrations of DO at the site along with the production of Fe(II) in contaminated areas were two indicators that intrinsic bioremediation, both aerobic and anaerobic, was occurring at the site in 1994. Hydrocarbons were initially oxidized using oxygen as the terminal electron acceptor, and when DO concentrations became sufficiently low, ferric iron (Fe(III)) was utilized as the electron acceptor. The concentrations of nitrate were sufficiently low, eliminating the possibility of nitrate reduction as a method of biodegradation. Concentrations of sulfate were less than 1.0 mg/L in two of the wells sampled indicating the possibility of sulfate reduction. In 1994, the levels of sulfide were below detection indicating that sulfate reduction at the site had yet to begin.

Dissolved inorganic carbon (DIC) and methane concentrations were also measured at the site. As the hydrocarbon contamination increased and the dissolved oxygen concentrations decreased, the DIC concentrations tended to increase. The high levels of DIC in the contaminated regions of the aquifer indicated the mineralization of organics to CO_2. As DIC concentrations increased, dissolved Fe(II) concentrations were also observed to increase indicating that Fe(III) reduction was a major terminal electron accepting process (TEAP) in the shallow, anaerobic part of the contaminated aquifer. Methane was not detected in any of the samples taken in 1994. These results indicated that although there were anaerobic conditions present in the aquifer, methanogenesis had not yet been initiated. No evidence of sulfate reduction or methanogenesis indicated that the plume was still relatively new.

2.4.3 Laboratory Experiments

The two main processes that affect the attenuation of petroleum hydrocarbon contaminants from the source area are adsorption and biodegradation (Landmeyer et al., 1996). Research was done in 1994 regarding the determination of adsorption coefficients for benzene and toluene. The samples collected from the site in February of that year were used to estimate the amount of each compound adsorbed to the sediment material from Laurel Bay. To obtain the linear adsorption coefficients, the compounds were dissolved in a solution of ground water and MTBE to represent in situ conditions. Concentrations were then measured after equilibrium was achieved to determine the the amount adsorbed. The linear adsorption coefficient was found by regressing the concentrations of the contaminant measured against the concentrations of the contaminant added to the solution.

The values of k_D found for toluene in the silty sand from the Laurel Bay site ranged from 0.057 to 0.14 ft^3/mg. For benzene, values of k_D at the site ranged from 0.057 to 0.2831 ft^3/mg.

These values are all very low, and suggested to Landmeyer et al. (1996) that little benzene or toluene was being adsorbed to the aquifer solids. Low adsorption coefficients indicate there will be little retardation of the contaminants relative to the groundwater flow, and the contaminated sediments will not be a continual source of contamination to the groundwater. The retardation factors for benzene and toluene range from 1.26 to 1.64 and from 1.26 to 2.30, respectively.

Biodegradation rates were estimated using different methods for MTBE, benzene, and toluene. Both aerobic and anaerobic rates of microbial degradation of toluene were found by quantifying the rate of production of radiolabeled $^{14}CO_2$ from a known amount of radiolabeled toluene added to a microcosm containing saturated sediment from LB-EX-8 (-0.64 to –0.003, respectively). The anaerobic microbial degradation of benzene was estimated using the digital solute-transport model SUTRA (Saturated and Unsaturated TRAnsport) (Voss, 1984). Iterative calibration simulations were performed to reproduce benzene concentrations observed in 1993 and 1994 in order to estimate an anaerobic biodegradation rate for benzene. The biodegradation potentials of MTBE were studied by quantifying the production of carbon dioxide from a known amount of uniformly labeled (UL) ^{14}C-MTBE added to microcosms containing aquifer material.

2.4.4 Solute Transport Simulations

Field and laboratory tests performed at Laurel Bay indicated a range of values possible for the hydraulic gradient, hydraulic conductivity, adsorption isotherms, and microbial degradation rates. These values are summarized in Table 2.1.

The two parameters subject to the largest degree of uncertainty were K_{aq}, the hydraulic conductivity, and K_{bio}, the microbial degradation rate. There was a standard deviation of 3.3 ft/day in the hydraulic conductivity measurements indicating a high degree of variability. There were order of magnitude variations between the aerobic and anaerobic rates of degradation for toluene as well as between the anaerobic rates for benzene and toluene.

Due to the significant variation in these parameters, an exploratory modeling approach was used to find the hydrocarbon distributions resulting from a range of values. The goal of this approach was to reproduce extreme conditions to determine the possibility of transport to the nearest POC. The most probable values shown in the table above were used to construct what was described as a Standard Model. This model assumed constant water-table gradients, the aquifer remained anaerobic, and the aquifer material had low tendency to adsorb benzene and toluene.

The model was set up with the free-product source area located on the upgradient side. The nearest POC, the property line on the southern edge of the site, provided the downgradient model boundary. The Standard Model was not intended to represent actual parameter values but to act as a method for comparison as certain parameters were varied. The results produced when parameters were varied were compared to the Standard Model results to assess the impact caused by the parameter variation on contaminant transport.

		Most Probable Values		
Parameter		**High Estimate**	**Low Estimate**	**Best Estimate**
Hydraulic gradient (ft/ft)		0.0046	0.0046	0.0046
Hydraulic conductivity (ft/day)		17.3	8.9	11.1
Microbial degradation rate (per day)	Toluene	-0.64 (aerobic)	-0.003 (anaerobic)	-0.003 (anaerobic)
Adsorption rate (ft^3/mg)	Toluene	5.00E-09	2.00E-09	2.00E-09
Microbial degradation rate (per day)	Benzene	-- (aerobic)	-0.00025 (anaerobic)	-0.00025 (anaerobic)
Adsorption rate (ft^3/mg)	Benzene	1.00E-08	2.00E-09	2.00E-09

Table 2.1 Most probable values for certain Laurel Bay site parameters

The Standard Model for toluene transport for 1994 was based on the most probable values for toluene shown Table 2.1. It was assumed toluene was leaching into the ground water system at a concentration of 50 mg/L beginning in late 1991 and that it was undergoing anaerobic biodegradation. The resulting contaminant distribution was compared to what was observed in the field. The model simulated the plume moving around 100 feet farther downgradient than what was seen in the field. This difference was explained by the fact that there were no downgradient wells in the field to accurately characterize the shape of the plume using field data. Since there were no downgradient wells, it was not possible to determine the actual length of the contaminant plume in 1994. This Standard Model indicated that the toluene plume achieved steady state conditions by the year 2001.

The Conservative Model, or the worst case scenario, simulated toluene transport from a constant source using no biodegradation or adsorption. The plume was not predicted to move more rapidly than the rate of ground water flow. The results did indicate, however, that the

dispersive effects of the silty sand grains lead to the toluene plume migrating ahead of the ground water flow. Using this model, the toluene plume, as delineated by the 0.1 mg/L contour, was shown to have moved 600 feet downgradient from the source area. The rate of toluene transport for these simulated conditions was found to be 200 ft/year, and that would imply the plume would reach the Broad River around 18 years from the time of the study.

When the hydraulic conductivity, K_{aq}, was varied in the toluene simulations, it was found that higher values of K_{aq} resulted in a larger plume. There was over a 300 feet difference between the simulation using the minimum value for K_{aq}, 8.9 ft/day, and the simulation using the maximum value for K_{aq}, 17.3 ft/day. Higher hydraulic conductivity values resulted in higher groundwater flow rates, and that led to the increased travel distance of the plume.

When the model was run using the aerobic biodegradation rate, the toluene contamination remained within 50 feet of the source area as of 1994. The geochemical conditions in the field implied there was more anaerobic biodegradation occurring in the body of the plume than aerobic biodegradation. Aerobic biodegradation was most likely occurring near the top of the plume, which was exposed to rain water infiltration, and along the edges of the plume where there was contact with non-contaminated groundwater. When the adsorption rate was varied within the range seen in Table 2.1 it was shown that it does not significantly retard toluene transport at Laurel Bay.

Toluene simulations were run using minimum and maximum values for all the parameters listed in Table 2.1. It was shown that even when maximum hydraulic conductivity values were used, the use of the aerobic biodegradation rates had a larger impact on the shape and travel distance of the plume. This combination of parameters kept the plume within 200 feet of the source area. These results indicated that by inducing aerobic conditions in the aquifer, toluene concentrations could be controlled and potentially reduced.

Simulations were also run where the contaminant source was removed from the aquifer. The parameters entered for this model were identical to those of the Standard Model. Removal of the source had a significant impact on the maximum toluene concentrations seen in the plume over time. One year after the source was removed concentrations were predicted to decrease by an order of magnitude.

Benzene simulations were run using the same approach that was used for toluene. A Standard Model was again constructed using the most probable values from Table 2.1. This Standard Model was again used as a means of comparison when parameter values were varied to determine their impact on benzene transport.

Two benzene Standard Models were run, one for 1993 and one for 1994. Each model was run with the best estimate values from Table 2.1, and the benzene plume was simulated as originating from a constant source. It was found that in order to simulate the benzene concentrations seen in the field in 1994, the source of benzene contamination had to be removed from the model simulation in 1993. Even with that variation, the benzene plume, delineated by the 1.0 ppb contour, reaches 50 feet further (to 400) downgradient than was observed in the field in 1994. This difference was again explained by the lack of downgradient wells available to aid in plume characterization. Transport simulations were run out until 2044, and the indicated the contamination would not reach the nearest POC by that time.

The worst case simulation depicted neither adsorption nor biodegradation. Dispersive effects caused by the aquifer material caused the contaminants to migrate further than was predicted by purely advective flow. This conservative scenario predicted concentrations of benzene of 1.0 ppb 470 feet downgradient from the source area after three years of transport. The rate of benzene transport under these conditions was estimated to be 157 ft/year, and that would result in benzene reaching the nearest POC after around 23 years. Source removal was also simulated. Once the source was removed, benzene concentrations over time were predicted to decrease due to dilution by ground water. When the hydraulic conductivity was increased, the plume length increased, and that was what was observed for toluene.

The results of these simulations indicated that no range of feasible input parameters, hydrologic, geochemical, or microbial, would result in the transport of BTEX compounds to the nearest POC. The contaminants were effectively isolated to the site under the conditions at that time, and they were not likely to affect adjacent surface water bodies in the future. Intrinsic bioremediation was determined to be a possible remediation alternative at the Laurel Bay site, and the removal of the source of contamination and/or the contaminated sediments would have accelerated the intrinsic bioremediation process.

2.4.5 1998 Study

In 1998, a study was conducted by Landmeyer et al. to determine the fate of MTBE relative to benzene in a gasoline-contaminated aquifer. Prior to this study, 5 additional wells were installed at the site. Five multi-level sampling wells were installed between 1996 and 1997. Figure 2.2 shows the locations of all of the wells at the site relative to the source area, which is found in the circled area near wells LB-EX-1 and LB-EX-3. Using the concentration data measured at the site between 1993 and 1998, contours for both benzene and MTBE were created. The contours were generated for 1993, 1994, 1996, January and July 1997, and 1998.

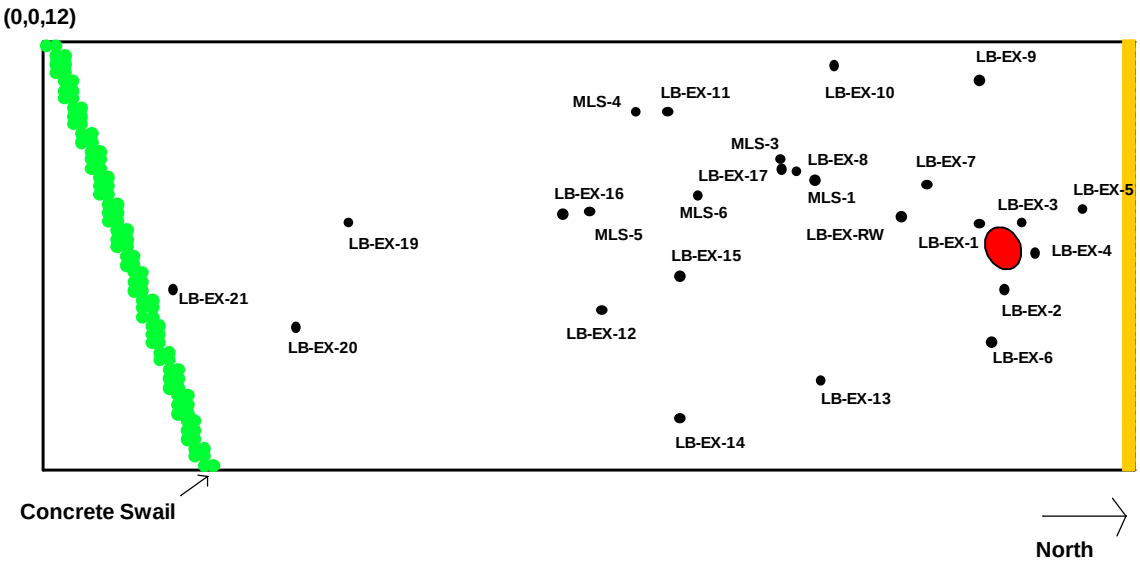

Figure 2.2 Location of monitoring wells relative to the source area

The area of MTBE contamination was delineated by the 20 µg/L contour while the extents of the benzene plume were marked by the 5.0 µg/L contour. A drinking water advisory was recently issued for MTBE for concentrations ranging from 20 µg/L to 40 µg/L (December 1997), so the most conservative was chosen. 5.0 µg/L was selected to define the area of benzene in the aquifer since as of 1998, it was the EPA drinking water MCL.

By April 1993, MTBE concentrations of 20 µg/L were observed around 100 meters downgradient from the source area with maximum concentrations around 250 mg/L in the source area. It was assumed that MTBE moved at the rate of groundwater advection, so the fact that MTBE traveled that distance indicates that the contaminant release could have occurred as early as 1988. Benzene concentrations of 5.0 µg/L were found 83 meters downgradient from the contaminant leak. Benzene traveled around 80 % of the distance traveled by MTBE over the same duration due to its lower solubility, higher adsorption, and higher biodegradation potential. The retardation factor for benzene was about 1.25.

The March 1994 data indicated both the MTBE and benzene plumes had traveled an additional 30 meters downgradient. There were decreases observed in benzene concentrations from 1993 seen in some of the more contaminated wells close to the source area. The increase in the spread of the contamination in the transverse direction was explained by lower recharge amounts permitting more dispersion processes to occur.

By June 1996, concentrations of MTBE and benzene of 18 mg/L and 1.0 mg/L were observed in LB-EX-21. This well was furthest downgradient from the source area, closest to the

swail. It was estimated that the contaminants had been transported to LB-EX-21 sometime in early 1995 because contamination was observed at the time the well was installed.

The lowest water table elevations of the five-year study were recorded during the seven-month time span from January 1997 to July 1997. This was used as a possible explanation for the fact that similar benzene and MTBE concentration distributions were seen for both those sampling dates. The center of the MTBE plume was observed to have traveled in the downgradient direction with decreasing maximum concentrations since 1996. The benzene plume did not exhibit the same trends. Both plumes were observed to be spreading more in the transverse horizontal direction in the area of the site with lower groundwater flow rates while they continued to be narrow closer to the concrete swail where flow rates were higher.

In January 1998, the 20 μg/L and 5 μg/L contours for MTBE and benzene were similar to those from 1997, but the highest MTBE contour, 10,000 μg/L, moved around 61 meters downgradient from its 1997 location. Increases in hydraulic gradients in the region where the plume was traveling along with increased recharge resulting from above average rainfall from July 1997 to January 1998 were used to explain the increased travel distance of the MTBE plume. The increase in recharge also resulted in a narrowing effect evident in both the MTBE and benzene plumes.

Concentrations of both benzene and MTBE were observed to increase as depth in the aquifer increased with the highest MTBE and benzene concentrations not found near the water table. This is in contrast to what is typically seen with a LNAPL spill. This observation suggested that recharge events were causing dissolved phase MTBE and benzene to be displaced deeper into the aquifer. Over time, the maximum concentrations of both contaminants appeared to move deeper within the aquifer as well as in the downgradient direction.

3.0 Numerical Models

3.1 Groundwater Model

It is necessary to develop a groundwater model that best represents the actual site conditions since contaminant flow is impacted by the groundwater flow. Based on the geological and hydrogeological studies of the Laurel Bay site, a model of the groundwater system was developed using the Department of Defense Groundwater Modeling System (GMS) which employs the MODFLOW finite difference code. The accuracy of the model was determined through comparisons with the available water table elevation data.

3.1.1 Conceptual Model

The formulation of a conceptual model that adequately depicts the groundwater flow system is the first step in a computer modeling study (Anderson and Woessner, 1992). A conceptual model of the Laurel Bay site was used to simplify the more complex field conditions. The first step in designing a conceptual model of the site was the identification of the model boundaries.

Geologic information for the Laurel Bay area indicated a shallow, unconfined water table aquifer made up of fine-grained silty sand immediately beneath the ground surface. The sand layer extends around 38 feet below the land surface, and it is part of the upper aquifer as defined in the site Contamination Assessment Report (ABB Environmental Services, 1993). A thick, clay-confining layer, or aquitard, lies beneath the sand layer. It is assumed that no groundwater flowed vertically through the confining layer. Since there is no evidence indicating the plume travels into the clay layer, the groundwater model has just one hydrostratigraphic layer. Regional hydrogeological data indicates that the upper aquifer consists of deposits of varying lithology, thickness, and permeability indicating the possibility of varying hydraulic conductivities within the model boundaries (ABB Environmental Services, 1993).

Water enters the modeled flow system in one of two ways. Groundwater flows from the groundwater divide located north of the source area into the model domain. The second input method is through recharge. Precipitation data for Beaufort County indicates that the area receives around 50 inches of rain a year (http://www.ncdc.noaa.gov/pub/data/coop-precip/south-carolina.txt). A commonly used method of estimating recharge based on some percentage of average annual precipitation was used to determine the recharge rate across the site (Anderson and Woessner, 1992). Groundwater flow only exits the model through the concrete swail. The swail is modeled as a drain, and since the head in the aquifer is greater than the drain

elevation, water exits the model through the drain at a rate proportional to the drain's conductance.

3.1.2 Mathematical Model

Once the conceptual model had been developed, the next step in the groundwater modeling study involved selecting a computer code with which to run the model. The computer code uses the governing equations to solve the mathematical model numerically. MODFLOW was the computer code used in the groundwater model of the Laurel Bay site. MODFLOW is a finite difference code that has the ability to simulate the three-dimensional movement of groundwater through a porous material described by the following governing equation

$$\frac{\partial}{\partial x}\left(K_{xx}\frac{\partial h}{\partial x}\right)+\frac{\partial}{\partial y}\left(K_{yy}\frac{\partial h}{\partial y}\right)+\frac{\partial}{\partial z}\left(K_{zz}\frac{\partial h}{\partial z}\right)-W=S_s\frac{\partial h}{\partial t} \qquad (3.1)$$

where

K_{xx}, K_{yy},and K_{zz} are the hydraulic conductivity values along the x, y, and z coordinate axes, which are assumed to be parallel to the major axes of hydraulic conductivity (L/t);

h is the hydraulic head (L);

W is the volumetric flux per unit volume representing sources/sinks of water (t^{-1});

S_s is the specific storage of the porous material (L^{-1}); and

t is time (t).

Equation 3.1 represents flow under nonequilibrium conditions in a heterogeneous and anisotropic aquifer. Steady-state conditions are assumed in this flow model.

The second step in developing the mathematical model involves specifying the initial boundary conditions. The eastern and western boundaries in the Laurel Bay model are flow lines and are specified as no-flow boundaries, described by $\frac{\partial h}{\partial x}=0$. The northern boundary of the model is also a specified flow boundary, and it is defined using $\frac{\partial h}{\partial x}=f$ where f is determined based on recharge rates and the area between the boundary and the groundwater divide. The calculation is discussed in more detail in Section 3.1.3. The final boundary is the drain, which is a head-dependent flux boundary.

The rate of flux between a drain and the surrounding aquifer is found using the following equation

$$QD=CD(h-d) \qquad (3.2)$$

where

QD is the rate at which water is removed from the model (L/t);

CD is the assigned conductance of the drain (L/t);

h is the head in the aquifer surrounding the drain (L); and

d is the elevation of the drain (L).

MODFLOW only calculates flow into the drain. If the elevation of the drain is greater than the head in the surrounding aquifer ($d > h$), the flux is zero.

The upper and lower model boundaries are the water table and the clay aquitard. MODFLOW uses the Dupuit Assumptions to model flow in the top layer of the three-dimensional model, so it only requires the specification of side and bottom boundary conditions for the model domain. The model then calculates the water table location as a part of the solution. The aquitard is a no-flow boundary that defines the bottom of the model domain.

3.1.3 Model Grid and Boundary Conditions

The dimensions and location of the model grid were based on the boundary conditions established by the conceptual model. The length of the model grid is 250 meters extending from around 30 meters north of the source area to the concrete swail in the south. The swail represents the southern boundary of the model. The width of the grid is 98 meters. This distance is based on the predicted location of the contaminant plume estimated from site data (Landmeyer et al., 1996). The model grid was designed to capture the entire plume with extra distance on either side to allow for possible natural deviations in flow or error in plume delineation. Each of the grid cells is 2 meters long by 2 meters wide, so the model is 125 cells long and 49 cells wide. The actual model grid can be seen in Figure 3.1 with the southwestern most point of the grid (0,0,12) defined as the origin. The site features and the outer boundaries of the model grid can be seen in Figure 3.2.

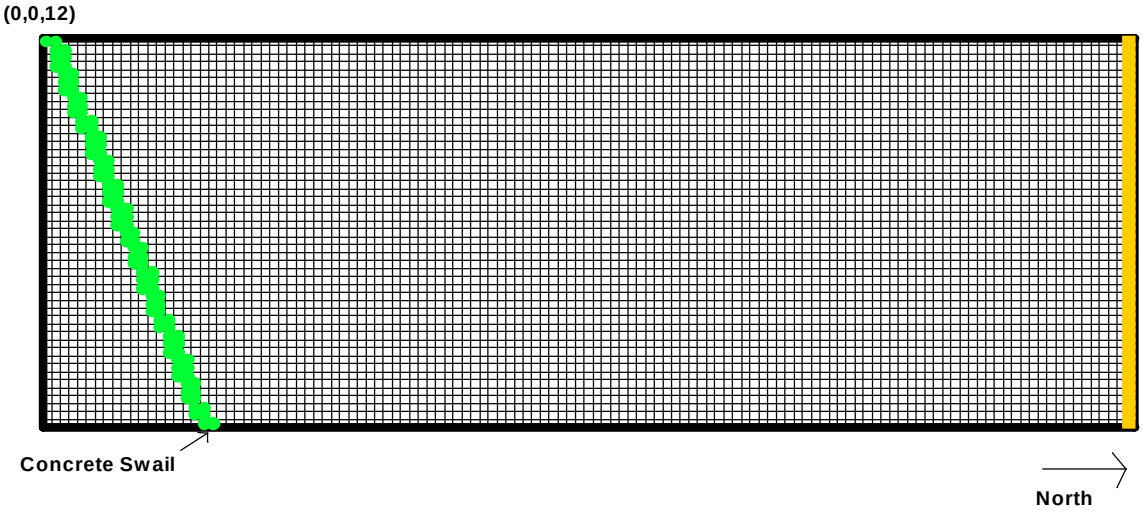

Figure 3.1 Model grid

The total depth of the model is 12 meters based on the 40-foot approximation of depth from the ground surface to the confining clay layer. The model is divided into 4 layers. Since the groundwater flow was confined to just the upper unconfined aquifer at the Laurel Bay site, one model layer could have been used. Multiple layers are used to model the vertical migration of the plume that was observed in the field (Landmeyer et al., 1996). The bottom three layers are each 2.25 meters thick with the top layer being 5.25 meters thick. The top layer is defined as unconfined with the bottom two layers defined as confined. The second layer is defined as confined/unconfined type 3. Under this condition, the layer can vary between being fully confined (i.e., fully saturated) and being unconfined. The transmissivity in this layer can vary depending on the hydraulic conductivity and saturated thickness, and the storage coefficient can alternate between confined and unconfined values.

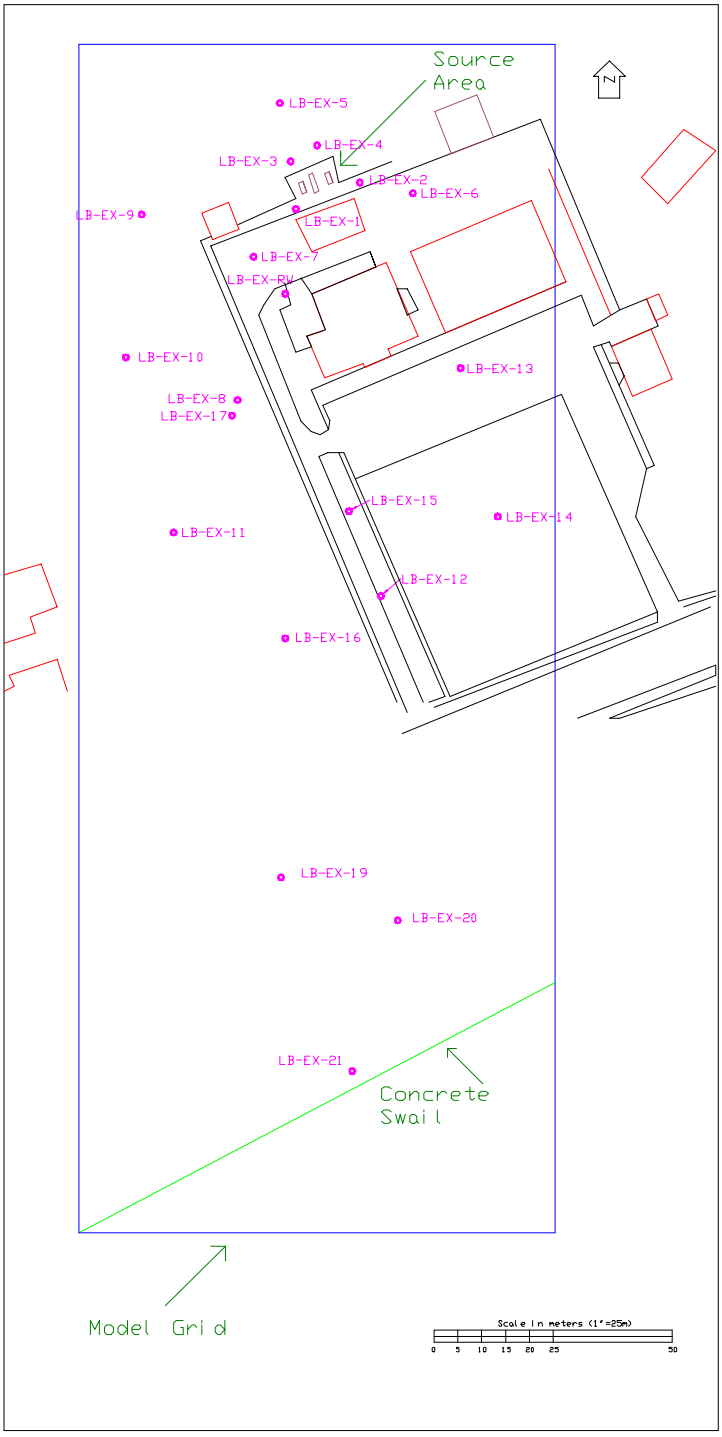

Figure 3.2 Site features and model grid outer boundaries (modified from Brauner, 1995)

The specified flux through the northern boundary is found using the Dupuit Equation given by

$$q' = \frac{1}{2} K \left(\frac{h_1^2 - h_2^2}{L} \right) \tag{3.3}$$

where

q' is the flow per unit width;

K is the hydraulic conductivity

h_1 is the head at the origin;

h_2 is the head at L; and

L is the flow length.

The Dupuit Equation is based on several assumptions assumed valid at Laurel Bay: steady, unconfined flow, hydraulic gradient is equal to the slope of the water table, and for small water-table gradients, the streamlines are horizontal and the equipotential lines are vertical. A wetlands region is located about 4000 feet from the concrete swail. Equation (3.3) can be modified to incorporate boundary conditions:

$$h^2 = h_1^2 - \frac{\left(h_1^2 - h_2^2\right)x}{L} + \frac{w}{K}(L - x)x \tag{3.4}$$

where

w is the recharge rate;

x is the distance from the origin to where h is being determined;

L is the distance to the wetlands;

h_2 is the corresponding head at the wetland region; and

h_1 is the head at the swail.

Using data from several monitoring wells, simultaneous equations were solved to yield values for recharge rate, the head at the wetlands area, and the head at the concrete swail. Once recharge rate and boundary conditions were calculated, it was possible to estimate the distance to the groundwater divide:

$$d = \frac{L}{2} - \frac{K}{w} \frac{\left(h_1^2 - h_2^2\right)}{2L} \tag{3.5}$$

Solving equations (3.4) and (3.5) yielded the following results:

h_1 = 17.5 feet (5.33 meters);

h_2 = 32.4 feet (9.88 meters);

K = 11.1 feet/day (3.383 meters/day);

w = 0.005 feet/day (0.0015 meters/day);

L = 4000 feet (1219.1 meters); and

d = 2200 feet (670.5 meters).

The purpose of this analysis was to calculate a groundwater inflow rate at the upgradient boundary. Based on the estimated recharge rate and the area of land from the groundwater divide to the back boundary of the model grid, it was possible to determine the amount of groundwater flowing into the model grid. This northern boundary was established as a constant flow boundary with Q_{well} specified at each of the 196 grid cells using MODFLOW's well package. A representation of the system can be seen in Figure 3.3.

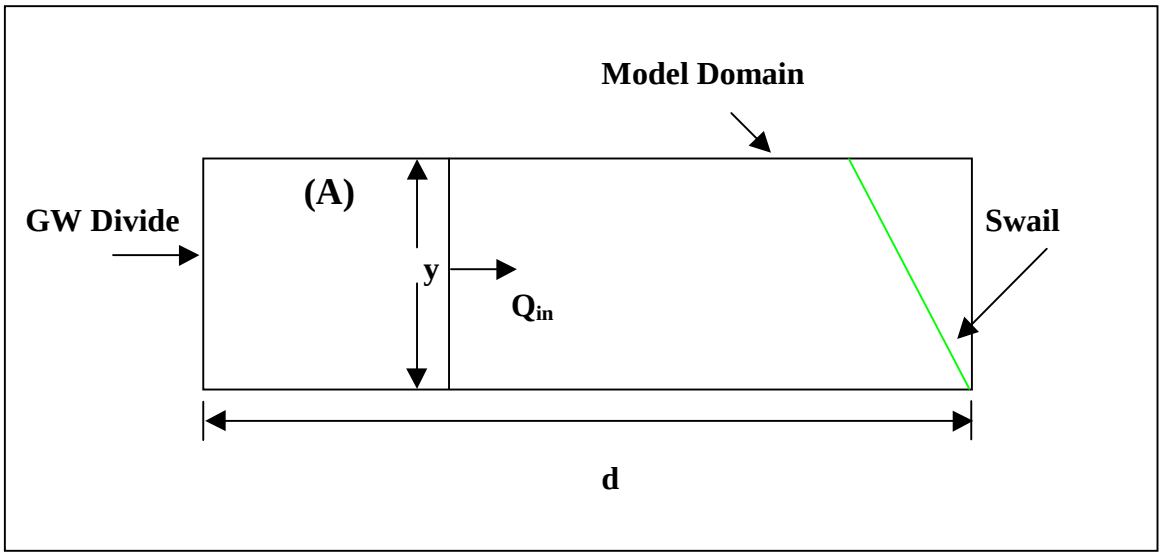

Figure 3.3 Depiction of method used to calculate groundwater inflow

Q_{in} was used to determine the specified Q_{well} at each of the cells along the constant flow boundary. The well package in MODFLOW simulates the inflow. A well is located in each of the 196 cells located along that boundary. The initial amount of water injected into each cell was found using:

$$Q_{well} = \frac{wA}{196} \tag{3.6}$$

where

w is the rate of recharge over the area; and

A is the area of land from the back boundary to the groundwater divide.

The water table in layer 1 does not reach the top of the cells in that layer, so $Q_{well,}$ for each cell in that layer was multiplied by a factor of 0.35. That factor was based on the assumption that the maximum head at the boundary would be 8.5 meters rather than 12 meters, or the top of each cell. Calculations can be seen in Appendix A, and the results show Q_{in} is 54.5 meters^3/day and Q_{well} varies from 0.097 to 0.28 meters^3/day. These values were later varied during calibration of the flow model.

The swail was assigned as the southern model boundary based on the observations in the field of groundwater leaving the subsurface through the swail (Landmeyer and Widdowson, personal communication, 1998). Using the drain package in MODFLOW, the swail is simulated as a drain. The bottom elevation of the swail is 17.5 feet, or 5.3337 meters, from the bottom of the aquifer, and it is located in the second layer. The actual width of the drain was approximated as 30 feet or 9.1436 meters. Half of the drain was simulated in the model, so it was placed in 2 grid cells. From the origin, the concrete swail is angled at 20° in the northeasterly direction. For this reason, all of the cells south of the angled drain were inactivated since as it has already been stated, all flow will exit the model through the drain. The land adjacent to the swail slopes downward into the swail at around a 9.4° angle. To simulate the sloping land surface, 20 cells were inactivated in the top layer. Calculations based on the elevation of the swail bottom, the land surface elevation and the width of the swail indicated that twenty cells needed to be inactivated, and they can be seen in Appendix A.

The boundaries on the eastern and western sides of the model grid are no-flow boundaries. These were determined based on the reported groundwater flow direction (Landmeyer et al., 1996). No values are assigned to the model cells along those boundaries because MODFLOW simulates all boundaries as no-flow unless otherwise specified.

3.1.4 Model Parameters

Figure 3.4 shows the location of the contaminant source area and monitoring wells. Over 22 monitoring wells were installed as a part of contamination assessment activities and are in use measuring the elevation of the groundwater table as well as to define the horizontal and vertical extent of groundwater contamination. The wells are numbered sequentially from LB-EX-1 through LB-EX-21 along with a well LB-EX-RW. The locations of all the wells that fell within

the model grid can be seen in Figure 3.4. The only well that does not fall within the grid used for this research is LB-EX-18.

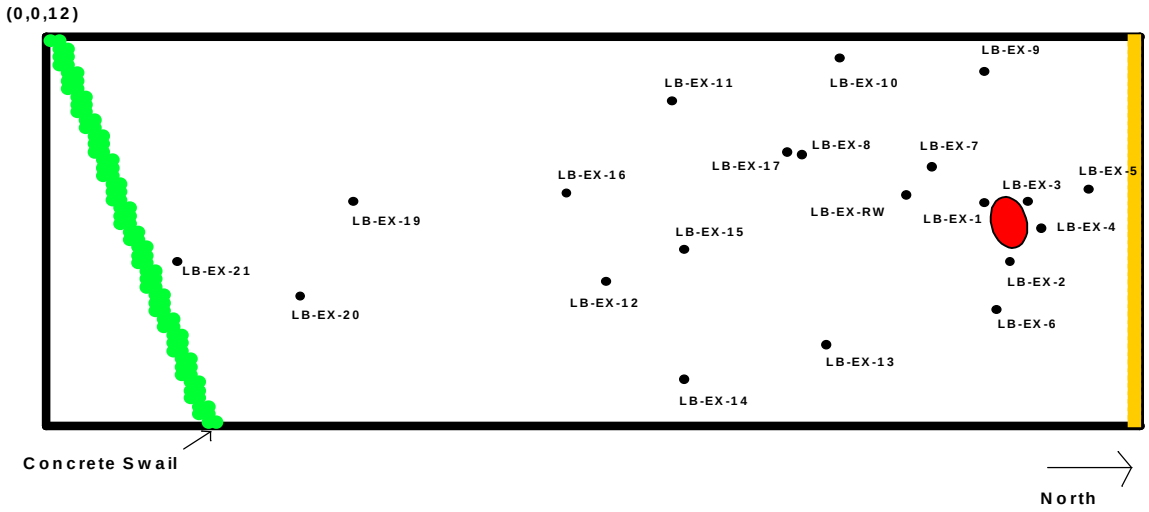

Figure 3.4 Location of monitoring wells within the model grid

The mean hydraulic conductivity at the site was 11.1 ft/day, or 3.387 meters/day (Landmeyer et al., 1996). This value was used as a starting point for the estimate of both hydraulic conductivity and transmissivity at the site. The initial transmissivity value used in the bottom three layers of the model was 7.52 m^2/day. K was later varied during calibration of the flow model.

MODFLOW accounts for vertical flow with the parameter VCONT, and it can be calculated in a number of ways depending on the type of layers through which the flow is being simulated. For Laurel Bay, the vertical flow was within a single hydrostratigraphic unit, the silty sand aquifer. The vertical conductance was found using the following equations:

$$VCONT = \frac{Kz_{i,j}}{\Delta z_{k+1/2}} \quad \text{and} \tag{3.7}$$

$$\Delta z_{k+1/2} = \frac{\Delta v_k}{2} + \frac{\Delta v_{k+1}}{2} \tag{3.8}$$

where

$Kz_{i,j}$ is the hydraulic conductivity in the vertical z direction;

Δv_k is the thickness of the upper layer; and

Δv_{k+1} is the thickness of the lower layer.

$Kz_{i,j}$ was not known and was estimated during calibration, which is the common practice (Anderson and Woessner, 1992). A value commonly used for the ratio of vertical to horizontal hydraulic conductivity is 0.01 with it ranging as high as 0.1. Since available cross sections of the contaminant plume showed that there was significant vertical migration of the plume, $Kz_{i,j}$ was estimated as 0.2 $Kx_{i,j}$. During calibration of the flow model, $Kz_{i,j}$ was varied. There was not a significant difference between the head levels when the ratio was 0.1 compared with 0.2.

Drain conductance is not a parameter that can be determined from field tests, so a conductance value for the drain simulating the concrete swail was estimated. Equation (3.9) was used to initially estimate the conductance of the drain. Conductance was varied as a method of calibration.

$$CD = \frac{Kz_{i,j}}{b} Lw \tag{3.9}$$

where

$Kz_{i,j}$ is the horizontal conductivity in the direction of flow;

b is the cell thickness;

L is the cell length; and

w is the cell width.

The recharge rate was variable within the model grid resulting from land surface variations influencing recharge. These included a sandy region of high permeability as well as a large amount of paved areas that allow for minimal recharge. For that reason, the model grid was divided up into 6 regions based on the various features. The initial estimate of recharge over the entire area was 20 inches with that value being used in the regions subjected to average recharge (Landmeyer et al., 1998). Figure 3.5 shows the model grid with the recharge areas labeled A through F. The red area of the grid indicates the inactive cells.

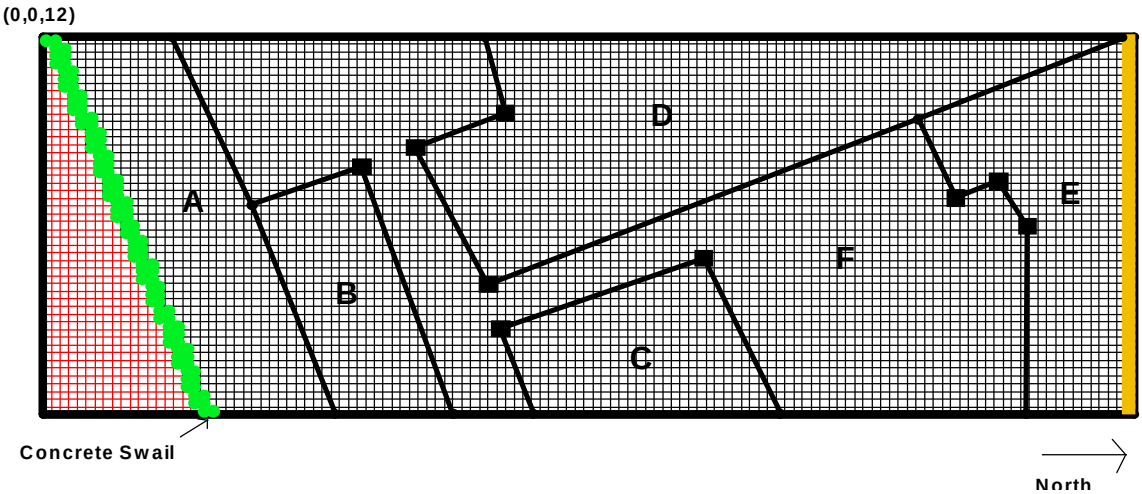

Figure 3.5 Recharge areas within the model grid

The initial recharge rate estimates for each area can be seen in Table 3.1. These values were varied during calibration of the flow model.

Area	Recharge Rate (inches/year)
A	10.0
B	20.0
C	20.0
D	45.0
E	20.0
F	10.0

Table 3.1 Initial recharge rates by areas defined in Figure 3.5

3.1.5 Model Calibration

When calibrating the groundwater model, the goal is to find a set of aquifer parameters, boundary conditions, and hydrologic stresses that result in hydraulic head and flow values similar to what are observed in the field (Anderson and Woessner, 1992). In this study, the hydraulic head levels from the model simulation were compared to the field measured values for twenty wells at the site.

Due to the shallow permeable nature of the water table aquifer being modeled, recharge events in the field can significantly impact the flow gradients and directions. Consequently, head levels were also used to calculate the hydraulic gradients and flow angles predicted by the model, and they were then compared with those that occurred in the field. Five triangles running along the entire length of the model were used to determine the gradients and flow directions. These

triangles were composed of wells LB-EX-19, LB-EX-20, and LB-EX-21; LB-EX-3, LB-EX-4, and LB-EX-5; LB-EX-14, LB-EX-16, and LB-EX-20; LB-EX-13, LB-EX-15, and LB-EX-7; and wells LB-EX-13, 15, and LB-EX-1. The hydraulic gradients, i, and flow directions, β, were calculated using the method by Widdowson (1999), and details on the calculations can be seen in Appendix A.

Calibration was achieved using a trial-and-error technique varying certain parameters, and it was quantified with error analysis. The parameters that were varied included Q_{well}, K, $Kz_{i,j}$, drain conductance, and recharge rates. Since the model was steady-state, the model simulated head values were compared with the field average head levels. It was assumed that the field maximum and minimum head levels were due to specific recharge events not simulated directly by the model. For each simulation, the mean error, mean absolute error, and root mean squared error were calculated. Once the simulation yielding the lowest errors was found, parameters were varied to assess the impact on flow gradients and directions. More details on the analysis of the gradient and flow direction error can be found in Appendix A. The parameters that resulted in the best match of gradients and flow directions without increasing the error with respect to the hydraulic head levels were selected. Sample groundwater flow model input is presented in Appendix D.

$Kx_{i,j}$ and $Kz_{i,j}$ were varied in an attempt to simulate the vertical migration of the plume observed in the field (Landmeyer et al., 1998). Cross-sections of the plume over time indicated vertical migration of the contamination to depths equivalent to layer 3 of the groundwater model (Landmeyer et al., 1998). Hydraulic conductivity was increased in layer 3 resulting in a flow pattern more similar to what was observed in the field. The increase also caused the gradient in some regions of the model to be lower than it was in the field. Consequently, the hydraulic conductivity within layer 3 was varied using higher $Kx_{i,j,}$ values in the lower gradient regions. The original estimate of $Kx_{i,j}$ was 3.38 meters per day based on site measurements, and during calibration, it was increased slightly to 3.51 meters per day. This value of $Kx_{i,j}$ was used in layers 1, 2, and 4 as well as in the areas of layer 3 where the steeper gradients were observed in the field. The value of $Kz_{i,j}$ was increased from 0.2 $Kx_{i,j}$ to 0.4 $Kx_{i,j}$ to increase the vertical flow of the contaminant plume. This change had an impact on the VCONT calculation made by MODFLOW simulating the flow between the layers.

Recharge rates were altered in each of the six regions. Changes in the recharge rates had a significant impact on the model head levels. Increasing recharge rates resulted in increasing head values. As the recharge rates were altered, the specified flux into the upgradient boundary

was varied as well since it was based on the recharge rate. The final values used in each region can be seen in Table 3.2.

Area	Recharge Rate (inches/year)
A	14.3
B	20.0
C	20.0
D	60.0
E	26.0
F	10.0

Table 3.2 Calibrated recharge rates by areas defined in Figure 3.5

The parameter subject to the greatest degree of uncertainty was the drain conductance. The initial estimate of conductance was 1.20 based on Equation (3.9). As the conductance of the drain was increased, it led to a decrease in the head values along the entire length of the site. During calibration, the conductance value was increased to 2.50.

3.1.6 Calibration Results

Model calibration yielded a groundwater flow model that produced heads, flow gradients and flow directions similar to those observed in the field. The model output head levels at each node in the grid. Sample output from the groundwater flow model can be seen in Appendix E. Figure 3.6 shows calibrated water table contours in the uppermost active model layer.

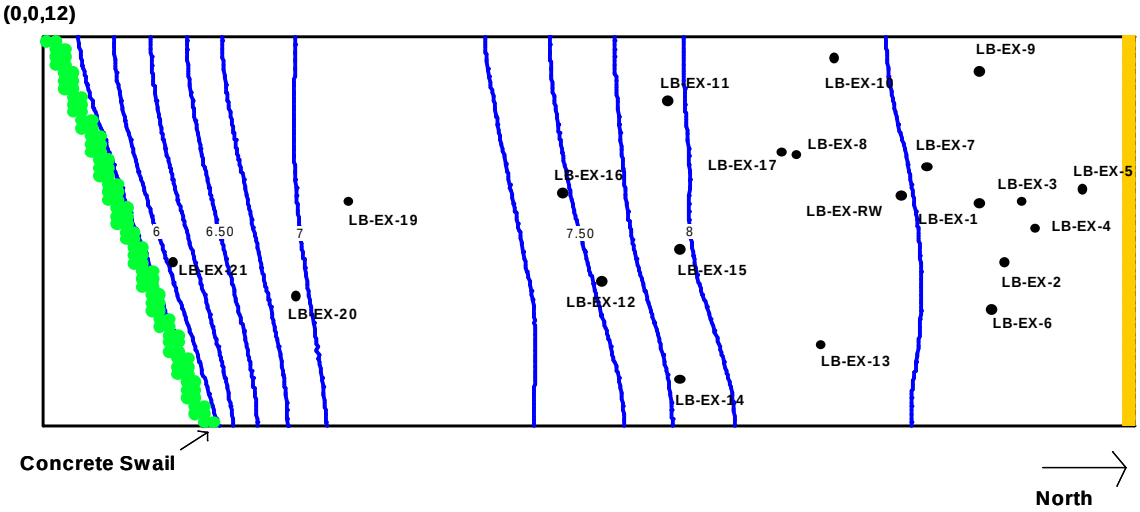

Figure 3.6 Model simulated water table contours

The results of the error analysis on the head levels are presented in Table 3.3 and Table 3.4. Table 3.3 shows the comparisons in heads at every well. For each well, the maximum, minimum, and average head measured between April 1993 and January 1998 is listed. The maximum and minimum heads are shown to exhibit the fluctuation of head levels in the shallow aquifer caused by recharge events at the site. It can be seen that head levels vary by up to a meter at some of the wells. The simulated head is h_s, and it is compared to the average head from the field for the error analysis. The residual represents the difference between the average head and h_s. The mean error, mean absolute error, and root mean squared error of the model can be seen in Table 3.4.

Well Number	Maximum Head (meters)	Minimum Head (meters)	Average Head h_m (meters)	h_s (meters)	Residual h_m-h_s (meters)
LB-EX-1	8.76	7.99	8.32	8.30	0.02
LB-EX-3	8.80	7.91	8.37	8.32	0.05
LB-EX-4	8.80	7.92	8.38	8.33	0.05
LB-EX-5	8.84	7.93	8.41	8.35	0.05
LB-EX-6	8.77	8.77	8.77	8.30	0.47
LB-EX-7	8.73	7.85	8.22	8.27	-0.04
LB-EX-8	8.59	7.73	8.17	8.17	-0.01
LB-EX-9	8.76	7.85	8.32	8.31	0.01
LB-EX-10	8.63	7.76	8.21	8.21	0.00
LB-EX-11	9.12	8.01	8.20	7.94	0.26
LB-EX-12	8.23	7.39	7.81	7.53	0.28
LB-EX-13	8.61	7.80	8.21	8.18	0.04
LB-EX-14	8.45	7.69	8.09	7.79	0.30
LB-EX-15	8.43	7.63	8.03	7.95	0.08
LB-EX-16	8.14	7.30	7.70	7.47	0.23
LB-EX-17	7.76	7.61	7.68	8.15	-0.47
LB-EX-19	7.38	6.89	7.07	7.07	0.01
LB-EX-20	7.18	6.73	6.92	6.92	0.00
LB-EX-21	6.27	5.60	5.94	6.02	-0.08
LB-EX-RW	8.73	7.84	8.21	8.24	-0.04

Table 3.3 Head level comparison showing maximum, minimum, and field average head, the model simulated head levels, and the residual used in the error calculations

Mean Error	Mean Absolute Error	Root Mean Squared Error
0.061	0.125	0.195

Table 3.4 Groundwater flow model error based on comparison of field average and model simulated head levels

Figures 3.7, 3.8, and 3.9 compare the simulated heads with the average, maximum, and minimum field measured values, respectively. The field measured head values fall along the x-axis with the simulated head values along the y-axis. Darker lines on the plots are the best-fit linear regression equation for the data points. Equations and R^2 values are shown on the plots. The other line represents a one-to-one correspondence between model simulated head levels and field measured head levels (y = x). Comparison of the model simulated heads with the average heads yielded the best fit with an R^2 value of 0.9139. Comparison with the maximum and minimum heads resulted in R^2 values of 0.8396 and 0.8643, respectively. These figures show that the model data best simulated the average head levels observed in the field. This would be expected since the recharge to the model domain was simulated as an average over time due to the steady-state nature of the model.

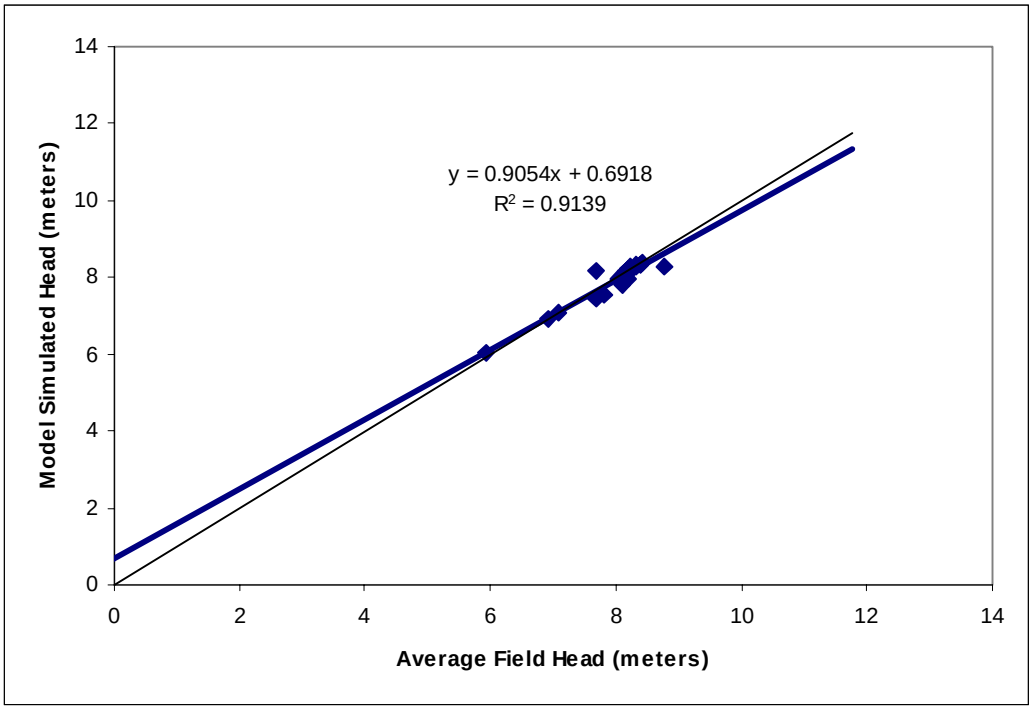

Figure 3.7 Model simulated heads versus field average heads

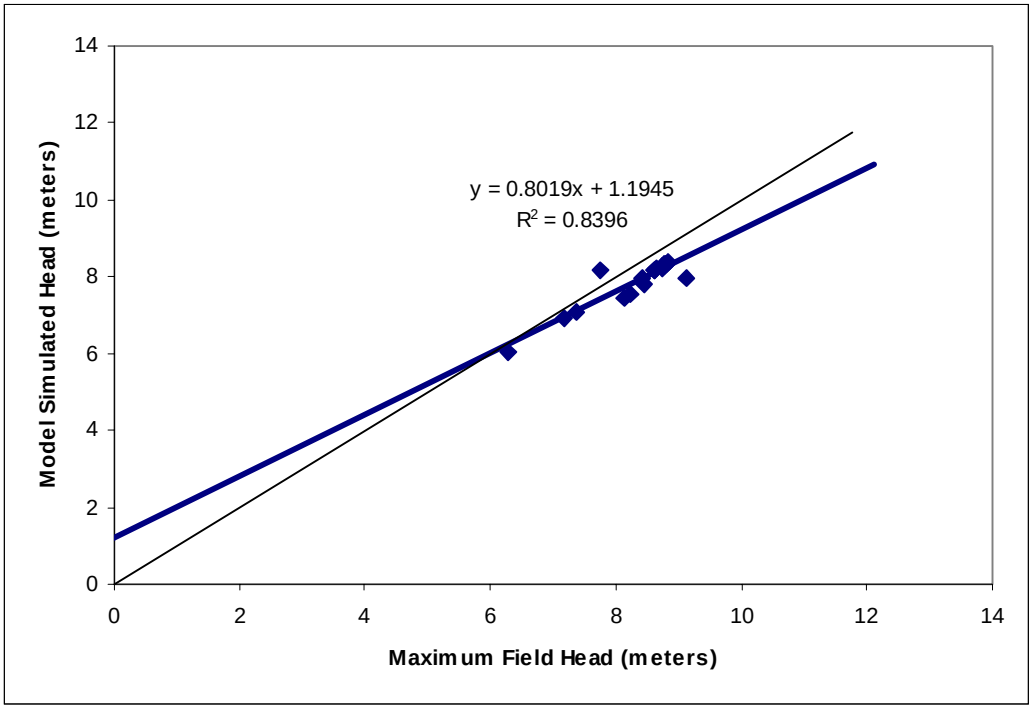

Figure 3.8 Model simulated heads versus field maximum heads

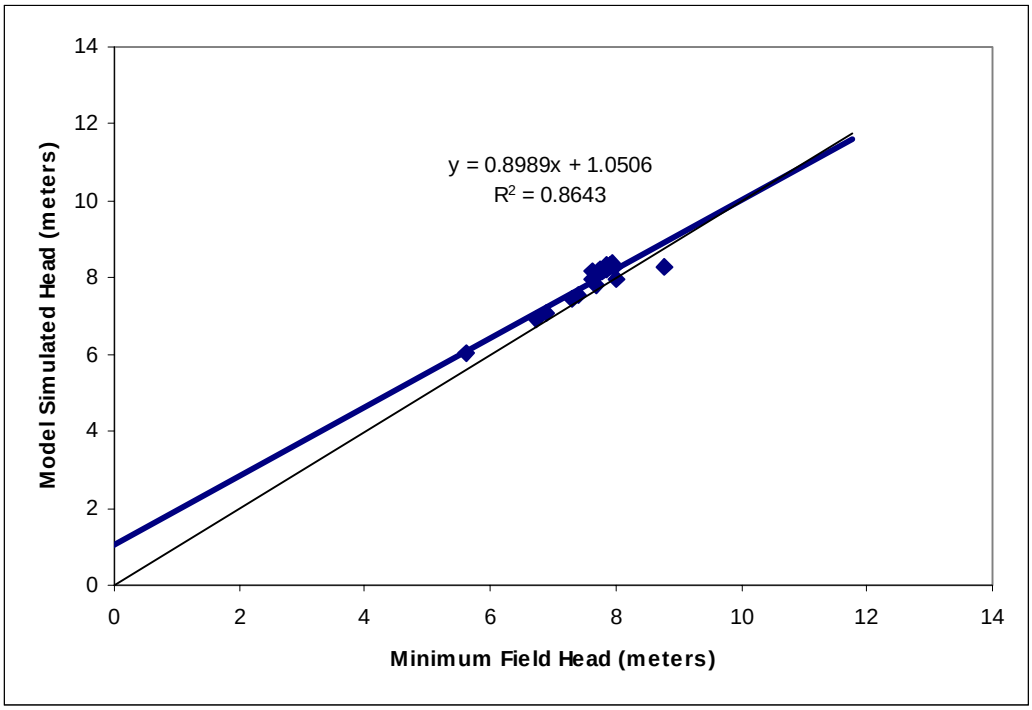

Figure 3.9 Model simulated heads versus field minimum heads

Results of the gradient and β calculations are presented in Table 3.5 and Table 3.6. The tables compare the gradient and flow directions based on the calibrated model simulation with those calculated based on the average measured heads, the maximum measured heads, and the minimum measured heads. All the flow directions are angles in degrees. Table 3.5 shows the gradients in the field varied slightly depending on whether the head levels were average, maximum, or minimum. The model gradient fell within the range seen in the field for triangle 2. For triangles 1 and 3, the model gradient fell just below the range seen in the field, and for triangles 4 and 5, it fell just above the field range. The model gradients most closely resemble the field average gradients followed by the field maximum and field minimum gradients. The root mean squared error for these was found to be 0.0022, 0.0026, and 0.0036, respectively.

From Table 3.6 it can be seen that the flow direction in the field varied significantly depending upon the head conditions showing factors such as recharge events can alter flow directions considerably. The model simulated flow direction was always within the range observed in the field. As with the gradient comparisons, the model simulated flow directions match most closely with the field average flow direction followed by the field maximum and field minimum flow directions. The root mean squared error for these values was found to be 8.9, 9.0 , and 15.0, respectively.

Triangle	Wells	Model Gradient	Field Average Gradient	Field Maximum Gradient	Field Minimum Gradient
1	19,20,21	0.03036	0.03327	0.03074	0.03812
2	3,4,5	0.00245	0.00292	0.00380	0.00189
3	14,16,20	0.00964	0.01310	0.01509	0.01059
4	13,15,7	0.00612	0.00454	0.00536	0.00436
5	13,15,1	0.00577	0.00468	0.00495	0.00519

Table 3.5 Hydraulic gradient comparison between model and field average, minimum, and maximum values for five areas in the model domain

Triangle	Wells	Model β	Field Average β	Field Maximum β	Field Minimum β
1	19,20,21	36.45	37.13	32.67	37.91
2	3,4,5	3.33	16.27	3.15	28.51
3	14,16,20	5.49	9.38	20.46	0.83
4	13,15,7	31.05	45.63	22.25	34.54
5	13,15,1	29.10	28.45	19.61	7.63

Table 3.6 Flow direction comparison between model and field average, minimum, and maximum for five areas in the model domain

3.2 Contaminant Transport Model

The next step in the research was conceptualization of the contaminant transport model and development of the mathematical model for solute transport and both aerobic and anaerobic biodegradation. Equations solved using SEAM3D to simulate contaminant transport, NAPL dissolution, substrate utilization and microbial growth are described in Appendix B (Waddill and Widdowson, 1998). Many of the model input parameters and details were based upon the work by Waddill and Widdowson (1997). The detail in this section is provided to ensure that all differences between the models is known.

3.2.1 Model Domain and Simulation Times

The groundwater flow model described in the Section 3.1 was coupled with the contaminant transport model. Consequently, the same model grid was used for each, and the hydraulic head output for the steady state groundwater model was used as the head condition for the transient contaminant transport simulation. Initial time for the running of the simulations was selected as December 15, 1990 which was when the tanks failed the test for tightness. Simulations ran to 836, 1170, 1992, 2206, 2387, and 2571 days to compare the model results with the field data measured in April 1993, March 1994, June 1996, January 1997, July 1997, and January 1998. The length of each transport time step was calculated by the model and was less than 1 day. One biodegradation time step was simulated for each transport step.

3.2.2 NAPL Constituents

The major contaminants of concern at the Laurel Bay site were the BTEX compounds, benzene, toluene, ethylbenzene, and xylene due to the regulatory concerns regarding their potential toxicity. Consequently, the BTEX compounds were treated individually to assess the natural attenuation potential of each. All of the aliphatic compounds were lumped together as one compound because they tend to have an inherently low solubility. MTBE, methyl-tertiary-butyl ether, was simulated as a tracer due to its very high solubility and the fact that it travels with the groundwater virtually unretarded. All other constituents not accounted for by specific model variables were assumed inconsequential.

Mass fractions of each of the components in the NAPL used in the model were within ranges specified by the literature. Table 3.7 shows the mass fractions of the various components that have been measured or used in simulations.

Component	Sigsby et al. (1987) No-lead Regular (g/g)	Sigsby et al. (1987) No-lead Premium (g/g)	Baehr and Corapcioglu (1987) (g/g)	Rixey et al. (1991) (g/g)	Parr et al. (1991) (g/g)	Rixey and Dorch (1992) (g/g)
Benzene	1.76	1.96	1.14	1.0	1.94	1.0
Toluene	5.54	20.25	6.07	7.0	4.73	5.0
Ethylbenzene	1.17	0.94	--	9.0*	2.0	10.0
Xylenes	7.04	4.21	--	--	9.65	--
Total aromatics	31.23	44.20	27.52	39.0	--	36.0
Total aliphatics	68.77	55.80	52.26	61.0	--	64.0
Heavy ends	--	--	20.21	--	--	--

*total of ethylbenzene and xylene

Table 3.7 Mass fractions of gasoline components

Mass fractions used in the model for benzene, toluene, ethylbenzene, xylene, and the aliphatic compounds are shown in Table 3.8, and they were initially selected based on an average of the values in Table 3.7. Mass fractions of the 'other aromatics' compound and MTBE were initially estimated as 0.10 and 0.03 respectively (Waddill and Widdowson, 1997). Based on the results of the initial simulations, the fractions were varied in an attempt to match up the model results with the concentrations observed in the field. Values used in the final simulation are presented in Table 3.9.

Component	Mass Fraction
MTBE	0.03
Benzene	0.01
Toluene	0.08
Ethylbenzene	0.05
Xylenes	0.12
Other aromatics	0.1
Aliphatics	0.55
Inerts	0.06

Table 3.8 Initial mass fractions in NAPL

Component	Mass Fraction
MTBE	0.005
Benzene	0.01
Toluene	0.085
Ethylbenzene	0.06
Xylenes	0.14
Other aromatics	0.109
Aliphatics	0.5
Inerts	0.089

Table 3.9 Mass fractions in NAPL for contaminant transport model

3.2.3 NAPL Mass Loading

Information contained in the1993 Contamination Assessment Report was used to determine what values to input into the NAPL package of SEAM3D (ABB Environmental Services, 1993). Two of the underground storage tanks failed a tightness test in December 1990. By November 1991, only one tank was still found to be leaking, so it was emptied and taken out of service with the remaining tanks removed in late 1993 along with the surrounding sediments. Based on that data, the estimated time for NAPL leakage into the subsurface is 330 days, and the time to excavation has been estimated at 1000 days. The approximate extent of the contaminant plume by 1993 was around 22 meters in diameter encompassing LB-EX-1 and LB-EX-7 (ABB Environmental Services, 1993).

Figure 3.10 shows the leak was simulated as beginning in eighteen cells in the region where the tanks were located, labeled with the number 1. Using the approach taken by Waddill and Widdowson (1997), the time scheduling for the mass loading was determined using both the estimated average velocity of the NAPL and the 2 meter by 2 meter size of the cells. The average contaminant velocity was found to be 0.032 m/day.

In all, there were thirteen different schedules of mass loading all beginning 62.5 days apart, and the cells corresponding to each schedule can be seen in Figure 3.10. An average NAPL velocity was used to determine that it would take the free product 62.5 days to travel through one of the cells in the model grid. Based on this estimate, it was possible to determine the starting time for NAPL loading in each of the cells. Mass loading in the cells labeled with a 2 began on day 62.5 with loading in the cells labeled with 3 beginning on day 125. This sequential process was continued until the edge of the NAPL contamination, the cells labeled with 13, was reached. The mass loading in these cells began on day 750. Each period of mass loading lasted 330 days corresponding to the time span when the tanks were leaking into the subsurface.

Model cells where the NAPL was originally located were assigned excavation times of 1000 days corresponding with the time in late 1993 when the remaining tanks and sediments were excavated. After this excavation time, NAPL was no longer simulated in those cells. In the remaining cells, the excavation time was set to a value larger than the total simulation time, so the only method of NAPL elimination in those grid cells was through dissolution.

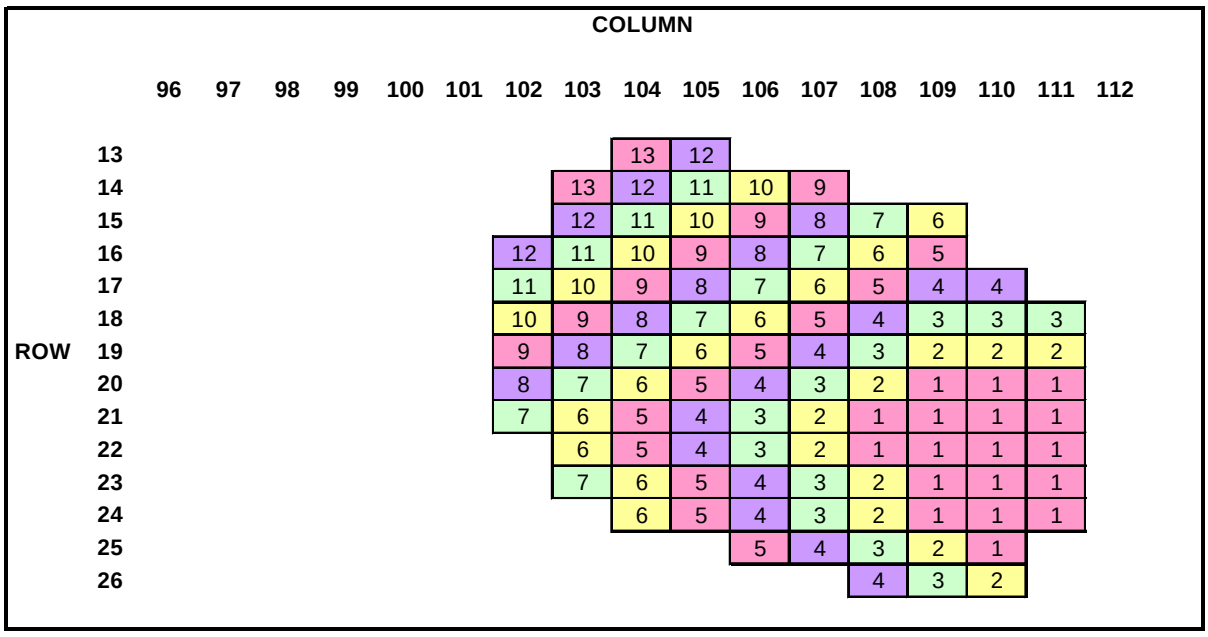

Figure 3.10 NAPL mass loading regions

Input parameters for the SEAM3D NAPL package include the soil bulk density, the density of the NAPL, and the porosity of the aquifer material, and they were used to determine the maximum and minimum NAPL concentrations possible in the soil (Waddill and Widdowson, 1997). The maximum concentration was found to be 0.035 g_{NAPL} per g_{soil} and the minimum concentration was found to be 0.00875 g_{NAPL} per g_{soil}. These concentrations were used to estimate the maximum amount of contaminant mass that could potentially enter each cell. An assumption was made that the contaminant concentrations decreased linearly as distance from the source increased. Based on that, the maximum possible masses calculated were 336 kg closest to the source area and 56 kg furthest from the source. Details on these calculations can be found in Appendix A.

The NAPL concentrations measured in the field were at least an order of magnitude less than those predicted based on the calculations described above and shown in Appendix A. To account for the difference, the values calculated for the model were decreased by a factor of $^1/_3$ to

better simulate what was observed in the field. Using these decreased mass values, the mass rate per day into each cell was found by dividing the total mass into the cell by the 330 day loading period.

Initial simulation runs indicated the need to alter the mass loading rates to more accurately depict the contaminant concentrations observed in the field. The original mass estimates for the cells in the source area were multiplied by a factor of ½ rather than the $^1/_3$ used previously. This value was decreased by 5 % for each subsequent loading region until region 10 was reached. In regions 10 through 13, the original mass estimate was multiplied by a factor of $^1/_{20}$. Less mass was used as the NAPL migrated further from the source area since there was more of an opportunity for mass loss or decreases in the plume velocity resulting from environmental conditions. The mass loading input parameters can be seen in Table 3.10.

NAPL Loading region	Start of mass loading (day)	End of mass loading (day)	Mass loading rate (grams/day)	Total NAPL mass added to block (grams)	Excavation (day)
1	0	330	509.1	168000	1000
2	62.5	392.5	305.5	100800	90000
3	125	455	271.5	89600	90000
4	187.5	517.5	178.2	58800	90000
5	250	580	152.7	50400	90000
6	312.5	642.5	127.3	42000	90000
7	375	705	67.9	22400	90000
8	437.5	767.5	50.9	16800	90000
9	500	830	33.9	11200	90000
10	562.5	892.5	8.5	2800	90000
11	625	955	8.5	2800	90000
12	687.5	1017.5	8.5	2800	90000
13	750	1080	8.5	2800	90000

Table 3.10 NAPL mass loading input parameters

3.2.4 Electron Acceptors

Based on the Landmeyer et al. (1996) report, the contaminant transport site model simulated aerobic biodegradation along with iron reduction, sulfate reduction, and methanogenesis. The initial concentrations of oxygen, sulfate, and solid phase Fe(III) were 5.0 g/m^3, 10.0 g/m^3 and 100µg/g, respectively, at all nodes in the interior of the grid, which were based on measurements taken at uncontaminated wells at the site (Landmeyer et al., 1996). Concentrations of oxygen and sulfate were specified using the SEAM3D source/sink mixing package at the upgradient flow boundary. Initial estimates for input concentrations were 5.0 g/m^3 for oxygen and 15.0 g/m^3 for sulfate in the top layer with the values decreasing by 1.0 g/m^3 in

each subsequent layer. The values in the top layer were based on the initial concentrations of each component in the recharge. Concentrations were decreased as depth increased to account for the fact that not all of the DO and SO_4 entering the aquifer in the recharge will filter down to the bottom of the aquifer. Utilization of the compounds and movement with the groundwater flow closer to the land surface will result in lower concentrations reaching the aquifer bottom. Concentrations of DO and sulfate in the recharge were 5.0 g/m^3 and 15.0 g/m^3, respectively. All other substrates, products, and MTBE were assigned initial concentrations of zero at all nodes and within the source/sink mixing package. Both dissolved oxygen and sulfate were also introduced into the system in recharge.

3.2.5 Transport Parameters

The longitudinal dispersivity (α_x) value used by Waddill and Widdowson (1997) was 8.0 meters. Since they did not vary K between layers, they needed to use a higher dispersion to better simulate vertical flow. An initial longitudinal dispersivity of 1.0 meter was used in this model of the Laurel Bay site due to the multiple model layers. The ratio of transverse horizontal to longitudinal dispersivity was chosen to be 0.10 and the ratio of transverse vertical to longitudinal was chosen to be 0.01. The effective molecular diffusion coefficient was 0.0001. When attempting to match the model simulations with the field data, the value for α_x was varied. The value used for α_x that led to the closest match with field data was 0.1 meters, and that is what was used in the final contaminant transport simulation. It has been suggested that longitudinal dispersivity can be estimated as about 0.1 of the flow length (Fetter, 1993). Since the flow length simulated by this model is less than 250 meters, a longitudinal dispersivity of 0.10 meters was a reasonable estimate.

The soil bulk density was chosen as 1.6×10^6 g/m^3, and this is typical of a sandy soil (Carsel and Parrish, 1988). When calculating the retardation factor for the various components, the linear adsorption isotherm was used. Retardation factors were found for all of the substrates and Fe(II). All of the electron acceptors, MTBE, H_2S, and CH_4 were all assumed to be completely in solution by Landmeyer et al. (1996), so they were subject to no retardation. Landmeyer et al. (1996) measured the distribution coefficient, k_D, for benzene and toluene, and the smallest of the values they measured, 0.057 cm^3/g, was used as the distribution coefficient for each substrate. The distribution coefficient for Fe(II) was selected as 0.328 cm^3/gram (Waddill and Widdowson, 1997). The k_D values were varied during calibration, but the initial values were found to yield the concentrations closest to those observed in the field in combination with the

other parameters. The final values used are presented in Table 3.11 along with their corresponding retardation factors.

Compound	Sorption Coefficient (m^3/gram)	Retardation Factor
MTBE	0	1.0
Benzene	5.76E-08	1.26
Toluene	5.76E-08	1.26
Ethylbenzene	5.76E-08	1.26
Xylenes	5.76E-08	1.26
Other Aromatics	5.76E-08	1.26
Aliphatics	5.76E-08	1.26
Ferrous Iron (Fe(II))	3.28E-07	2.5

Table 3.11 Sorption coefficients and retardation factors used in the contaminant transport model

3.2.6 Biodegradation Parameters

The parameters selected to model biodegradation in the model were based upon both laboratory measurements and values used in previous site models (Landmeyer et al., 1996; Waddill and Widdowson, 1997). Initial parameter estimations are presented in Table 3.12 and Table 3.13. These values were then altered, if necessary, during calibration of the transport model. Parameters used in the calibrated contaminant transport model are shown in Table 3.14 and Table 3.15. The parameters defined in Tables 3.12 and 3.14 are the substrate half saturation coefficient ($K^s_{x,ls,le}$), the electron acceptor half saturation coefficient ($K^e_{x,ls,le}$), the yield coefficient ($Y_{x,ls,le}$), the electron acceptor use coefficient ($\gamma_{x,ls.le}$), the inhibition coefficient ($\kappa_{le,li}$), the product generation terms ($\xi_{x,ls}$),the initial microbial biomass (M_x), and the effective death term (K_{dx}^{bk}). Tables 3.13 and 3.15 show the maximum specific rates of substrate utilization ($\nu^{max}_{x,ls,le}$).

EA	$K^s_{x,ls,le}$ (g/m^3)	$K^e_{x,le}$ (g/m^3)	$Y_{x,ls,le}$ (g/g)	$\gamma_{x,ls,le}$ (g/g)	$\kappa_{le,li}$ (g/m^3)	$\xi_{x,li}$ (g/g)	M_x (g/m^3)	k_{dx}^{bk} (day^{-1})
O_2	5.0	0.5	0.5	3.2	0.1	--	0.3	0.29
Fe(III)	5.0	--	0.2	42.0	10.0	0.2	0.01	0.0012
SO_4	5.0	0.5	0.2	4.5	0.5	0.8	0.01	0.0012
CH_4	5.0	--	0.0	--	--	0.8	0.35	0.0

Table 3.12 Initial biodegradation input parameters

Microcolony	EA	Benzene	Toluene	Ethylbenzene	Xylene	Other Aromatics	Aliphatics
		(day^{-1})	(day^{-1})	(day^{-1})	(day^{-1})	(day^{-1})	(day^{-1})
Aerobes	**O_2**	0.64	0.64	0.64	0.64	0.64	0.64
Iron reducers	**Fe(III)**	0.0009	0.009	0.009	0.009	0.009	0.0
Sulfate reducers	**SO_4**	0.0009	0.009	0.009	0.009	0.009	0.0
Methanogens	**CH_4**	0.0003	0.003	0.003	0.003	0.003	0.0

Table 3.13 Initial maximum specific rate of substrate utilization ($V^{max}_{x,ls,le}$) for each microbial population

EA	$K^s_{x,ls,le}$	$K^e_{x,le}$	$Y_{x,ls,le}$	$\gamma_{x,ls,le}$	$\kappa_{le,li}$	$\xi_{x,li}$	M_x	k_{dx}^{bk}
	(g/m^3)	(g/m^3)	(g/g)	(g/g)	(g/m^3)	(g/g)	(g/m^3)	(day^{-1})
O_2	5.0	0.5	0.5	3.2	2.5	--	0.3	0.386
Fe(III)	5.0	--	0.2	42.0	20	0.2	0.01	0.0012
SO_4	10.0	0.5	0.2	4.5	5.0	0.5	0.01	0.0008
CH_4	10.0	--	0.0	--	--	0.8	0.085	0.0

Table 3.14 Calibrated biodegradation input parameters

Microcolony	EA	Benzene	Toluene	Ethylbenzene	Xylene	Other Aromatics	Aliphatics
		(day^{-1})	(day^{-1})	(day^{-1})	(day^{-1})	(day^{-1})	(day^{-1})
Aerobes	**O_2**	0.85	0.85	0.85	0.85	0.85	0.85
Iron reducers	**Fe(III)**	0.0001	0.012	0.0001	0.012	0.012	0.0
Sulfate reducers	**SO_4**	0.0006	0.006	0.006	0.006	0.006	0.0
Methanogens	**CH_4**	0.0003	0.003	0.003	0.003	0.003	0.0

Table 3.15 Calibrated maximum specific rate of substrate utilization ($V^{max}_{x,ls,le}$) for each microbial population

3.3 SEAM3D Model Calibration

A significant amount of field measured data was available from the Laurel Bay site for model calibration. Concentrations of contaminants, electron acceptors, and end products were measured beginning no later than March 1994 and continued through 1997 (Landmeyer et al., 1996; and Landmeyer, personal communication). The model was first calibrated to the earliest possible data set from the field that included electron acceptor and end product data (1994).

An error analysis was performed as a part of the calibration process. The mean error, mean absolute error, and the root mean squared error were calculated for the BTEX compounds, the electron acceptors, and the end products. These calculations were made for all of the wells

within the model. The errors were also normalized by dividing the difference between the measured and simulated concentrations by the maximum concentration measured for that component at any time anywhere within the grid (Zheng and Bennett, 1995). Normalization was performed to account for the large concentration variations that existed between contaminants as well as among different wells for the same contaminant.

SEAM3D allows the user to look at output concentrations for all the hydrocarbons, tracers, the mobile electron acceptors and end products at any specified node within the model grid. Observation points were set up for the nodes corresponding to the 21 wells falling within the model grid with comparisons made at 8 wells along the transect. Wells LB-EX-3, LB-EX-1, LB-EX-RW, LB-EX-17, LB-EX-15, LB-EX-16, LB-EX-19, and LB-EX-21 were the wells along the transect, and they can be seen in Figure 3.11. For the wells that did not fall directly along the transect, the distance from the source area was determined based on the point where a perpendicular line from the well met the transect. Well LB-EX-17 falls the furthest from the centerline, 16.3 meters. Simulated concentrations of MTBE, each BTEX compound, aqueous electron acceptors, and aqueous end products were compared to field measured values.

Wells LB-EX-19 and LB-EX-21 were not installed until following the 1994 field sampling, so comparisons for those two wells were not made in that year. No data was available on the electron acceptors and end products at well LB-EX-17 for comparison at any of the dates. Also, concentrations of sulfate and methane were only measured at LB-EX-3, LB-EX-1, and LB-EX-RW in 1996. There were no MTBE concentrations available in January 1997 or July 1997 at any of the wells. In July 1997, no sampling occurred at LB-EX-3 for any of the components, and no concentration data was available for sulfate and methane. Since all the wells except LB-EX-17 were screened through portions of the top two layers, the model produced concentration data was found by averaging the concentrations for layers 1 and 2. Well LB-EX-17 is the deep well with the screen running through the bottom layer, so the concentrations found in layer 4 were used as a comparison.

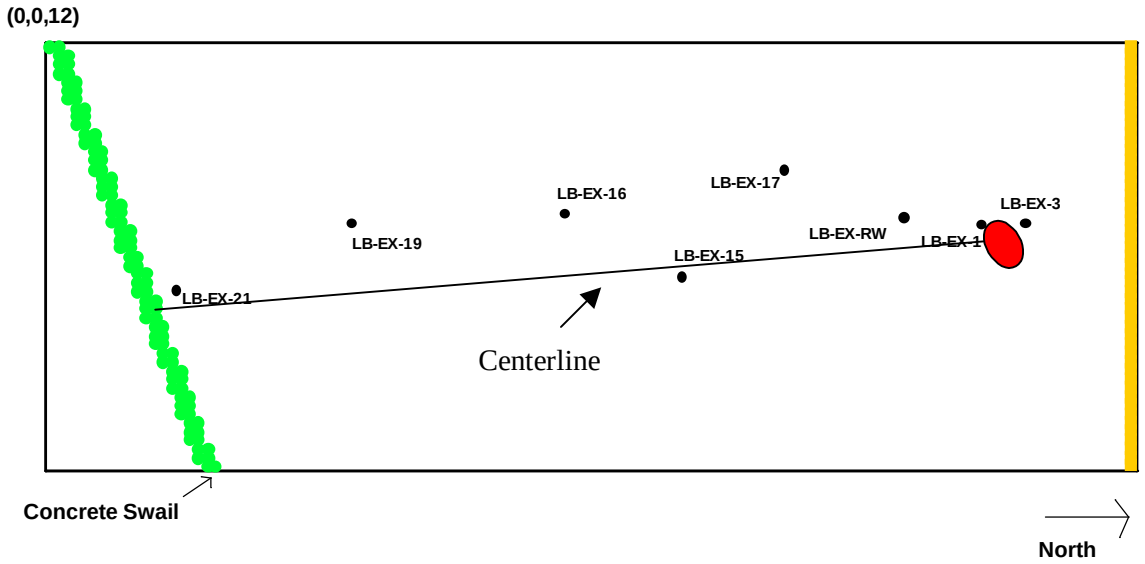

Figure 3.11 Wells falling along the plume transect

The model was calibrated by adjusting input parameters using a trial and error approach. The goal was to minimize the error while best matching up concentrations along the plume transect. Once a simulation was found that resulted in lowest root mean squared error, the concentrations along the transect were then compared. It was found that slight changes to most of the parameters did not alter the root mean squared error. Input parameters varied included contaminant mass fractions in the NAPL, rates and region of NAPL mass loading, concentration of electron acceptors in the recharge water, longitudinal dispersivity, substrate half saturation constants, maximum specific rates of substrate utilization, generation coefficients, initial microbial biomass concentrations, and inhibition coefficients. Sample contaminant transport model input is presented in Appendix F.

3.4 Model Verification

Since it was possible that the parameter values used in the calibrated model did not accurately represent field values or a non-unique solution was determined, model verification was performed. The goal of verification was to determine if the calibrated parameters accurately depicted plume conditions and concentrations at another time. Field data for verification was available for June 1996, and January and July 1997, so concentrations of the hydrocarbons and geochemical indicators were compared at the wells along the plume transect for all three dates.

Error analysis was performed using the January 1997 data since it was the most comprehensive data set from the field after 1994. The root mean squared error for the BTEX compounds in 1997 was compared with the error from 1994.

4.0 Results and Discussion

4.1 Error Analysis

Tables 4.1 through 4.4 present error results for transport model calibration (1994 data) for benzene, toluene, ethylbenzene, and xylene, respectively. Tables 4.5 through 4.8 present error analysis results for transport model verification (January 1997 data) for each of the BTEX compounds, respectively. The contaminant concentrations were taken from the SEAM3D output data file. Sample model output is presented in Appendix G. All of the concentrations are in μg/L, and the 'NS' in the measured concentration column indicates no sampling of the compound occurred at that well. Wells that were not sampled were not included in the error analysis. From the tables, it can be seen that the model simulates the plume location as well as the concentrations relatively well. In 1994, the model simulates contaminant concentrations of zero at wells LB-EX-4, LB-EX-5, LB-EX-10, LB-EX-11, LB-EX-13, and LB-EX-14. Contamination was not detected at these wells in the field either. In 1997, low levels of contamination were measured at wells LB-EX-13 and LB-EX-14 in the field, while the model simulated concentrations of zero. The best matches are at wells LB-EX-1, LB-EX-7, and LB-EX-RW in 1994. These were the wells of highest contamination indicating the model is able to simulate the travel path of the plume center. In general for the wells containing contamination, the model simulates concentrations of the same magnitude as what was observed in the field in both 1994 and January 1997.

Table 4.9 shows the mean error, mean absolute error, root mean squared error, and the normalized root mean squared error. As was discussed in Section 3.3, the root mean squared error was normalized by dividing the residual by the maximum concentration of the compound measured at the site (Zheng and Bennett, 1995). The benzene residuals were normalized using 16,000 μg/L, toluene with 43,000 μg/L, ethylbenzene with 4895 μg/L, and xylene with 23,000 μg/L. For each compound aside from ethylbenzene, those maximum concentrations were measured in 1993, with that for ethylbenzene measured in 1994. The errors for each of the BTEX compounds decrease between 1994 and 1997 indicating the model is more accurately predicting contaminant concentrations over time. The root mean squared error for benzene decreases from 2561 to 1115, from 6061 to 5004 for toluene, from 1541 to 1414 for ethylbenzene, and from 5078 to 3750 for xylene.

Tables 4.1 through 4.8 show that both the model simulated and field measured concentrations vary significantly, ranging from zero up to several thousand μg/L. That could cause the mean error, mean absolute error, and root mean squared error values seen in Table 4.9

to be significantly impacted by a single highly contaminated well. When comparing the errors between the compounds, the normalized root mean squared error is used since toluene and xylene represent higher mass fractions in the NAPL and thus higher concentrations than benzene and ethylbenzene. Table 4.9 shows that toluene has the lowest normalized root mean squared error in 1994 at 0.14 followed by benzene (0.16), xylene (0.22), and ethylbenzene (0.31). In 1997, benzene has the lowest normalized root mean squared error at 0.07 followed by toluene (0.12), xylene (0.16), and ethylbenzene (0.29).

Well	Measured Concentration C_m	Simulated Concentration C_s	Residual C_m-C_s	Normalized Residual
LB-EX-1	8450	11321	-2871	-0.179
LB-EX-2	NS	33.7	--	--
LB-EX-3	6.1	4.7	1.4	0.000
LB-EX-4	0	0.0	0.0	0.000
LB-EX-5	0	0.0	0.0	0.000
LB-EX-6	NS	0.0	--	--
LB-EX-7	9450	10898	-1448	-0.090
LB-EX-8	9180	0.3	9180	0.574
LB-EX-9	36.6	0.0	36.6	0.002
LB-EX-10	0	0.0	0.0	0.000
LB-EX-11	0	0.0	0.0	0.000
LB-EX-12	0	47.4	-47.4	-0.003
LB-EX-13	0	0.0	0.0	0.000
LB-EX-14	0	0.0	0.0	0.000
LB-EX-15	6.7	157	-150	-0.009
LB-EX-16	6.5	2.4	4.1	0.000
LB-EX-17	NS	1.0	--	--
LB-EX-19	NS	0.1	--	--
LB-EX-20	NS	10.7	--	--
LB-EX-21	NS	26.2	--	--
LB-EX-RW	8650	6725	1925	0.120

Table 4.1 1994 benzene concentrations for error analysis

Well	Measured Concentration C_m	Simulated Concentration C_s	Residual C_m-C_s	Normalized Residual
LB-EX-1	20600	21943	-1343	-0.031
LB-EX-2	NS	103	--	--
LB-EX-3	22.2	11.6	10.6	0.000
LB-EX-4	0	0.0	0.0	0.000
LB-EX-5	0	0.0	0.0	0.000
LB-EX-6	NS	0.0	--	--
LB-EX-7	22300	28353	-6053	-0.141
LB-EX-8	22500	1.0	22499	0.523
LB-EX-9	132	0.0	132	0.003
LB-EX-10	0	0.0	0.0	0.000
LB-EX-11	0	0.0	0.0	0.000
LB-EX-12	0	93.5	-93.5	-0.002
LB-EX-13	0	0.0	0.0	0.000
LB-EX-14	0	0.0	0.0	0.000
LB-EX-15	6.1	304.0	-298	-0.007
LB-EX-16	0	6.0	-6.0	0.000
LB-EX-17	NS	2.7	--	--
LB-EX-19	NS	0.3	--	--
LB-EX-20	NS	21.5	--	--
LB-EX-21	NS	55.4	--	--
LB-EX-RW	16100	13591	2509	0.058

Table 4.2 1994 toluene concentrations for error analysis

Well	Measured Concentration C_m	Simulated Concentration C_s	Residual C_m-C_s	Normalized Residual
LB-EX-1	0	3866	-3866	-0.790
LB-EX-2	NS	19.2	--	--
LB-EX-3	0	2.0	-2.0	0.000
LB-EX-4	0	0.0	0.0	0.000
LB-EX-5	0	0.0	0.0	0.000
LB-EX-6	NS	0.0	--	--
LB-EX-7	3100	6018	-2918	-0.596
LB-EX-8	2400	0.3	2400	0.490
LB-EX-9	11.8	0.0	11.8	0.002
LB-EX-10	0	0.0	0.0	0.000
LB-EX-11	0	0.0	0.0	0.000
LB-EX-12	0	16.2	-16.2	-0.003
LB-EX-13	0	0.0	0.0	0.000
LB-EX-14	0	0.0	0.0	0.000
LB-EX-15	5.9	53.3	-47.4	-0.010
LB-EX-16	0	1.2	-1.2	0.000
LB-EX-17	NS	0.6	--	--
LB-EX-19	NS	0.1	--	--
LB-EX-20	NS	3.8	--	--
LB-EX-21	NS	9.9	--	--
LB-EX-RW	0	2531	-2531	-0.517

Table 4.3 1994 ethylbenzene concentrations for error analysis

Well	Measured Concentration C_m	Simulated Concentration C_s	Residual C_m-C_s	Normalized Residual
LB-EX-1	13850	11114	2736	0.119
LB-EX-2	NS	57.4	--	--
LB-EX-3	258	6.0	252	0.011
LB-EX-4	0	0.0	0.0	0.000
LB-EX-5	0	0.0	0.0	0.000
LB-EX-6	NS	0.0	--	--
LB-EX-7	15100	17115	-2015	-0.088
LB-EX-8	19350	0.8	19349	0.841
LB-EX-9	60.7	0.0	60.7	0.003
LB-EX-10	0	0.0	0.0	0.000
LB-EX-11	0	0.0	0.0	0.000
LB-EX-12	0	47.3	-47.3	-0.002
LB-EX-13	0	0.0	0.0	0.000
LB-EX-14	0	0.0	0.0	0.000
LB-EX-15	11.4	153	-142	-0.006
LB-EX-16	0	3.6	-3.6	0.000
LB-EX-17	NS	1.7	--	--
LB-EX-19	NS	0.2	--	--
LB-EX-20	NS	11.0	--	--
LB-EX-21	NS	29.1	--	--
LB-EX-RW	7900	7020	880	0.038

Table 4.4 1994 xylene concentrations for error analysis

Well	Measured Concentration C_m	Simulated Concentration C_s	Residual C_m-C_s	Normalized Residual
LB-EX-1	1830	1718	112	0.007
LB-EX-2	NS	15.5	--	--
LB-EX-3	0	0.0	0.0	0.000
LB-EX-4	0	0.0	0.0	0.000
LB-EX-5	0	0.0	0.0	0.000
LB-EX-6	NS	0.0	--	--
LB-EX-7	1470	5202	-3732	-0.233
LB-EX-8	945	40.8	904	0.057
LB-EX-9	0	0.0	0.0	0.000
LB-EX-10	0	0.0	0.0	0.000
LB-EX-11	NS	0.0	--	--
LB-EX-12	0	549	-549	-0.034
LB-EX-13	240	0.0	240	0.015
LB-EX-14	0	0.0	0.0	0.000
LB-EX-15	150	1533	-1383	-0.086
LB-EX-16	101	44.6	56.4	0.004
LB-EX-17	67	10.8	56.2	0.004
LB-EX-19	0	2.3	-2.3	0.000
LB-EX-20	0	104	-104	-0.006
LB-EX-21	2360	329	2031	0.127
LB-EX-RW	6210	5118	1092	0.068

Table 4.5 1997 benzene concentrations for error analysis

Well	Measured Concentration C_m	Simulated Concentration C_s	Residual C_m-C_s	Normalized Residual
LB-EX-1	14100	5068	9032	0.210
LB-EX-2	NS	84.8	--	--
LB-EX-3	0	0.1	-0.1	0.000
LB-EX-4	0	0.0	0.0	0.000
LB-EX-5	0	0.0	0.0	0.000
LB-EX-6	NS	0.0	--	--
LB-EX-7	4030	22091	-18061	-0.420
LB-EX-8	309	185	124	0.003
LB-EX-9	0	0.0	0.0	0.000
LB-EX-10	0	0.0	0.0	0.000
LB-EX-11	NS	0.0	--	--
LB-EX-12	8	986	-978	-0.023
LB-EX-13	330	0.0	330	0.008
LB-EX-14	30	0.0	30.0	0.001
LB-EX-15	0	2670	-2670	-0.062
LB-EX-16	54	112	-58.1	-0.001
LB-EX-17	120	31.9	88.1	0.002
LB-EX-19	7	5.5	1.5	0.000
LB-EX-20	0	187	-187	-0.004
LB-EX-21	860	659	201	0.005
LB-EX-RW	7650	13542	-5892	-0.137

Table 4.6 1997 toluene concentrations for error analysis

Well	Measured Concentration C_m	Simulated Concentration C_s	Residual C_m-C_s	Normalized Residual
LB-EX-1	1900	950	950	0.194
LB-EX-2	NS	19.4	--	--
LB-EX-3	0	0.0	0.0	0.000
LB-EX-4	0	0.0	0.0	0.000
LB-EX-5	0	0.0	0.0	0.000
LB-EX-6	NS	0.0	--	--
LB-EX-7	710	5667	-4957	-1.013
LB-EX-8	1550	79.4	1471	0.300
LB-EX-9	0	0.0	0.0	0.000
LB-EX-10	0	0.0	0.0	0.000
LB-EX-11	NS	0.0	--	--
LB-EX-12	0	185	-185	-0.038
LB-EX-13	350	0.0	350	0.072
LB-EX-14	8	0.0	8.0	0.002
LB-EX-15	0	517	-517	-0.106
LB-EX-16	17	26.5	-9.5	-0.002
LB-EX-17	10	9.7	0.3	0.000
LB-EX-19	0	1.3	-1.3	0.000
LB-EX-20	0	35.9	-35.9	-0.007
LB-EX-21	780	137	643	0.131
LB-EX-RW	5320	2584	2736	0.559

Table 4.7 1997 ethylbenzene concentrations for error analysis

Well	Measured Concentration C_m	Simulated Concentration C_s	Residual C_m-C_s	Normalized Residual
LB-EX-1	5750	2855	2895	0.126
LB-EX-2	NS	55.3	--	--
LB-EX-3	12	0.0	12.0	0.001
LB-EX-4	0	0.0	0.0	0.000
LB-EX-5	0	0.0	0.0	0.000
LB-EX-6	NS	0.0	--	--
LB-EX-7	2000	15982	-13982	-0.608
LB-EX-8	2200	186	2014	0.088
LB-EX-9	0	0.0	0.0	0.000
LB-EX-10	0	0.0	0.0	0.000
LB-EX-11	NS	0.0	--	--
LB-EX-12	0	473	-473	-0.021
LB-EX-13	510	0.0	510	0.022
LB-EX-14	26	0.0	26.0	0.001
LB-EX-15	0	1269	-1269	-0.055
LB-EX-16	63	67.7	-4.7	0.000
LB-EX-17	46	22.5	23.5	0.001
LB-EX-19	0	3.1	-3.1	0.000
LB-EX-20	0	89.5	-89.5	-0.004
LB-EX-21	670	339	331	0.014
LB-EX-RW	6800	7652	-852	-0.037

Table 4.8 1997 xylene concentrations for error analysis

Compound	Mean Error	Mean Absolute Error	Root Mean Squared Error	Normalized Root Mean Squared Error
Benzene-94	442	1044	2560	0.16
Benzene-97	-71.1	570	1115	0.07
Toluene-94	1157	2196	6061	0.14
Toluene-97	-1002	2092	5004	0.12
Ethylbenzene-94	-465	786	1541	0.31
Ethylbenzene-97	25.1	659	1414	0.29
Xylene-94	1405	1699	5078	0.22
Xylene-97	-724	1499	3749	0.16

Table 4.9 Results of error analysis

4.2 Plume Transect

Simulated and measured concentrations of benzene, toluene, ethylbenzene, and xylene are plotted in Figures 4.1 through 4.4, respectively. Each figure shows concentrations in March 1994, June 1996, January 1997, and July 1997. The solid line represents the model-simulated concentrations, and the symbols are the concentrations that were measured in the field.

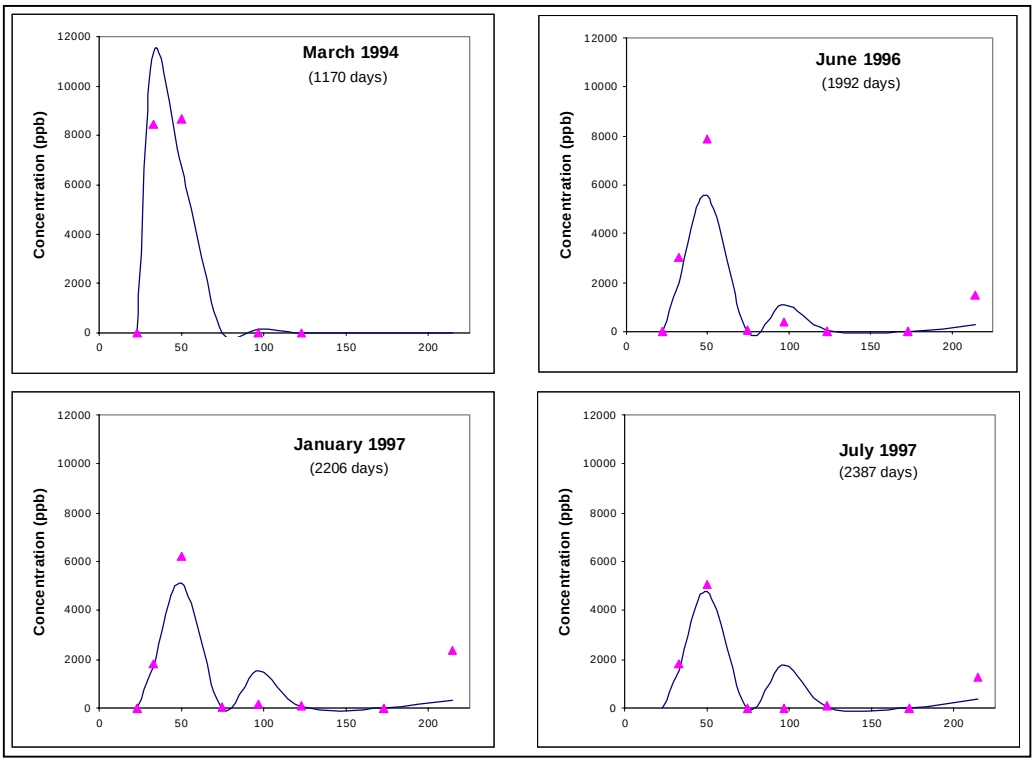

Figure 4.1 Benzene concentrations along the transect

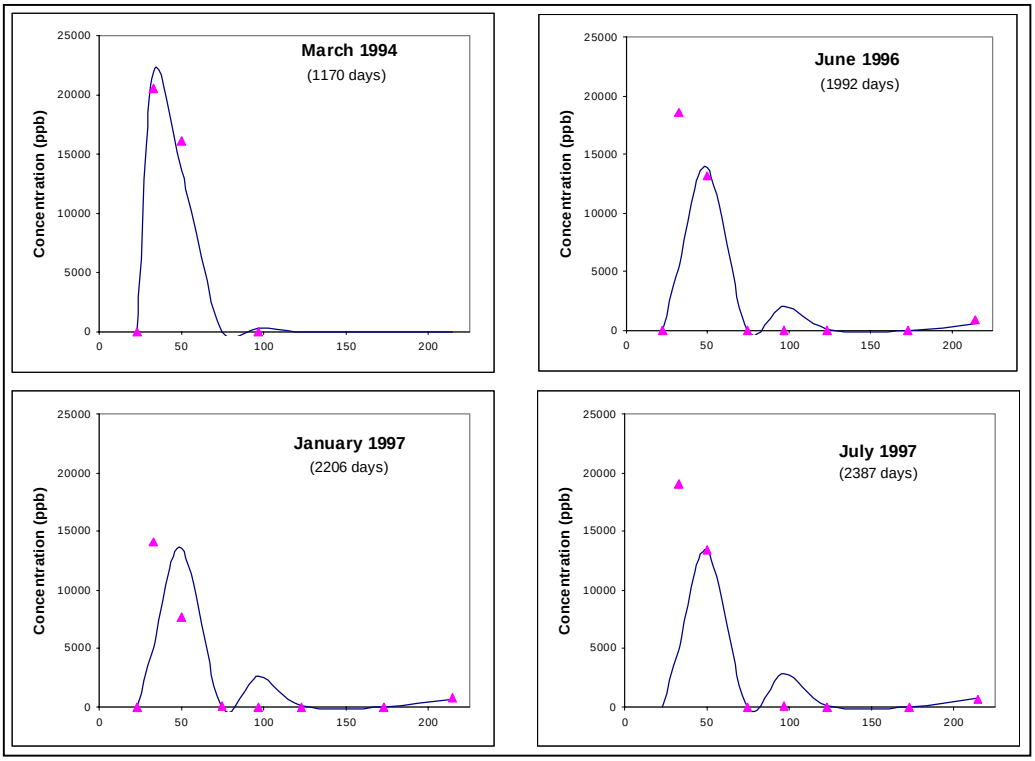

Figure 4.2 Toluene concentrations along the transect

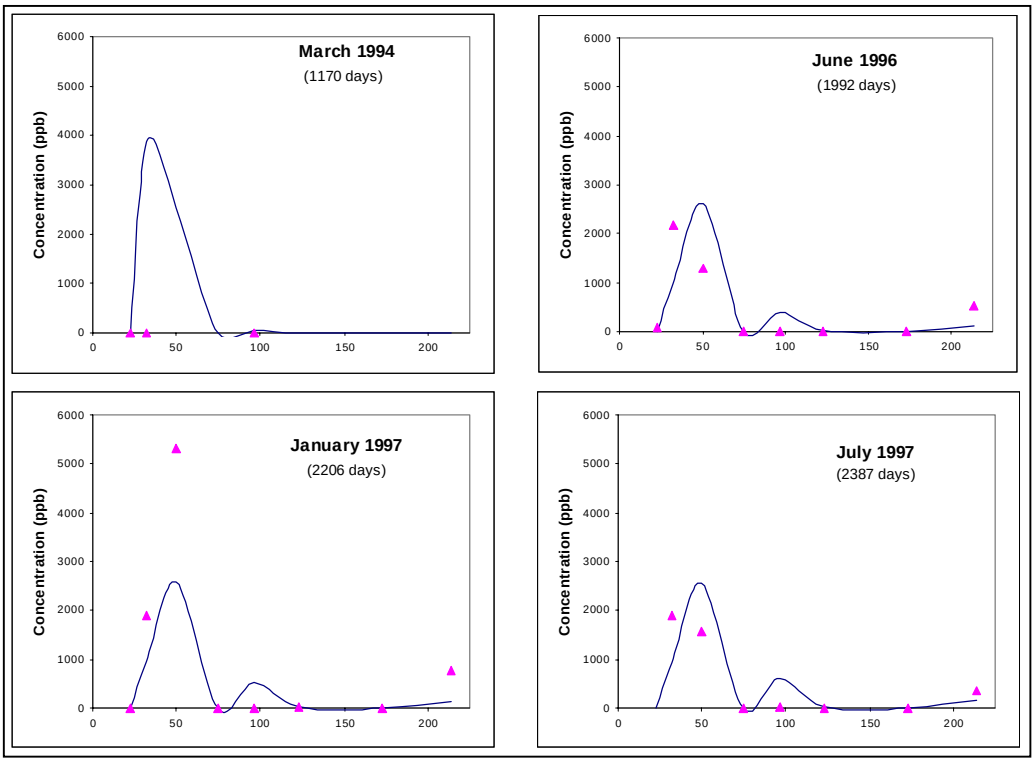

Figure 4.3 Ethylbenzene concentrations along the transect

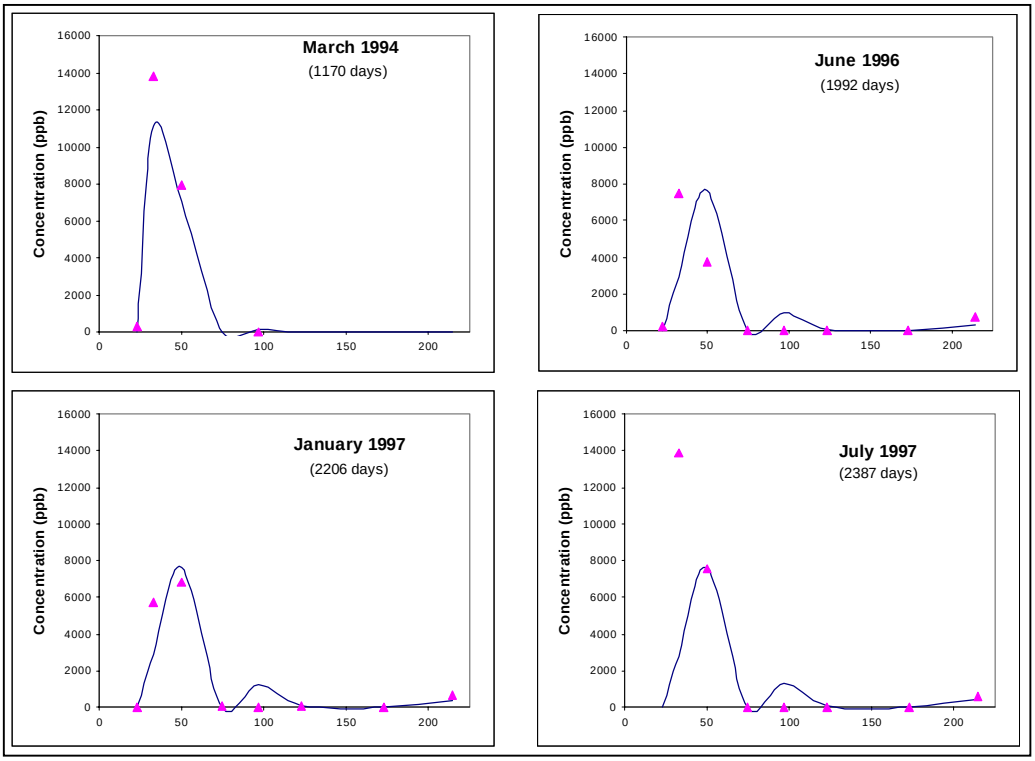

Figure 4.4 Xylene concentrations along the transect

The model results shown in Figures 4.1 through 4.4 indicate BTEX concentrations peaking right around the source area in 1994 indicating that the center of the plume had not traveled far since the release date 4 years earlier. The same trend is seen in the field data as well. Prior to the excavation of the source, that area remained the region of highest concentrations. In late 1993, the heavily contaminated sediment in the source area was removed, and the center of the plume began to travel downgradient. Due to a low contaminant transport velocity, it would not be expected that the center of the plume would have traveled a significant distance between the time of the source excavation and the 1994 sampling event less than 6 months later. Both the model and field data show higher concentrations at well LB-EX-21 than at wells between the swail and the source (Figures 4.1 through 4.4). It has been reported by Landmeyer et al. (1998) that recharge events at the site caused the plume to move deeper into the aquifer, and the model simulates this same trend. The plume begins to move towards the ground surface as it approaches the swail.

Figure 4.1 shows the benzene concentrations along the transect. The field data shows significant concentrations at wells LB-EX-1 and LB-EX-RW. The locations of the concentration peaks are simulated accurately by the model for each date, and they all appear to be around LB-EX-RW. The model underpredicts the peak concentrations in June 1996 and January 1997, but the field-measured concentration at LB-EX-RW falls right along the model-simulated curve in July 1997. Both the model and field data indicate decreasing maximum concentrations over time. This would be expected due to the potential for biodegradation of the contaminant as well as NAPL depletion.

Figures 4.1 and 4.3 show that the model underpredicts benzene and ethylbenzene concentrations at well LB-EX-21 over time. Possible causes of this could be overestimation of the sorption coefficient, which, as has already been discussed, does not significantly impact the model results or that the model did not accurately predict the plume travel direction. The sorption coefficient used in the model was the lowest value in the ranges found in the laboratory by Landmeyer et al. (1996) for benzene and toluene. It is also possible that the biodegradation rate for these compounds is overestimated. Figures 4.2 and 4.4 show that the model more accurately predicts the concentrations seen in the field at LB-EX-21 over time for toluene and xylene. In each of the figures (4.1 through 4.4), the model does exhibit the contaminant plume rising near the swail as was observed in the field (Landmeyer et al., 1998).

One other significant difference seen in Figures 4.1 through 4.4 is that simulated concentrations at well LB-EX-15 are much larger than the field concentrations for each of the BTEX compounds. Evidence from the site suggests a shift in the direction of the plume in the

area of well LB-EX-15. Since a steady-state flow model is being used, a shift over time can not be simulated. If there are relatively steep concentration gradients present along the plume edges and the direction of the contaminant flow is slightly off, there can be a significant difference between the model and field concentrations.

Figure 4.5 shows the MTBE concentrations along the transect. In 1994, the model simulated peak concentration is well below the peak seen in the field, but it is about the same distance downgradient from the source. The field and model data do not match up well for MTBE in 1996. During calibration, the initial mass fraction of MTBE was decreased because the model was simulating concentrations of MTBE significantly larger than any observed in the field. The field data shows that the MTBE is moving relatively quickly through the system as concentrations near the swail nearly equal those near the source in June 1996. The 1996 data shows that the model is simulating concentration increases in the same areas where they are observed in the field, near the source, near LB-EX-15, and near LB-EX-21. The increases near the source and the swail are not as significant in the model as the field, and that could have resulted from underestimating the initial mass fraction of MTBE in the NAPL plume.

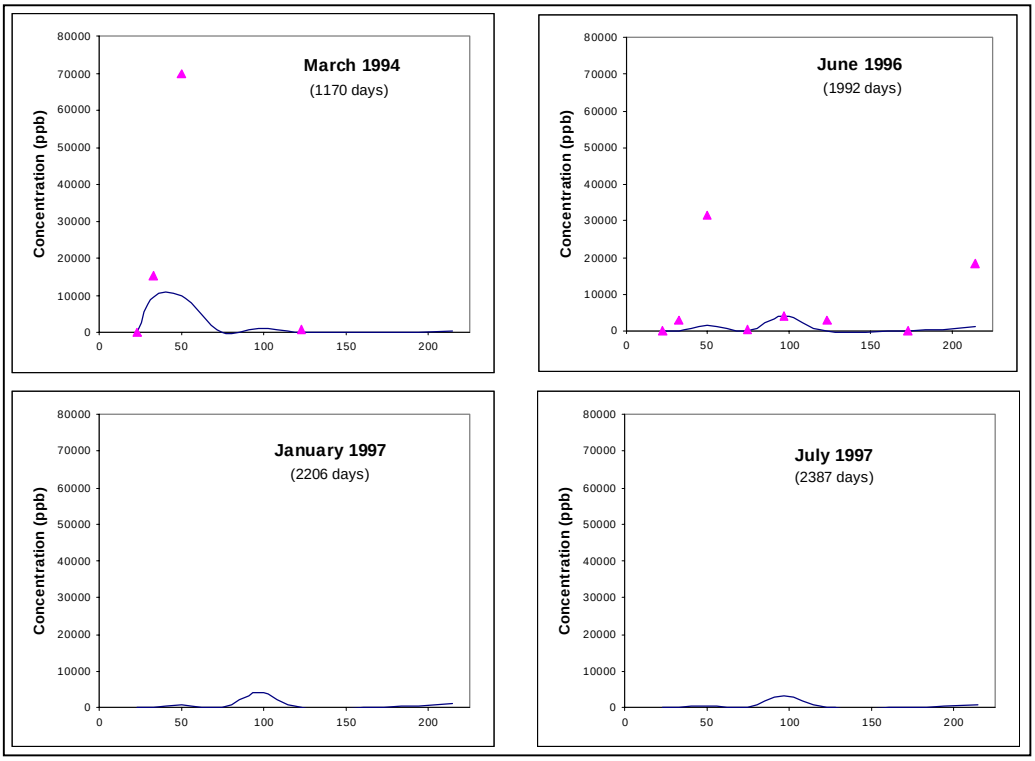

Figure 4.5 MTBE concentrations along the transect

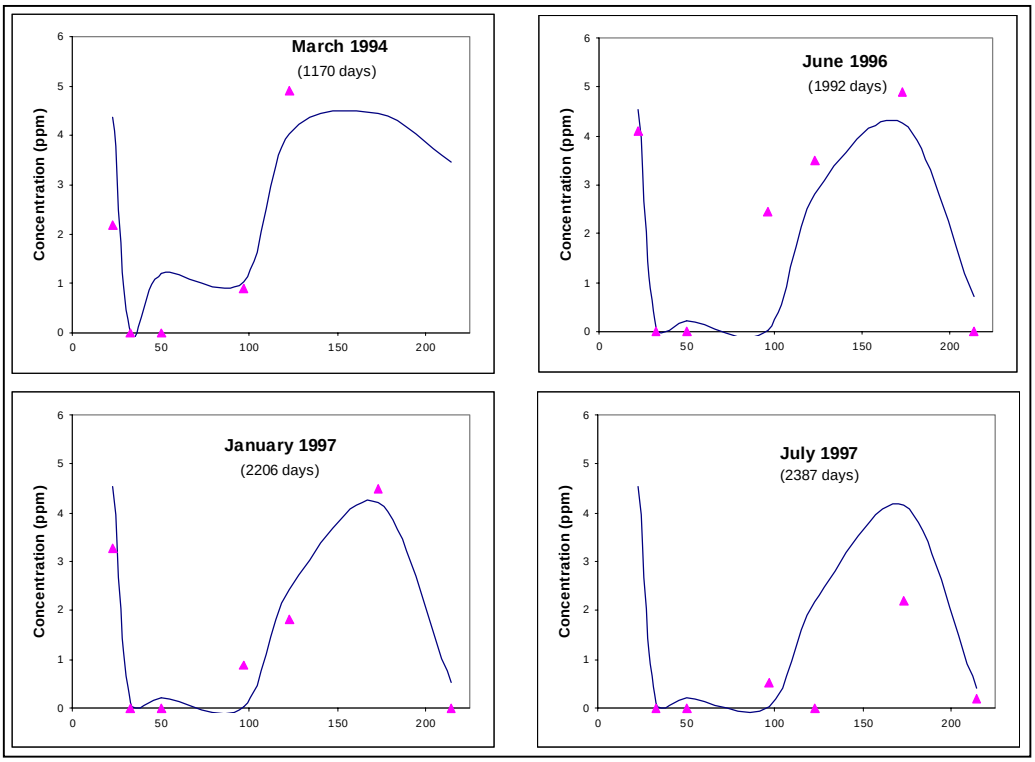

Figure 4.6 Dissolved oxygen concentrations along the transect

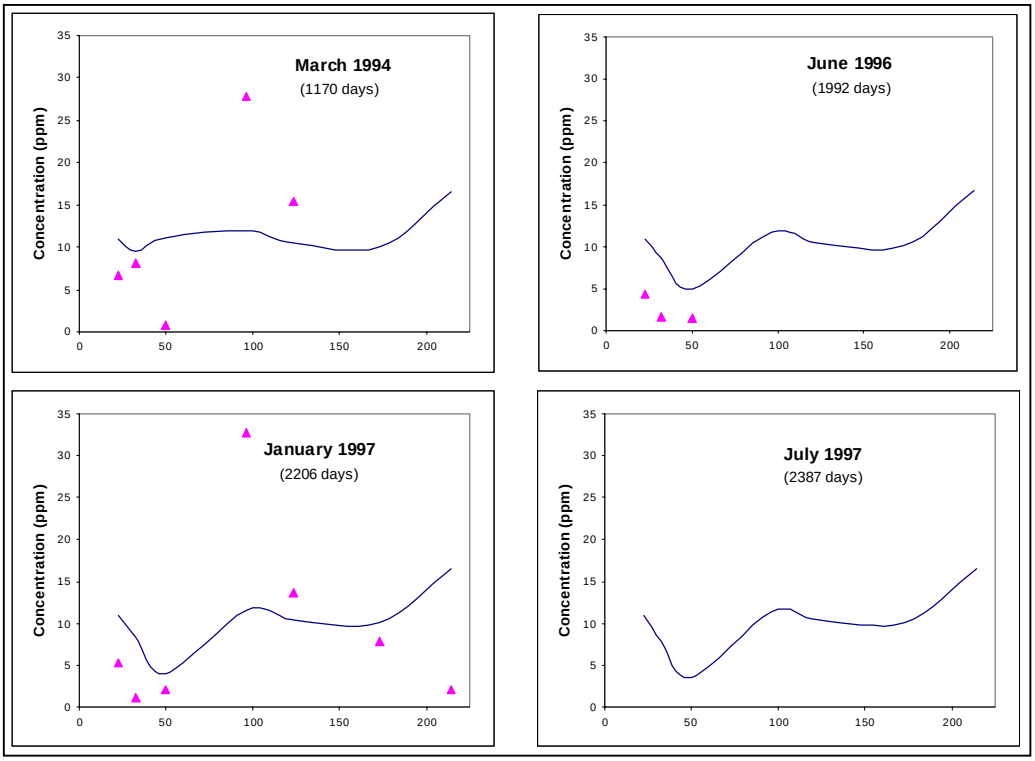

Figure 4.7 Sulfate concentrations along the transect

Figures 4.6 and 4.7 show simulated and measured concentrations of dissolved oxygen and sulfate along the transect. Figure 4.6 shows that the dissolved oxygen concentrations simulated using the model match up relatively well with those seen in the field for each date. The field DO concentrations fall primarily on or close to the curve generated by the model. Similarity between the calibrated model concentrations and the field concentrations indicates that the model is able to predict the regions of the Laurel Bay site where aerobic biodegradation is leading to decreased DO levels. In 1994, the model-simulated concentrations are not as low as those observed in the field in the area just downgradient of the source, near LB-EX-RW. One explanation of this is that other processes utilizing oxygen could be occurring in the field that are not simulated by SEAM3D. The only oxygen utilization process in SEAM3D is aerobic biodegradation, but many other oxidation reactions occur in the environment putting additional strain on oxygen levels.

In June 1996 and July 1997, the concentrations simulated by the model and those seen in the field follow the same shape. But, it can be seen in Figure 4.6 that in 1996, the model-predicted concentrations are slightly below actual concentrations, and in July 1997, they are slightly above. It is possible the differences could be attributed to recharge events at the site because DO is added to the model through recharge. Since the Laurel Bay site is small, recharge events will have a uniform effect across the entire site, and the concentration differences in these cases are uniform along the entire length of the transect. Since the model simulates steady-state flow conditions, it does not take into account individual recharge events that could result in sudden changes to the dissolved oxygen levels throughout the entire site.

The dissolved oxygen concentrations in both the field and the model can be used to follow the travel path of the contaminant plume. Upgradient of the source area, the concentrations of dissolved oxygen are at background levels. In the immediate vicinity of the source area where the contaminant concentrations are high, the microbes are using the DO to biodegrade the contaminants, so concentrations decrease. As distance from the source increases, the contaminant concentrations decrease significantly. Consequently, the DO concentrations rise since less aerobic biodegradation is necessary. Finally, in the region of the site near LB-EX-21 where contaminant concentrations increase, the DO concentrations tail off.

Figure 4.7 shows the sulfate concentrations along the length of the transect. The field data shows an initial concentration dip near the source area, and the model simulates a similar dip in June 1996 and January 1997. This is a region where the dissolved oxygen concentrations are less than 1.0 mg/L indicating the onset of anaerobic biodegradation. In 1994, the model concentrations of sulfate are essentially constant at around 10 mg/L along the entire length of the

transect. This indicates that the model has not begun using sulfate reduction as a primary TEAP. Before sulfate reduction will occur, even in anaerobic conditions, ferric iron is used as the terminal electron acceptor. Once the ferric iron concentrations have been reduced to a certain level, sulfate reduction will begin. In January 1997, Figure 4.7 shows that the concentration dip near the source is followed by concentration increases in both the field and the model. The concentrations in the field rise to a much higher level than those simulated by the model, and the peaks of both occur around LB-EX-15. Sulfate concentrations decrease continuously over the remaining length of the transect in the field indicating the possibility that sulfate reduction is occurring closer to the swail. The model simulates sulfate concentrations decreasing slightly after LB-EX-15 and then rising near LB-EX-21. Based on the sulfate concentrations near the swail, it is possible the model is not simulating sulfate reduction in that area even in January 1997.

Figures 4.8, 4.9, 4.10, and 4.11 show the concentrations of ferric iron, ferrous iron, sulfide, and methane along the transect. From those figures, it appears as though iron reduction is the only anaerobic TEAP occurring in the field in 1994. The field data indicates the presence of ferrous iron, but the concentrations of sulfide and methane are below detection levels. The model simulates low, but detectable, concentrations of both sulfide and methane in 1994 in the immediate area of the source. Since sulfide and methane are present, it can be assumed that the model is simulating both sulfate reduction and methanogenesis as terminal electron accepting processes as early as 1994.

If the field data is looked at more carefully, comparing the electron acceptors along with the end products, it can be seen that sulfate reduction could have been present in 1994 even though no concentrations of sulfide were detected. Field data in Figure 4.7 shows that sulfate levels decrease to close to zero near the source in 1994 which indicates that some process is utilizing the sulfate. Research has indicated that measuring the aqueous concentrations of sulfide underestimates the degree of sulfate reduction that is occurring (Kennedy et al., 1998). Sulfide reacts with ferrous iron yielding pyrite, and this reaction is not simulated by SEAM3D. It is possible that sulfide was being produced in small amounts at the site in 1994 and reacting with ferrous iron explaining why it was not detected by field testing.

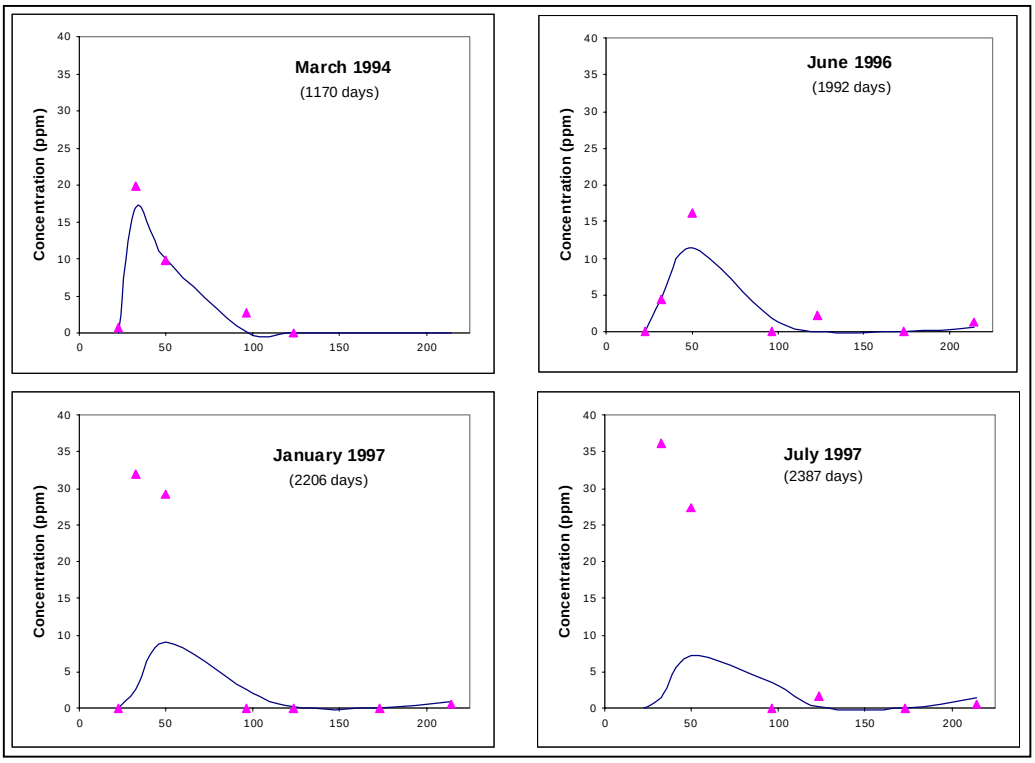

Figure 4.8 Ferrous iron concentrations along the transect

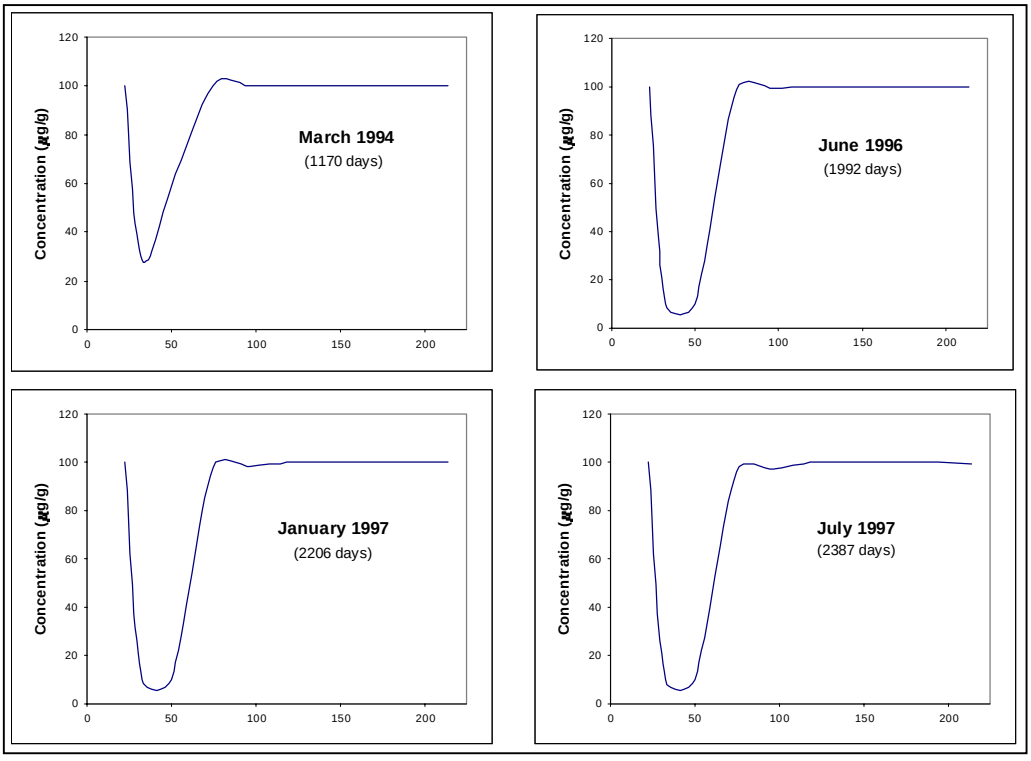

Figure 4.9 Ferric iron concentrations along the transect

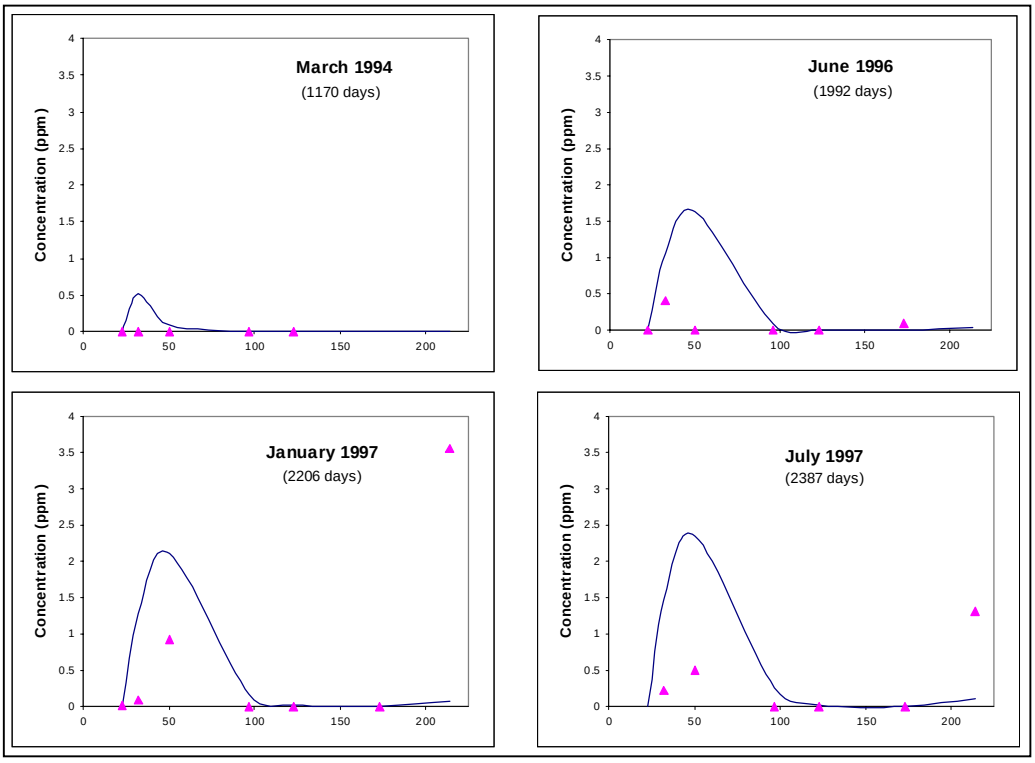

Figure 4.10 Sulfide concentrations along the transect

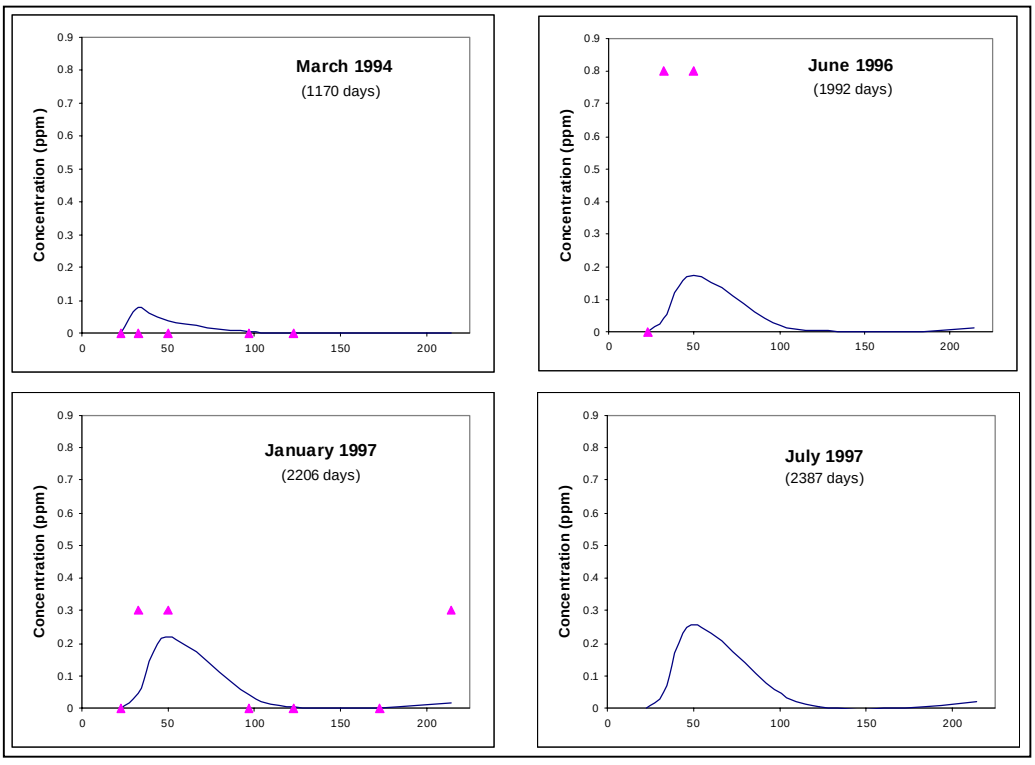

Figure 4.11 Methane concentrations along the transect

Figure 4.8 shows that the model simulates ferrous iron concentrations similar to what is seen in the field in 1994. The model curve peaks at around the same location, near LB-EX-1 and concentrations at LB-EX-3 and LB-EX-RW measured in the field fall along the model generated curve. In 1996, the field data and model results match well. The peaks are in the same location with the model peaking at a slightly lower concentration. There is also a rise in concentration seen for both sets of data near well LB-EX-21 at that time indicating the presence of iron reduction as a TEAP. Ferrous iron concentrations in both January and July 1997 fall well below the field concentrations. The model predicts the locations of the peaks, but as time goes by, the magnitude of the peak predicted by the model gets further from that seen in the field. As more of the area becomes anaerobic and more iron reduction is initiated, increases in the peak concentrations of ferrous iron would be expected. This would only be the case if there were a constant source of ferric iron were available to the microbes for use as an electron acceptor. In SEAM3D, each model cell was assigned a ferric iron concentration of 100 μg/g. Once that concentration decreases to 10 μg/g, iron reduction will no longer occur in that cell and ferrous iron concentrations will cease increasing. Figure 4.9 shows that the ferric iron levels in the area of highest ferrous iron concentrations are at the threshold level of 10 μg/g in 1997. This explains why the peak ferrous iron concentrations simulated by the model are much lower than those observed in the field.

The sulfide concentrations along the transect can be seen in Figure 4.10. Compared to the field data, the model simulated sulfide concentrations are higher over the entire length of the simulation. As has already been discussed, SEAM3D does not simulate the reaction of sulfide with ferrous iron forming pyrite. If this reaction is occurring at the site, greater concentrations of sulfide may be produced by sulfate reduction, but they are quickly diminished through reactions with the ferrous iron generated by iron reduction. Another difference between the field and model data seen in Figure 4.10 is that there is an order of magnitude difference between the sulfide concentrations at LB-EX-21. Beginning in January 1997, significant sulfide concentrations are seen in the field at LB-EX-21 indicating the presence of sulfate reduction as a terminal electron accepting process in that area. A concentration increase is simulated by the model, but it is not nearly as drastic as that observed in the field. Figure 4.8 shows that the model is predicting higher concentrations of ferrous iron than are seen in the field. It is possible that the model is simulating more iron reduction in that region delaying the complete onset of sulfate reduction closer to the swail. Consequently, higher sulfide concentrations are seen in the field data near LB-EX-21.

The concentrations of methane along the transect can be seen in Figure 4.11. The model simulates concentrations of methane less than 0.1 mg/L in 1994, and that is only slightly larger than the zero concentration levels seen in the field. Field data for methane is not available for July 1997, but Figure 4.11 shows that the location of the model peak corresponds to the location of the peak in the field for both June 1996 and January 1997. The maximum concentration simulated by the model is around 25 % of the peak measured in the field in June 1996 indicating the model is simulating less methanogenesis than is occurring in the field. In January 1997, two methane peaks are evident in the field. One is upgradient near the source area and the other is downgradient near well LB-EX-21. The model simulated concentrations at the upgradient peak are similar to what is seen in the field. Methane concentrations near LB-EX-21 are an order of magnitude below the field concentrations in January 1997 indicating less methanogenesis is simulated by the model in that area.

4.3 Areal Distributions

Benzene concentration distributions for 1994 and 1997 are shown in Figures 4.12 and 4.13 respectively. Since the regulatory standard with respect to benzene is 5 ppb or 0.005 mg/L, that is the minimum contour displayed in Figures 4.12 and 4.13. From Figure 4.12, it can be seen that the highest benzene concentrations, around 10.0 mg/L, remained in the top two layers in 1994. Vertical migration of benzene is apparent though with concentrations around the 5 ppb regulatory standard along the entire lengths of both layer 2 and layer 3. The model simulates concentrations of 5 ppb reaching the swail as early as 1994. This is contrary to reports from the site indicating that no contamination was detected in the region near the swail (Landmeyer et al., 1996). It should be noted, however, that there were no wells in that area of the site until after the 1994 sampling date, so it was not possible to measure contaminant concentrations there at that time. Also, Landmeyer et al. (1998) reported that contamination was detected in 1995 when wells LB-EX-19 through LB-EX-21 were installed. Since there was not complete plume delineation from the site in 1994, it is possible that the model's simulation of benzene transport is accurate.

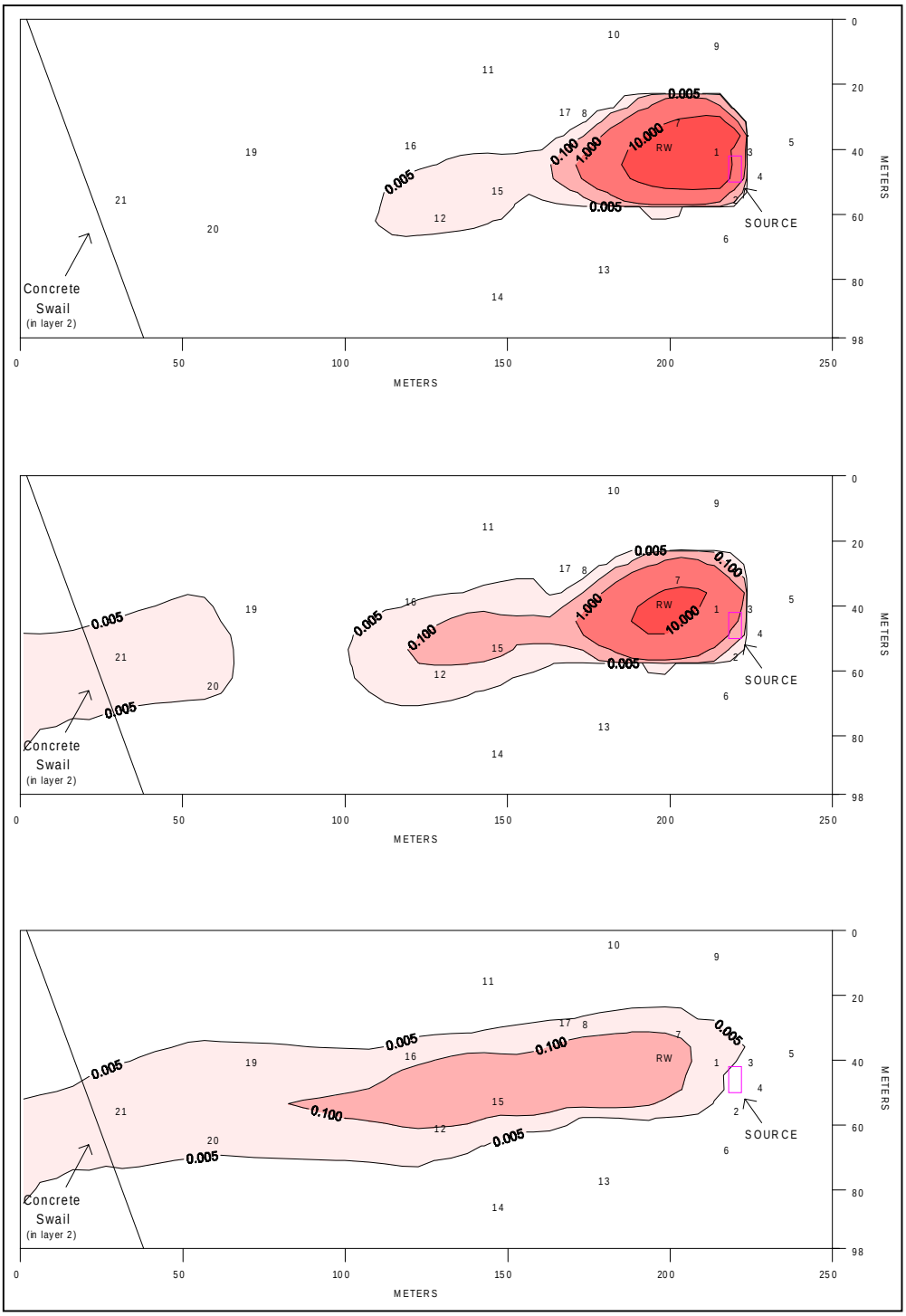

Figure 4.12 1994 benzene concentration distribution for model layers 1, 2, and 3 (layer 1 is the top contour with layer 3 being the bottom contour)

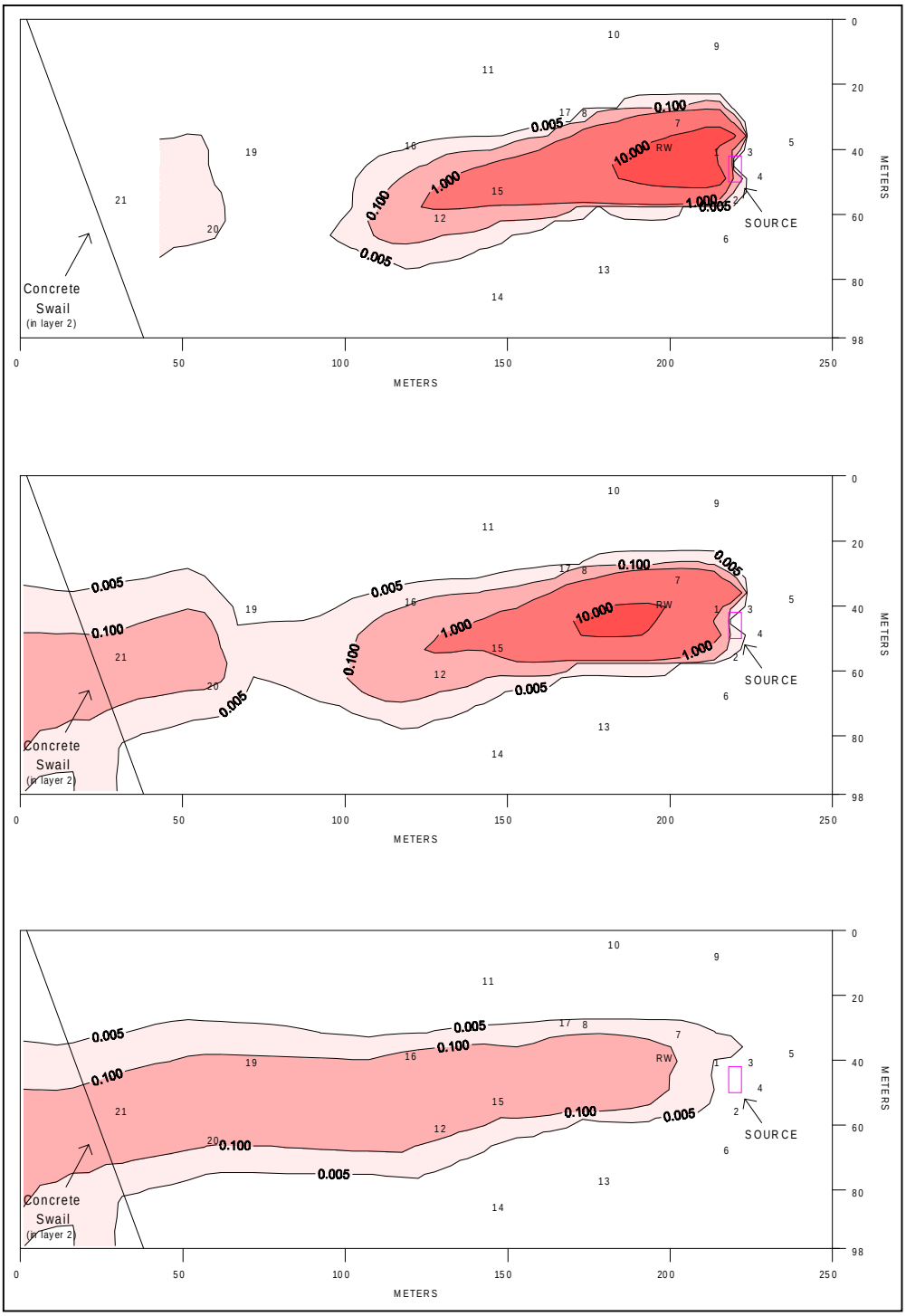

Figure 4.13 1997 benzene concentration distribution for model layers 1, 2, and 3 (layer 1 is the top contour with layer 3 being the bottom contour)

Landmeyer et al. (1998) reported that recharge events at Laurel Bay forced the dissolved contaminants deeper into the aquifer. This can be seen in Figure 4.12 which shows a discontinuity in the contaminant plume in layer 2 around 120 meters downgradient from the source. The plume moves into layer 3 where it travels continuously to the swail. The plume reemerges in layer 2 as flow is being pulled into the swail.

Figure 4.13 shows the benzene concentration distribution in 1997, so it can be used to trace the movement of benzene with time. The maximum concentrations of benzene in each of the layers are the same as they were in 1994, but they have shifted downgradient slightly towards the swail. The benzene concentrations reaching the swail are 10 ppb in layers 2 and 3 which is a concern since that is double the regulatory standard. The plume remains continuous through layer 2 with concentrations around 5 ppb in the region predicted to be uncontaminated in 1994. In general, the size of the plume increases in both length and width over time, and the concentration levels reaching the swail increase. Similar trends are seen over time with the other BTEX compounds, but their travel distances are smaller due to their lower solubilitites.

Concentration distributions of the two aqueous electron acceptors, dissolved oxygen and sulfate, in 1994 are shown in Figures 4.14 and 4.15, respectively and in 1997 are shown in Figures 4.16 and 4.17 respectively. In the dissolved oxygen figures, the darkest blue areas are the regions that are anaerobic with DO concentrations less than 0.5 mg/L. The white areas have DO concentrations greater than 3.0 mg/L. In the sulfate figures, the maximum contour represented is 10.0 mg/L which was the concentration in the recharge water.

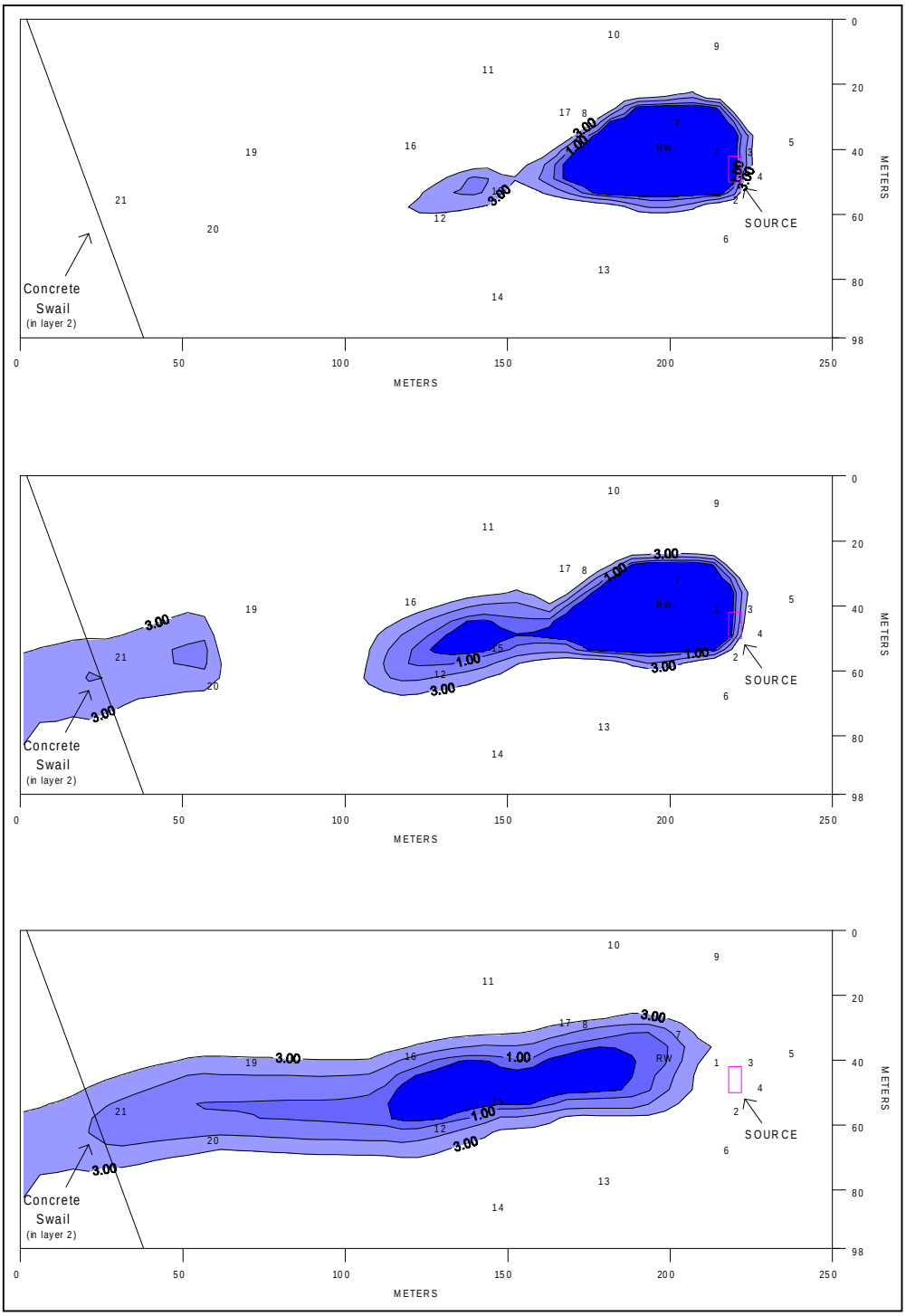

Figure 4.14 1994 dissolved oxygen concentration distribution for model layers 1, 2, and 3 (layer 1 is the top contour with layer 3 being the bottom contour)

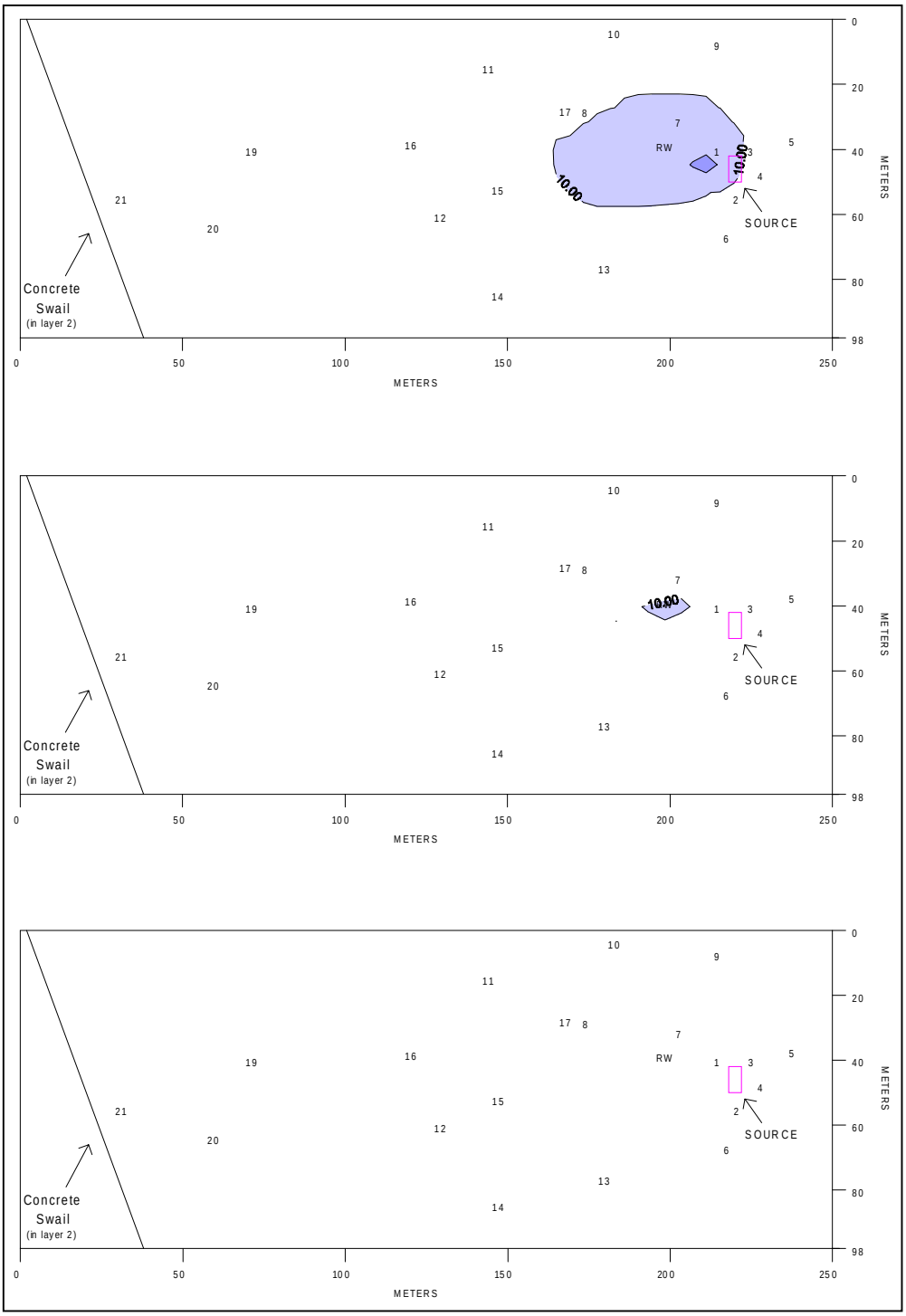

Figure 4.15 1994 sulfate concentration distribution for model layers 1, 2, and 3 (layer 1 is the top contour with layer 3 being the bottom contour)

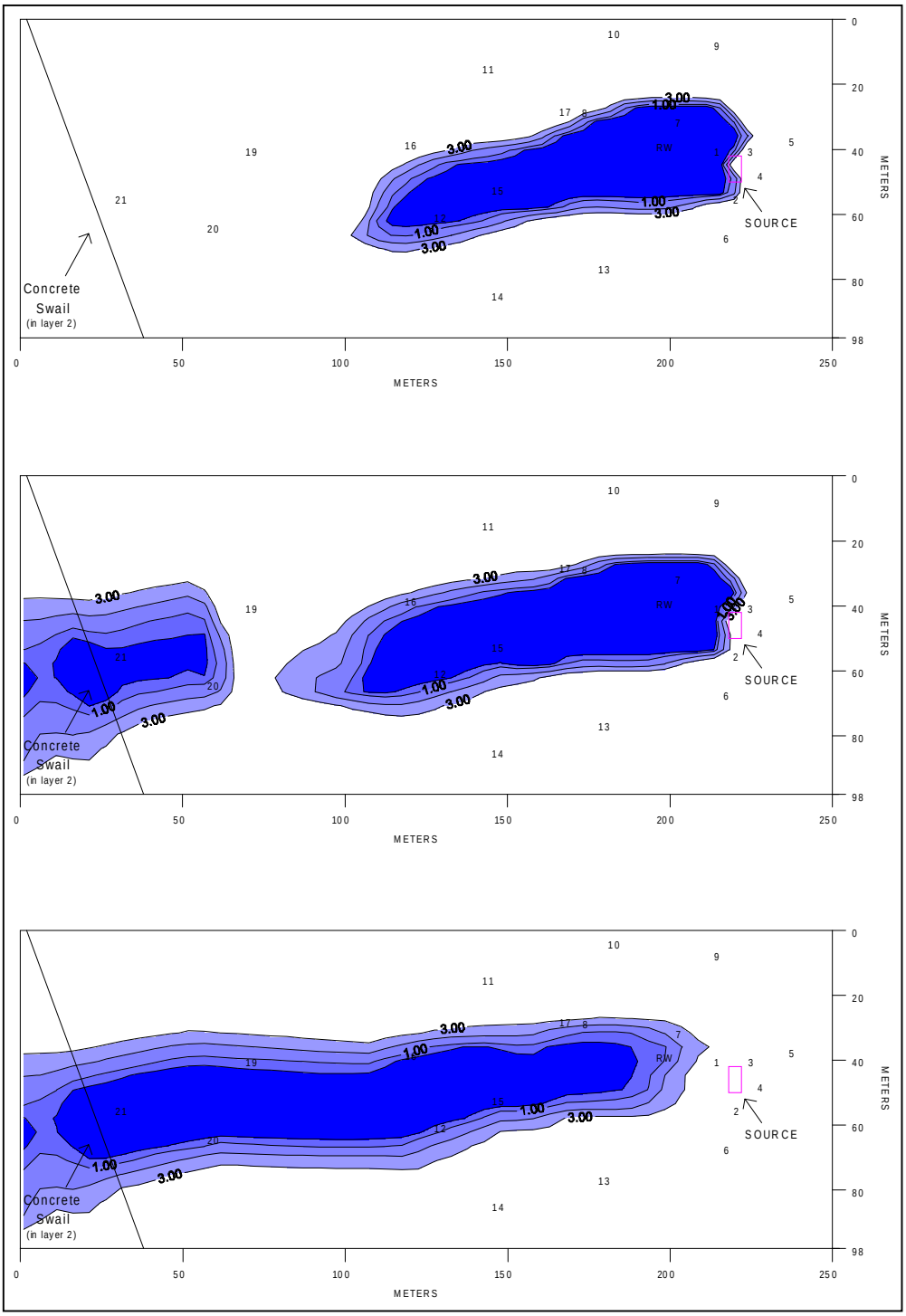

Figure 4.16 1997 dissolved oxygen concentration distribution for model layers 1, 2, and 3 (layer 1 is the top contour with layer 3 being the bottom contour)

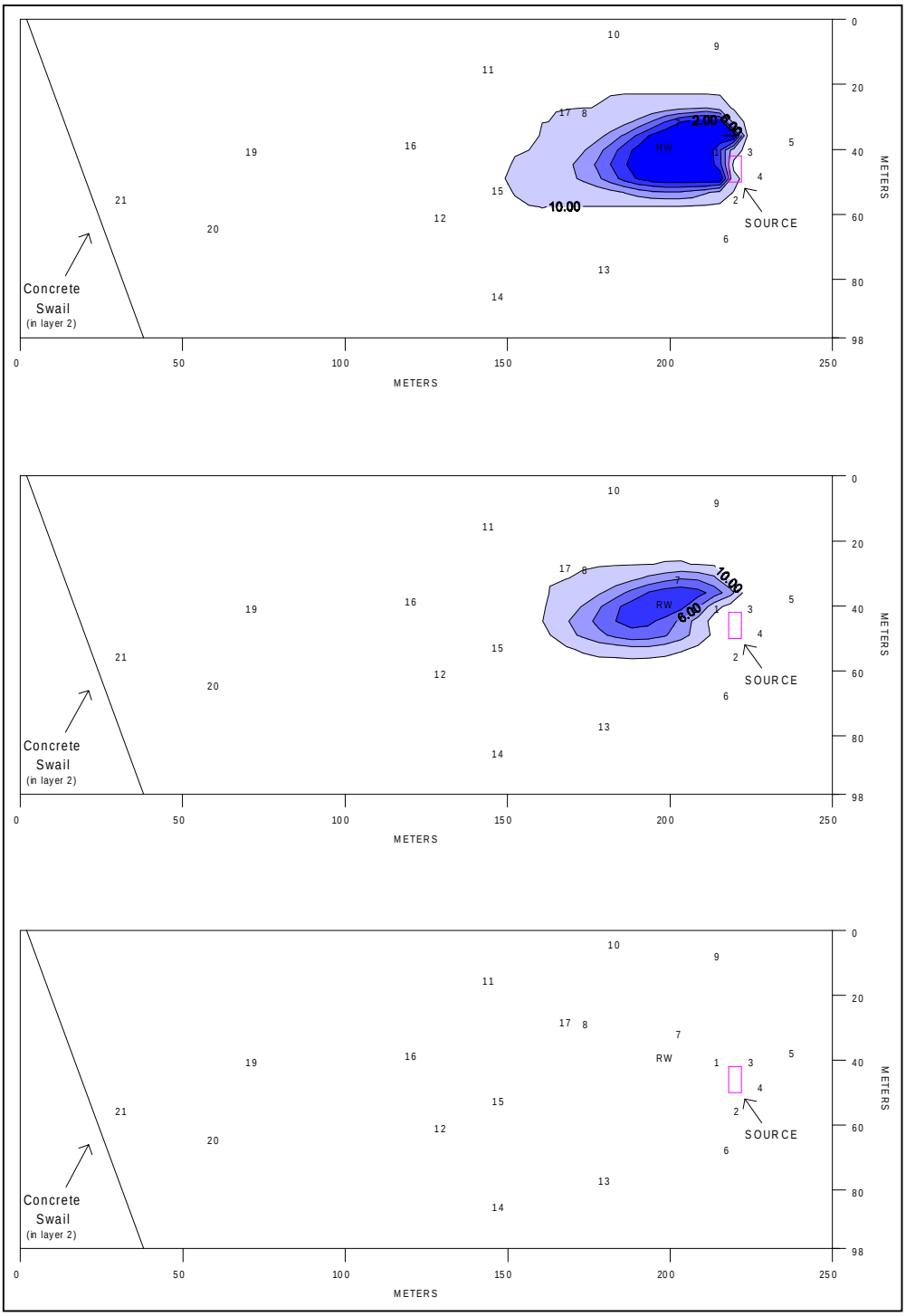

Figure 4.17 1997 sulfate concentration distribution for model layers 1, 2, and 3 (layer 1 is the top contour with layer 3 being the bottom contour)

The shapes of the DO plumes seen in both Figure 4.14 and 4.16 are similar to the shapes of the benzene plume in 1994 and 1997. Concentrations of DO are lowest in the regions with the highest concentrations of benzene contamination. Just as the length and width of the benzene plume increased during those three years, the size of the anaerobic portion of the plume increased as well. In 1994, Figure 4.15 shows that minimal sulfate reduction is occurring. There is a distinct region of sulfate concentrations slightly lower than background levels near the source area in layer 1. Figure 4.14 shows an anaerobic region in that same area. Since microbes prefer ferric iron to sulfate as an electron acceptor, they utilize iron reduction as a TEAP before sulfate reduction explaining the insignificant amount of sulfate reduction in 1994. Figure 4.17 shows that more sulfate is utilized as an electron acceptor in 1997. Sulfate concentrations decrease to close to zero in layers 1 and 2 near the source area indicating the presence of more sulfate reduction. As concentrations of both oxygen and ferric iron are diminished in that region (Figure 4.6, Figure 4.9, and Figure 4.16), the microbes turn to sulfate reduction to biodegrade the contamination.

The sequential trend of electron acceptor use can be seen with the end product concentration distributions as well. Figures 4.18 and 4.19 show the ferrous iron concentration distributions in 1994 and 1997, respectively, with the areas of darkest green delineated by the 30.0 mg/L contour. Since iron reduction yields more energy for the biodegrading microbes then sulfate reduction and methanogenesis, ferric iron is utilized in the anaerobic areas of the plume prior to sulfate and CO_2 as the preferred electron acceptor. The highest concentrations of ferrous iron are close to the areas of highest hydrocarbon concentration. Figure 4.18 shows that in 1994, the region of maximum Fe(II) concentration is just downgradient from the source where concentrations of DO are close to zero. Iron reduction is prevalent in layers 1 and 2 with maximum concentrations of ferrous iron around 30.0 mg/L. In layer 3, less iron reduction is occurring with maximum concentrations of around 0.1 mg/L.

By 1997, Figure 4.19 shows that iron reduction is occurring along the entire length of the plume. As more areas of the plume become anaerobic (Figure 4.16), iron reduction becomes the primary biodegradation method in those areas. The areas of maximum ferrous iron concentration shifted downgradient between 1994 and 1997. As concentrations of ferric iron decrease to the 10.0 μg/g minimum level necessary to support iron reduction, sulfate reduction is initiated in those regions (Figure 4.10).

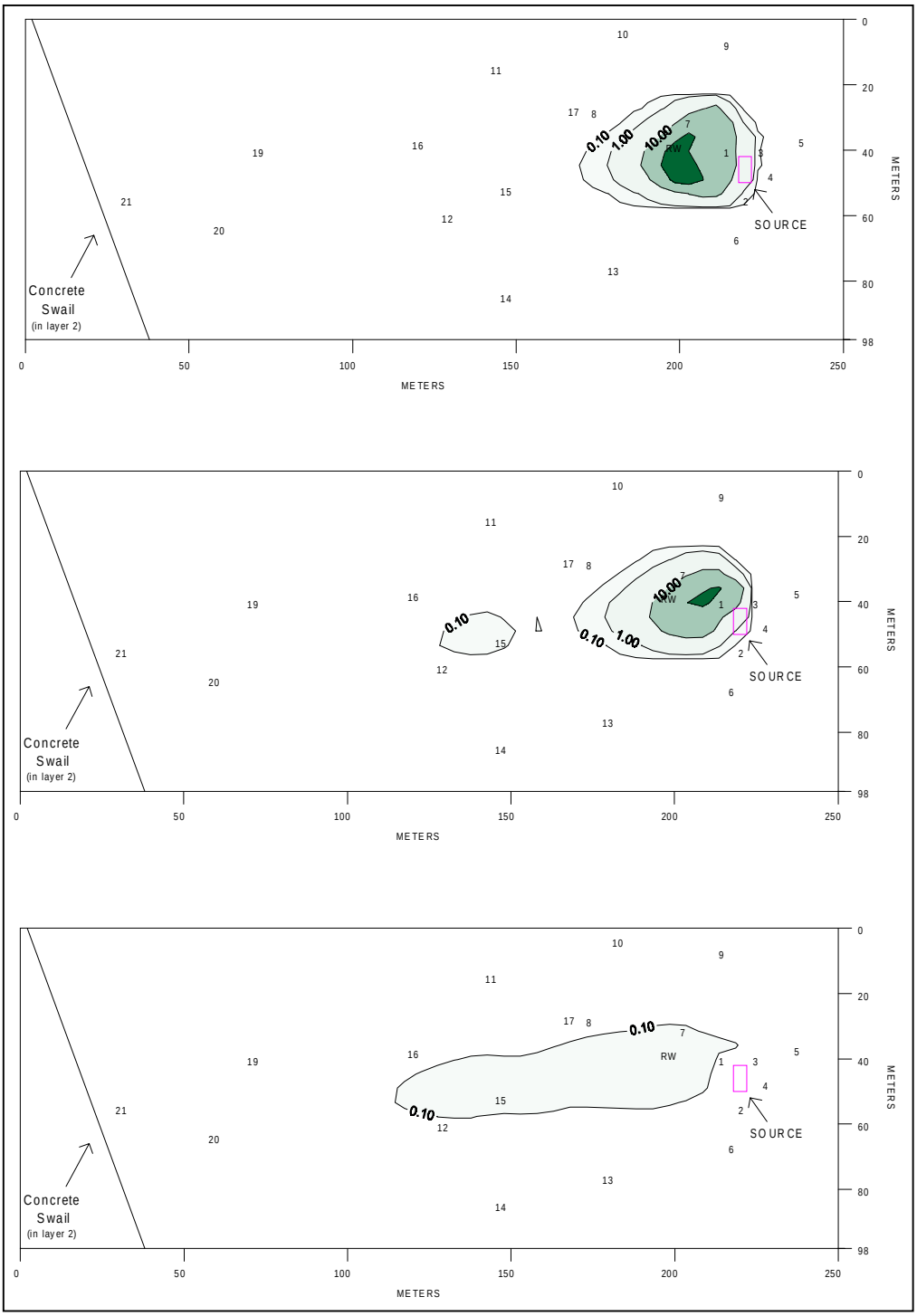

Figure 4.18 1994 ferrous iron concentration distribution for model layers 1, 2, and 3 (layer 1 is the top contour with layer 3 being the bottom contour)

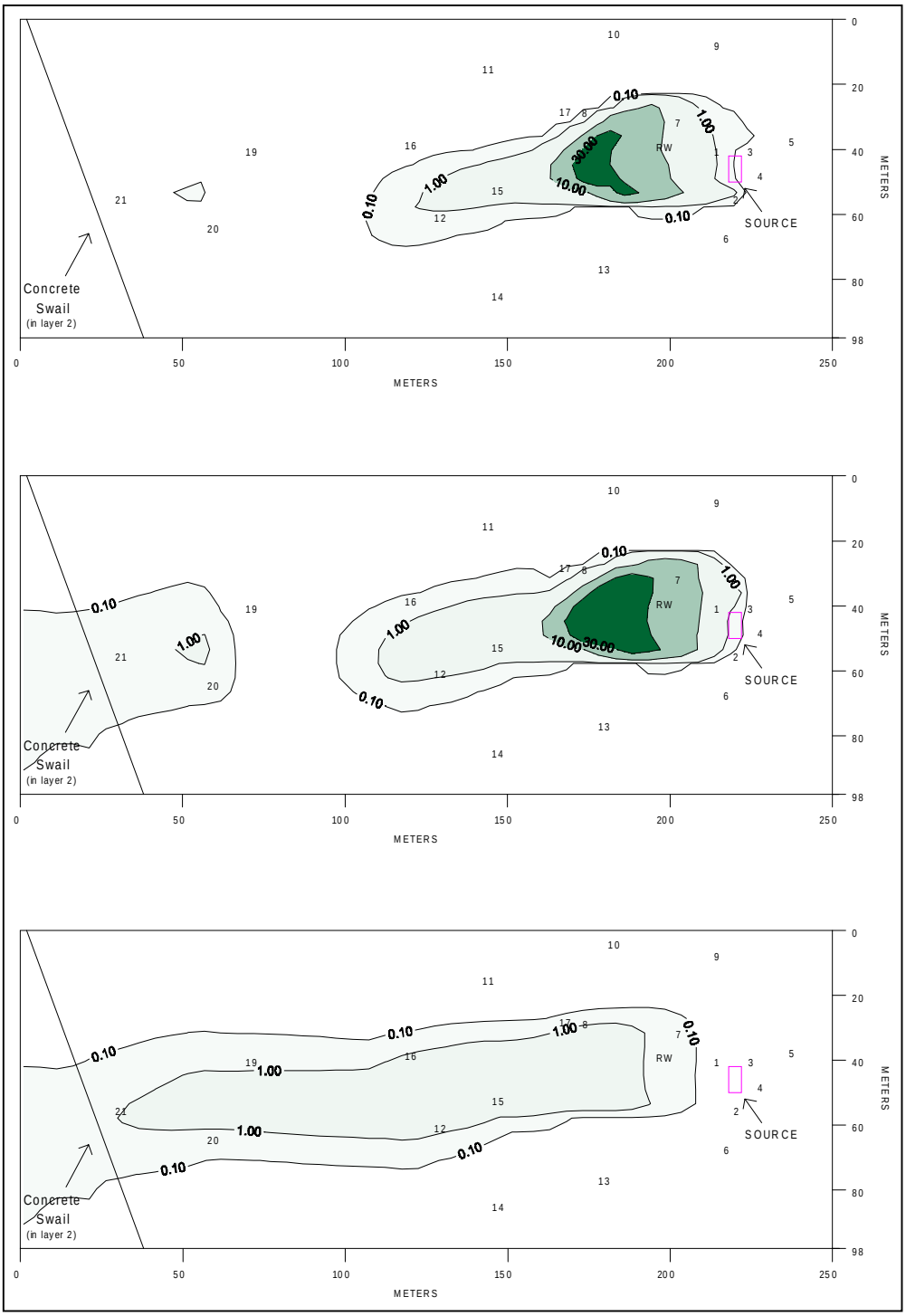

Figure 4.19 1997 ferrous iron concentration distribution for model layers 1, 2, and 3 (layer 1 is the top contour with layer 3 being the bottom contour)

5.0 Data Interpretation

SEAM3D performs mass balance calculations and ouputs two files containing these results. These files were used to study the biodegradation trends seen within the model. The first file (SMMASS.DAT) displays the total mass of each hydrocarbon constituent as well as the tracer in the aqueous, sorbed, and NAPL phases for every time step. The mass is totaled over the entire model domain by summing up the mass in each of the blocks in the grid, and it represents the mass over the entire grid at the end of each time step. It is not a cumulative value. The mass in the aqueous phase is found by dividing the aqueous concentration in each block by the porosity and then summed over the entire grid. For the sorbed phase mass, the solid phase concentration in each block is multiplied by the bulk density and the bulk volume. The NAPL mass in the domain is found in a similar way by multiplying the NAPL concentration by the bulk density and the bulk volume and then summing over the entire grid.

The second file (SMEAMASS.DAT) enables interpretation of biodegradation trends simulated by the model. This file contains the total mass of each hydrocarbon biodegraded by each TEAP at every time step. It is a cumulative calculation, so the mass of benzene, for example, degraded aerobically at step three is the sum of the benzene mass biodegraded at steps 1, 2, and 3. The program calculates the mass loss due to biodegradation using the following equation

$$M_{bio} = \frac{M}{\theta} v \left[\frac{S_1}{K_s + S_1} \right] \left[\frac{E_1}{K_s + E_1} \right] [\theta V_{cell}] \Delta t_{bio} \qquad (5.1)$$

where

M is the total contaminant mass at the initial transport step;

θ is the effective porosity;

S_1 is the substrate concentration at the initial transport step;

E_1 is the electron acceptor concentration at the initial transport step;

V_{cell} is the volume of the cell; and

Δt_{bio} represents the length of the transport step.

SEAM3D begins by calculating the mass of hydrocarbon 1, benzene in this model, lost due to aerobic biodegradation from the initial transport step, 1, to the final transport step, 2, in cell $i = 1, j = 1, k = 1$. It continues through the hydrocarbons, calculating the mass of each one biodegraded aerobically in transport step 2 based on the contaminant mass in the aqueous phase

in transport step 1. After all the mass lost due to aerobic biodegradation is calculated for transport step 2 for each hydrocarbon, the model then proceeds to calculate the mass loss for each hydrocarbon due to iron reduction. The losses due to sulfate reduction and then methanogenesis follow. SEAM3D then repeats the calculation for every cell in the grid for transport step 2 and sums them up to get the total mass loss due to each TEAP for each hydrocarbon in the given transport step. This process is then repeated for every transport step in the simulation.

5.1 Contaminant Mass

It was possible to study the mass trends for each hydrocarbon as well as the biodegradation trends and rates over time using a combination of both of the mass output files. Table 5.1 shows the magnitudes of each BTEX compound in the aqueous, adsorbed, and NAPL phases as well as the total mass. The percentage of the total aqueous and NAPL mass that each BTEX compound represents is shown in Table 5.2. The tables depict changes with time, containing data for 1 year, 2 years, 4 years, and 6 years from the beginning of the simulation.

	Benzene	Toluene	Ethylbenzene	Xylene
1 Year				
Aqueous Mass	5437	11017	1940	5786
Adsorbed Mass	1409	2855	503	1500
NAPL Mass	56022	432952	313199	729264
Total Mass	62868	446824	315642	736549
2 Years				
Aqueous Mass	10511	21822	3962	11695
Adsorbed Mass	2724	5656	1027	3031
NAPL Mass	68918	558155	409486	951953
Total Mass	82153	585634	414475	966679
4 Years				
Aqueous Mass	15851	34465	6960	18997
Adsorbed Mass	4109	8933	1804	4924
NAPL Mass	30636	294757	228908	528954
Total Mass	50596	338155	237673	552875
6 Years				
Aqueous Mass	17245	39894	8481	22580
Adsorbed Mass	4470	10341	2198	5853
NAPL Mass	22794	271776	223682	514332
Total Mass	44509	322010	234361	542764

Table 5.1 Mass distribution of each contaminant 1, 2, 4, and 6 years into the simulation (in grams)

	Benzene	Toluene	Ethylbenzene	Xylene
1 Year				
Aqueous Mass	22.5%	45.6%	8.0%	23.9%
NAPL Mass	3.7%	28.3%	20.5%	47.6%
2 Years				
Aqueous Mass	21.9%	45.5%	8.3%	24.4%
NAPL Mass	3.5%	28.1%	20.6%	47.9%
4 Years				
Aqueous Mass	20.8%	45.2%	9.1%	24.9%
NAPL Mass	2.8%	27.2%	21.1%	48.8%
6 Years				
Aqueous Mass	19.6%	45.2%	9.6%	25.6%
NAPL Mass	2.2%	26.3%	21.7%	49.8%

Table 5.2 Mass distribution of BTEX compounds within the aqueous and NAPL phases

Table 5.1 shows that the total mass of contamination is greatest after 2 years. There is a significant decrease between the second and fourth years in the total mass of each of the BTEX compounds. The mass of benzene decreases from 82 kg to 51 kg, and the mass of xylene decreases from 967 kg to 553 kg during those two years. In late 1993, around 3 years into the simulation, the remaining tanks and sediments in the source area were excavated. When this occurred, a large amount of the contaminant mass was removed accounting for the significant loss in total mass of the BTEX compounds seen between late 1992 and late 1994. A similar decrease is not observed in the mass of contamination in the aqueous phase, which is the actual mass in the contaminant plume.

Table 5.2 can be used to compare the BTEX distribution within the aqueous and NAPL phases. It shows that the contaminant distribution remains essentially the same during the entire 6 year simulation. At each of the 4 dates, toluene makes up the largest percentage in the aqueous phase (45.6 – 45.2 %) followed by xylene (23.9 – 25.6 %), benzene (22.5 – 19.6 %), and ethylbenzene (8.0 – 9.6 %). Benzene accounts for the lowest percentage in the NAPL phase over all 6 years (3.7 – 2.2 %) followed by ethylbenzene (20.5 –21.7 %), toluene (28.3 –26.3 %), and xylene (47.6 – 49.8 %). Since benzene is the most soluble of the BTEX compounds, it would be expected to represent the highest percentage of mass in the aqueous phase and the lowest in the NAPL phase followed by toluene, xylene, and ethylbenzene, respectively. The observed discrepancies are caused by the mass fractions of each compound present in the NAPL plume. The initial mass fraction of benzene, 0.01, is much lower than that of toluene, 0.085, and xylene, 0.14 (Table 3.9). Consequently, it represents a lower percentage of the aqueous mass. The initial

mass fraction of ethylbenzene, 0.04, is less than half that of toluene and less than a third of that of xylene. Consequently, ethylbenzene accounts for a lower percentage in the NAPL phase than would be expected.

5.2 Contaminant Mass Loss

5.2.1 Magnitude

The effects of each TEAP on both the net and the cumulative total contaminant mass loss can be seen in Table 5.3. It shows both the net and cumulative mass losses in grams for 1 year, 2 years, 4 years, and 6 years from the beginning of the simulation. The percentages of net and cumulative mass loss are shown for each TEAP as well.

Of the electron acceptors simulated in this model, O_2 provides the highest amount of Gibbs Free Energy for the microbial populations followed by Fe(III), SO_4^{-2}, and CO_2. Consequently, if dissolved oxygen is available as an electron acceptor, aerobic biodegradation results in the largest amount of mass loss. This is simulated in the model and is shown Table 5.3. The amount of net mass loss due to aerobic biodegradation is larger than the loss due to the sum of the three anaerobic processes. This can be seen at each of the times. After 1 year, 1.6 kg are biodegraded aerobically with 0.11 kg biodegraded anaerobically, and similarly, after 6 years, the net mass loss due to aerobic biodegradation is 19.0 kg compared to 7.0 kg biodegraded anaerobically.

Aerobic biodegradation results in the highest percentage of contaminant mass loss during the first year of the simulation with 93.9% of the mass biodegraded aerobically. Since the site was simulated with background DO concentrations of 5.0 mg/L, aerobic biodegradation began once the contamination entered the aquifer. Aerobic biodegradation of BTEX compounds occurs at a relatively rapid rate, so the plume quickly becomes anaerobic (Davis et al., 1994). Consequently, anaerobic processes begin to biodegrade the contaminants, so the percentage of mass loss due to aerobic biodegradation decreases to 71.6 % in the second year. As the plume spreads, it is exposed to uncontaminated aerobic groundwater as well as recharge water containing DO concentrations of 4.5 g/m^3. The percentage of net mass loss due to aerobic biodegradation increases between the fourth and sixth year from 68.3% to 72.9%, and it is most likely due to the reintroduction of DO into the anaerobic contaminant plume.

	Aerobic Biodegradation	Iron Reduction	Sulfate Reduction	Methanogenesis
1 Year				
Net Mass Loss	1596	94.0	3.9	5.5
Percent of net mass loss	93.9%	5.5%	0.2%	0.3%
Cumulative Mass Loss	1596	94.0	3.9	5.5
Percent of cumulative mass loss	93.9%	5.5%	0.2%	0.3%
2 Years				
Net Mass Loss	2438	930	15.6	19.4
Percent of net mass loss	71.6%	27.3%	0.5%	0.6%
Cumulative Mass Loss	4034	1024	19.5	24.8
Percent of cumulative mass loss	79.1%	20.1%	0.4%	0.5%
4 Years				
Net Mass Loss	12878	5536	291	163
Percent of net mass loss	68.3%	29.3%	1.5%	0.9%
Cumulative Mass Loss	16913	6560	310	188
Percent of cumulative mass loss	70.6%	27.4%	1.3%	0.8%
6 Years				
Net Mass Loss	18965	5090	1470	477
Percent of net mass loss	72.9%	19.6%	5.7%	1.8%
Cumulative Mass Loss	35878	11649	1780	665
Percent of cumulative mass loss	71.8%	23.3%	3.6%	1.3%

Table 5.3 Total hydrocarbon mass loss by each TEAP (in grams)

The model assumes that the organisms select a TEAP based on the amount of energy it provides in combination with the availability of the electron acceptor. Consequently, it would be expected that microbes, once anaerobic conditions exist, would select Fe(III), followed by SO_4^{-2} and finally CO_2 provided they are all available in the subsurface, so methanogenesis would result in the least amount of mass loss. An apparent contradiction to this exists in the first 2 years of the simulation where methanogenesis accounts for a greater percentage of total mass biodegraded than sulfate reduction. The initial population of methanogens, 0.085 g/m^3, is nearly an order of magnitude larger than that for sulfate reducers, 0.01 g/m^3, so they require less of a growth period before the initiation of biodegradation. Once the sulfate reducers had the opportunity to grow,

they surpassed the methanogens with respect to total mass biodegraded, and that can be seen in the later time results in Table 5.3.

The utilization of ferric iron as an electron acceptor follows dissolved oxygen at the Laurel Bay site. Table 5.3 shows the percentage of net mass loss due to iron reduction increases from 5.5% during the first year to 27.3% in the second year. This increase can be explained by the greater prevalence of anaerobic regions within the contaminant plume. The net percentage of mass loss due to iron reduction continues to increase until the fourth year, but it decreases from 29.3% to 19.6% during the last two years of the simulation. A threshold concentration of 10 μg/g was entered for ferric iron, so once the concentration in a cell reached this level, iron reduction ceases within the cell. Figure 4.9 shows that threshold concentrations are achieved as early as March 1994.

Table 5.3 shows that the percentage net mass loss due to sulfate reduction, 0.2%, is less than that due to iron reduction, 5.5%. The percent of net mass loss due to sulfate reduction increases consistently over the 6 years being compared. Sulfate reduction results in a larger percentage of net mass loss over time since the population of sulfate reducers has to go through an initial period of growth due to their low initial concentration, 0.01 g/m^3. Also, as the size of the anaerobic portion of the plume is growing and more model cells are reaching threshold concentrations of ferric iron, sulfate reduction is selected as the next TEAP in the sequence. Table 5.3 shows that methanogenesis contributes the least amount to the contaminant mass loss over the six year simulation. By the sixth year, it only accounts for 1.8% of the net mass loss, and that is less than half the percentage lost due to sulfate reduction.

There is a significant increase in contaminant mass loss between the second and fourth years. The increase is evident in Table 5.3 for all of the TEAPs simulated. Aerobic biodegradation resulted in 4.0 kg of mass loss in the first 2 years of the simulation and 12.8 kg in the second two years. Similar mass loss increases are seen for iron reduction, 1.0 kg to 5.5 kg, sulfate reduction, 0.02 kg to 0.29 kg, and methanogenesis, 0.02 kg to 0.16 kg. It can be seen in Table 5.2 that the amount of contaminant mass in the aqueous phase increases during that period. Since the microbes are only able to biodegrade the contamination in the aqueous phase, the mass increase in that phase results in an increase in mass biodegraded.

Table 5.4 focuses on the individual contaminants within the hydrocarbon plume rather than on the contamination as a whole. It shows the mass of the BTEX compounds (in grams) biodegraded by each TEAP after 1 year, 2 years, 4 years, and 6 years. They are cumulative values.

	Aerobic Biodegradation	Iron Reduction	Sulfate Reduction	Methanogenesis	Total
1 Year					
Benzene	306	0.3	0.1	0.2	307
Toluene	611	50.3	1.7	2.4	666
Ethylbenzene	232	0.2	0.7	1.0	234
Xylene	447	43.0	1.3	1.9	493
2 Years					
Benzene	833	3.9	0.6	0.8	838
Toluene	1664	540	8.5	10.9	2224
Ethylbenzene	472	2.8	3.7	4.6	483
Xylene	1066	477	6.7	8.5	1557
4 Years					
Benzene	3558	23.8	10.0	6.0	3598
Toluene	7286	3538	130	81.1	11035
Ethylbenzene	1732	16.3	63.8	36.7	1849
Xylene	4336	2981	106	64.1	7488
6 Years					
Benzene	7395	40.9	51.6	20.1	7508
Toluene	15436	6357	739	286	22817
Ethylbenzene	3765	28.1	371	130	4295
Xylene	9281	5224	619	228	15352

Table 5.4 Cumulative mass of each BTEX compound biodegraded by TEAP (in grams)

Table 5.4 indicates that aerobic biodegradation accounts for 99.8% of the total amount of benzene biodegraded in the first year of the simulation. Compared with the 306.5 grams of benzene biodegraded aerobically, iron reduction accounts for 0.3 grams, sulfate reduction for 0.1 grams and methanogenesis accounts for 0.2 grams. This trend is observed through the entire six year simulation with 98.5%, or 7.4 out of 7.5 kg, of the benzene mass loss due to aerobic biodegradation after six years. Since benzene is the most soluble of the BTEX compounds, it dissolves into the aqueous phase prior to the other three compounds, so it is the first contaminant in the proper phase for biodegradation. Also, benzene travels near the front of the contaminant plume due to its higher solubility, so it is the first to enter the uncontaminated zones containing higher concentrations of dissolved oxygen.

Another reason for benzene's high percentage of mass loss due to aerobic biodegradation is that the maximum rates of substrate utilization for aerobic processes are over two orders of magnitude larger than for the anaerobic processes in the model. It has been reported by many researchers that benzene is resistant to microbial biodegradation in anaerobic conditions (Acton and Barker, 1992; Barker et al., 1987; Hutchins et al., 1991; Weiner et al., 1998). Benzene's maximum rate of substrate utilization for sulfate reduction and methanogenesis is an order of magnitude less than that for the toluene, ethylbenzene, and xylene. The maximum rate for iron reduction is less than that for sulfate reduction and methanogenesis. This is because there is

evidence that benzene biodegrades minimally using iron reduction under natural conditions with no outside stimulus (Lovley et al., 1994; Lovley, et al., 1996).

Toluene also exhibits a majority of mass loss due to aerobic biodegradation with 611.2 grams out of 665.7 grams, or 91.8%, biodegraded aerobically in the first year (Table 5.4). In contrast to benzene, the amount of toluene biodegraded by anaerobic processes increases over time. The maximum rate of substrate utilization for the iron reduction is two orders of magnitude larger for toluene than it is for benzene, and the rates for sulfate reduction and methanogenesis are an order of magnitude larger. That explains the larger amount of anaerobic biodegradation of toluene. After 6 years, iron reduction accounts for 6.4 kg of mass loss compared with 15.4 kg biodegraded aerobically. It can be seen that more toluene is biodegraded by methanogenesis than sulfate reduction initially, and that can be attributed to the growth period of the sulfate reducers. After 4 years, sulfate reduction results in more toluene mass loss than methanogenesis with 0.13 kg biodegraded by sulfate reducers and 0.081 kg lost due to methanogenesis.

Ethylbenzene results are similar to those for benzene. Most of the biodegradation is aerobic since the same maximum rate of substrate utilization for iron reduction is used for each contaminant. The rates of iron reduction are 0.0001 day^{-1} for benzene and ethylbenzene. More ethylbenzene is biodegraded using sulfate reduction and methanogenesis since the maximum rate of substrate utilization for those two processes are two orders of magnitude larger than that for iron reduction. After 1 year, 99.1% of the ethylbenzene is biodegraded aerobically. By the sixth year, aerobic biodegradation accounts for 87.7% of the total mass biodegraded.

Xylene exhibits results similar to toluene. Maximum rates of substrate utilization are the same for each TEAP for toluene and xylene. After 1 year, 0.45 kg of xylene are biodegraded aerobically compared with 0.49 kg of total biodegradation. Aerobic biodegradation accounts for 90.6%, the lowest percentage of the four BTEX compounds. The mass of xylene biodegraded aerobically after 6 years is 9.3 kg. That is 60.5% of the total mass of 15.3 kg of xylene biodegraded by that time.

Table 5.4 shows that ethylbenzene consistently accounts for the least mass lost due to biodegradation. It is followed in increasing order by benzene, xylene, and toluene. Since ethylbenzene is the least soluble of the BTEX compounds, it makes up the smallest percentage of the contamination in the aqueous phase (Table 5.2). Consequently, less ethylbenzene is bioavailable for the microbes to degrade.

Figure 5.1 shows the cumulative mass loss of the BTEX compounds over time with respect to each TEAP. They show graphical evidence of trends already discussed based on the tables. From the figure, it can be seen that majority of mass loss early in the simulation is due to aerobic biodegradation. The slopes are still positive at the end of the simulation indicating that aerobic biodegradation is still contributing to mass loss after 6 years. Iron reduction begins to degrade toluene and xylene around 500 days into the simulation, but it has no significant impact on the masses of benzene and ethylbenzene due to the lower rates of substrate utilization for those two compounds. The steepest portion of the curves for toluene and xylene are seen from 1000 to 1500 days indicating that the most significant amounts of mass loss occur at that time. As with the aerobic plot, the mass losses of toluene and xylene due to iron reduction are still climbing at the end of the simulation indicating iron reduction was still occurring.

Figure 5.1 shows that sulfate reduction begins to contribute to observable mass loss around 1000 days into the simulation. At around 1500 days, the amount of toluene, ethylbenzene, and xylene lost due to sulfate reduction increases rapidly, but the cumulative mass of benzene lost remains less than 0.10 kg through the entire simulation. Initiation of methanogenesis begins prior to sulfate reduction, but between 1000 and 1500 days, the cumulative mass loss due to sulfate reduction surpasses the amount lost due to methanogenesis. As with sulfate reduction, very little benzene is biodegraded by methanogens with less than 50 grams lost by the end of the simulation. The curves on both the sulfate reduction and methanogenesis plots have a steep slope at the end of the simulation. This indicates that the amount of mass lost due to both those TEAPs is significantly increasing as the simulation ends.

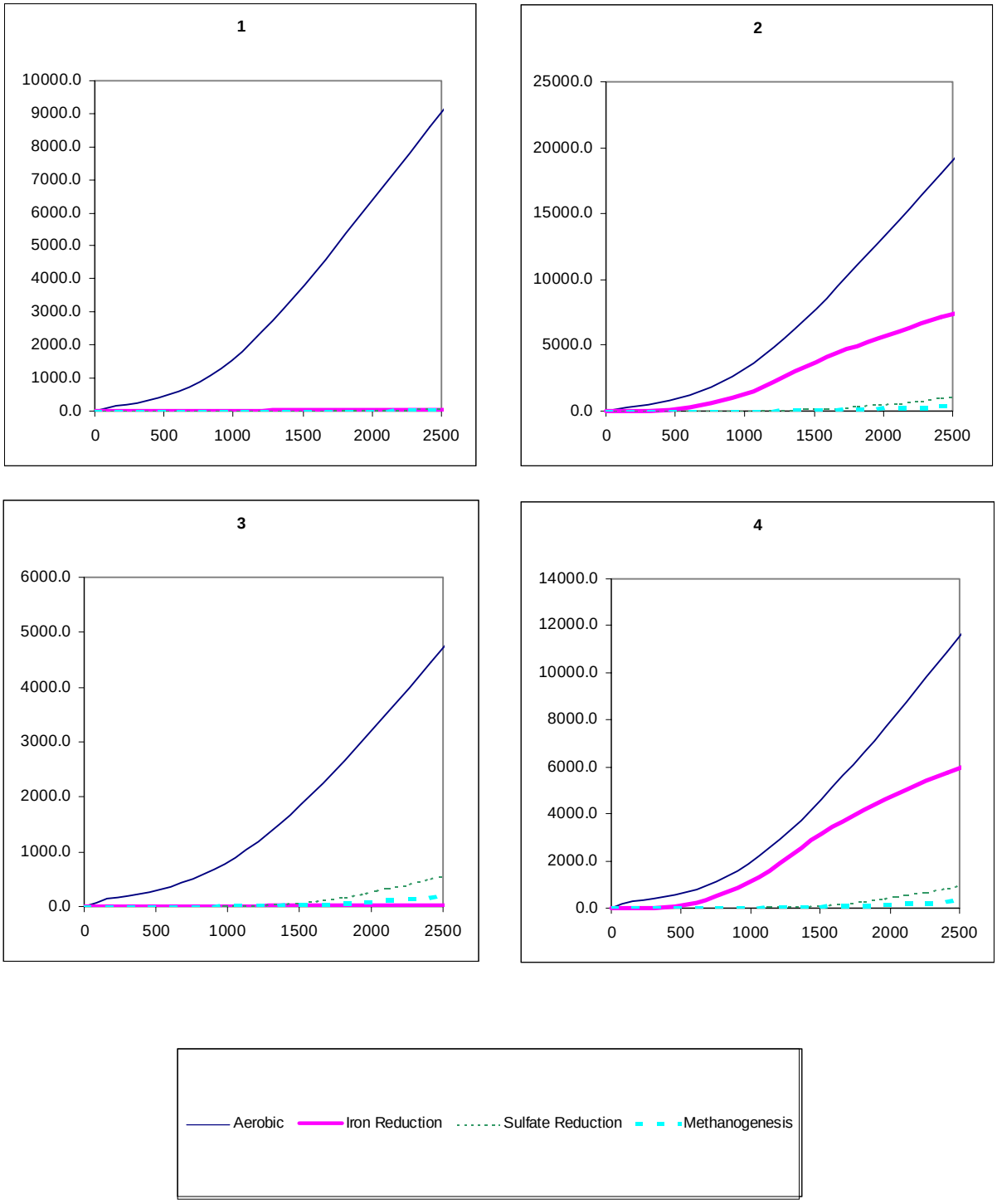

Figure 5.1 Cumulative mass loss (in grams) of the BTEX compounds over time (in days). Plot 1 represents the mass of benzene biodegraded by each TEAP. Plots 2, 3, and 4 show the mass of toluene, ethylbenzene, and xylene, respectively, biodegraded by each TEAP.

5.2.2 Rates of Contaminant Loss

Data from the two mass output files was used to calculate the rates of contaminant loss for each BTEX component. Rates were found for each TEAP at every time step. The rate at a particular time step (1) was found using the following equation

$$Rate = \frac{M_{bio\,2} - M_{bio\,1}}{\Delta t M_{total\,1}} \tag{5.2}$$

where

M_{bio2} was the cumulative mass of contaminant biodegraded by the end of time step 2;

M_{bio1} was the cumulative mass of contaminant biodegraded by the end of time step 1;

Δt was the length of the time step; and

M_{total1} was the total mass of the contaminant in the aqueous phase at the end of time step 1.

The changes in rate over the entire length of the simulation can be seen in Figure 5.2, and Table 5.5 shows the mass loss rates for each contaminant with respect to each TEAP. The units of rate are grams of contaminant biodegraded per day per total mass of contaminant in the aqueous phase.

		2 Days	1 Week	1 Month	1 Year	2 Years	4 Years	6 Years
Aerobic Biodegradation	Benzene	204800	8538	1290	146	207	314	307
	Toluene	61911	4006	979	146	202	300	287
	Ethylbenzene	62148	10155	1994	204	249	349	351
	Xylene	37066	5292	1261	171	221	322	315
Iron Reduction	Benzene	0.7	0.2	0.2	0.5	1.5	1.9	1.2
	Toluene	24.8	9.2	9.7	35.5	99.6	142	86.7
	Ethylbenzene	0.2	0.2	0.3	1.0	2.8	3.1	1.6
	Xylene	14.8	12.6	15.5	58.3	163	211	115
Sulfate Reduction	Benzene	0.4	0.1	0.1	0.1	0.3	1.9	4.1
	Toluene	1.8	0.7	0.6	0.9	1.7	11.6	28.9
	Ethylbenzene	1.5	1.6	1.7	2.1	4.4	28.8	67.2
	Xylene	1.1	0.9	0.9	1.3	2.6	17.5	43.2
Methanogenesis	Benzene	0.6	0.2	0.2	0.2	0.3	0.8	1.6
	Toluene	2.7	1.0	0.9	1.2	1.9	4.9	10.1
	Ethylbenzene	2.2	2.4	2.5	2.8	4.6	11.0	21.7
	Xylene	1.6	1.3	1.4	1.8	2.8	7.0	14.5

Table 5.5 Rates of biodegradation (x 10^6 day^{-1}) for each BTEX compound and TEAP

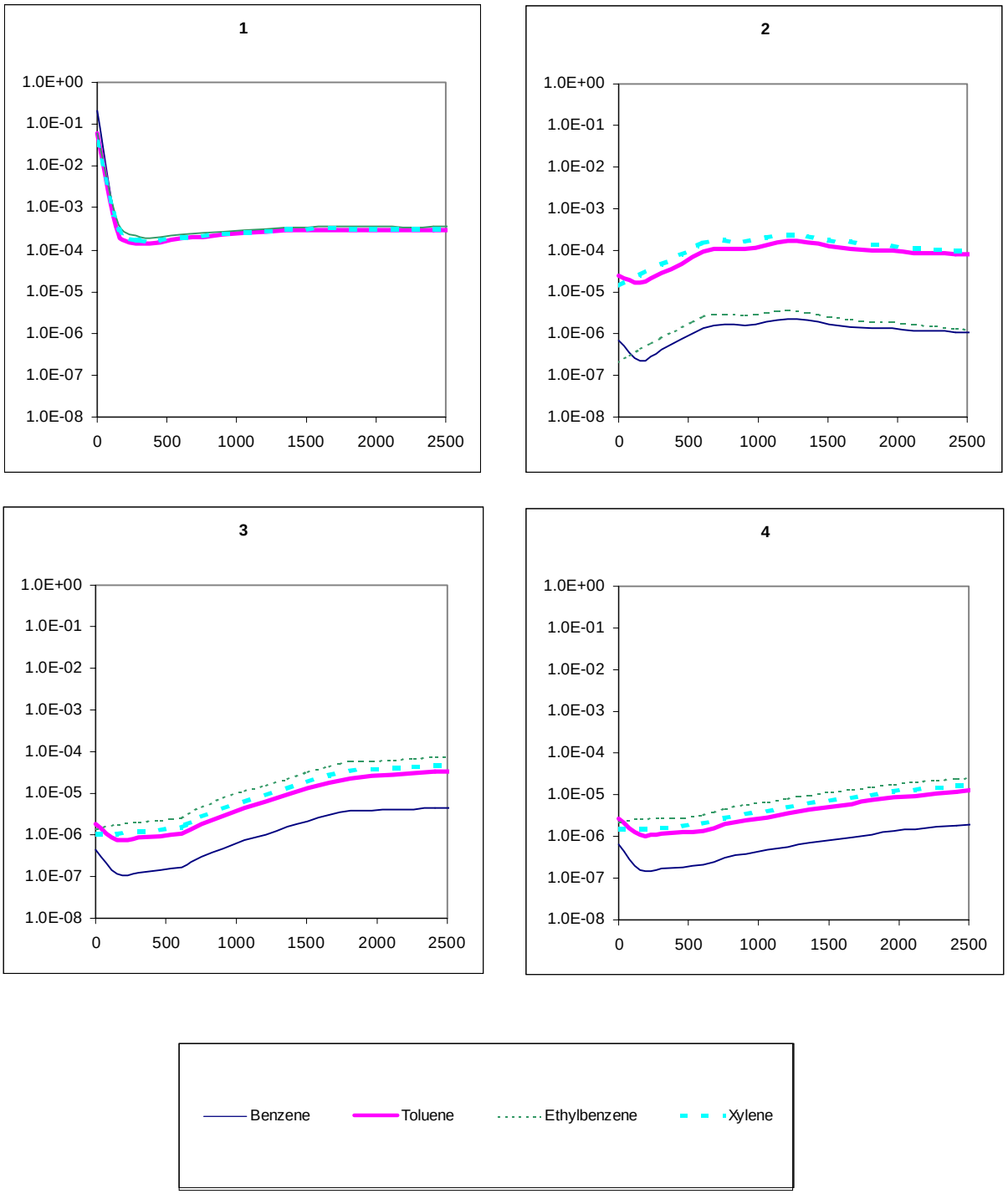

Figure 5.2 Rates of biodegradation (x 10^6 day^{-1}) over time (in days). Plot 1 shows loss rates due to aerobic biodegradation and plots 2, 3, and 4 show loss rates due to iron reduction, sulfate reduction, and methanogenesis respectively.

Both Table 5.5 and Figure 5.2 show that the aerobic biodegradation rates are high in the initial stages of the contaminant spill. This is true for each of the BTEX contaminants. By the second day, the rate of benzene mass loss is 0.20, and that is followed by a rate of 0.062 for toluene and ethylbenzene and 0.037 for xylene. As the dissolved oxygen near the source is quickly utilized and depleted by the microbes, there is rapid decrease in the aerobic rates during the first year of the simulation. After 1 year, the rate of mass loss for benzene is four orders of magnitude less than after 2 days, and the rates for the other three compounds are three orders of magnitude lower than the initial rates. Over time, a balance is achieved between oxygen loss from the plume through biodegradation and that added to the plume through recharge, groundwater inflow, and plume spreading. This balance is reflected in the rates as they begin to level off after 1 year becoming essentially constant over the remainder of the simulation. This trend is shown with the values in Table 5.5 and in Figure 5.2 as the curve tracing the rates levels off after 1 year.

Since the microbes prefer aerobic biodegradation, the rates for the three anaerobic processes are at least two orders of magnitude less than the aerobic rates for the first month of the simulation. The most significant difference is seen when comparing the aerobic and iron reduction rates for benzene. There is evidence indicating that benzene is not easily biodegraded in iron reducing conditions (Lovley et al., 1994; Lovley et al., 1996). Consequently, the maximum rate of ferric iron utilization is three orders of magnitude lower than the rate for aerobic biodegradation resulting in lower mass loss rates. A similar substrate utilization rate is used for ethylbenzene. The lower utilization rates for benzene and ethylbenzene explain the lower mass loss rates due to iron reduction when compared with toluene and xylene.

Figure 5.2 shows that the rates due to iron reduction climb over the first 2 years as the iron reducers grew and more of the plume became anaerobic. Rate increases are still evident until around year 4 when the rates begin to decrease for all of the BTEX compounds. This decrease is caused by the depletion of ferric iron in the most anaerobic regions of the plume. As the electron acceptor is depleted, the mass loss due to iron reduction slows and becomes dependent on the rate of depletion of DO.

The mass loss rates due to sulfate reduction are lower than the rates for aerobic biodegradation. For toluene and xylene, the loss rates are also lower than for iron reduction. This is expected since sulfate reduction is inhibited by both aerobic biodegradation and iron reduction. This inhibition in combination with a needed period of growth for the sulfate reducers results in very low rates of sulfate reduction in the first two years of the simulation. Table 5.5 and Figure 5.2 show that the rates of mass loss due to sulfate reduction begin to increase after around 2 years

increasing an order of magnitude by year 6. During this time, the anaerobic portion of the plume is increasing and threshold concentrations are being achieved in a larger number of model cells, so sulfate reduction becomes more prevalent.

After 0.005 years (2 days), the rates of mass lost due to methanogenesis are comparable with those for sulfate reduction. The initial biomass concentration of methanogens is 0.085 g/m^3 compared with an initial concentration of 0.01 g/m^3 for both sulfate and iron reducers. Consequently, less growth, if any, is required for the methanogen population, so they begin to biodegrade contaminants in the areas of the plume that rapidly become anaerobic at the onset of the simulation. The rates of mass loss due to methanogenesis decrease during the first year of the simulation for benzene, toluene, and xylene as the iron and sulfate reducers grow and begin inhibiting methanogenesis. The rates increase over the final 5 years of the simulation. Table 5.5 shows that the mass loss rates increase by 200% from year 2 to 4 as well as from year 4 to 6 indicating that methanogenesis is becoming a more significant mass loss mechanism over time.

Both Table 5.5 and Figure 5.2 show that the benzene's mass loss rates due to sulfate reduction and methanogenesis are at least an order of magnitude less than the rates for toluene, ethylbenzene, and xylene. Research has shown that significant amounts of benzene are not biodegraded anaerobically (Acton and Barker, 1992; Barker et al., 1987; Hutchins et al., 1991; Weiner et al., 1998). Consequently, the maximum rate of substrate utilization for benzene is an order of magnitude less for those two processes. Lower maximum rates of substrate utilization for benzene lead to lower rates of mass loss due to the anaerobic processes.

5.3 Long Term Simulation

The Laurel Bay contaminant transport simulation was run out for twenty years to study the long term effects on the contaminant mass distribution as well as the rates and magnitudes of contaminant mass loss. The results can be seen in Tables 5.6 through 5.9 and Figures 5.3 and 5.4. The tables compare values at 6 years, 10 years and 20 years from the start of the simulation.

Table 5.6 shows the mass distribution of the BTEX compounds within the aqueous and NAPL phases, and it is a continuation of the results presented in Table 5.2. The percentage of benzene in both the aqueous and NAPL phases continues to decrease through the 20 year simulation. Benzene accounts for 19.6% of the aqueous mass after 6 years and 4.1% after 20 years, and it accounts for 2.2% and 0.2% of the NAPL mass at those same times.

Due to its low solubility and high initial mass fraction (Table 3.9), Table 5.6 shows that after 20 years, xylene accounts for 55.5% of the NAPL phase contamination. The low solubility of ethylbenzene results in low percentages in the aqueous phase. After 20 years, 12.4% of the

aqueous mass is ethylbenzene. Toluene is the only one of the BTEX compounds where decreases in the percentages of NAPL mass are reflected by increases in the percentages of the aqueous phase mass. Toluene accounts for 26.3% of the NAPL mass after 6 years compared to 19.4% after 20 years, and 45.2% of the aqueous phase mass is toluene at year 6 compared with 47.2% at year 20.

	Benzene	Toluene	Ethylbenzene	Xylene
6 Years				
Aqueous Mass	19.6%	45.2%	9.6%	25.6%
NAPL Mass	2.2%	26.3%	21.7%	49.8%
10 Years				
Aqueous Mass	14.9%	46.4%	10.0%	28.7%
NAPL Mass	1.2%	24.4%	22.7%	51.6%
20 Years				
Aqueous Mass	4.1%	47.2%	12.4%	36.3%
NAPL Mass	0.2%	19.4%	25.0%	55.5%

Table 5.6 Long-term mass distribution of BTEX compounds within the aqueous and NAPL phases

The impact each TEAP has on the contaminant mass loss can be seen Table 5.9. The amount of mass biodegraded aerobically continues to be much larger than the mass biodegraded anaerobically. After 20 years, the net mass loss due to aerobic biodegradation is 83.2 kg compared with 41.2 kg due to the anaerobic processes. Biodegradation results in more significant mass losses in the second 10 years of the simulation than it does in the first 10 years for aerobic biodegradation, sulfate reduction and methanogenesis. Aerobic biodegradation in the first 10 years results in 74.5 kg of mass loss compared with 83.2 kg in the second ten years. The trend that is observed in the first 6 years towards more mass loss due to sulfate reduction and methanogenesis continues through the 20 year simulation. Sulfate reduction results in 6.7 kg of mass loss in the first 10 years compared with 17.3 kg in the latter 10 years. Similarly, methanogenesis results in just 2.6 kg through the first 10 years compared with 5.7 kg of mass loss over the next 10 years.

Table 5.7 shows that there are 18.2 kg of contaminant mass lost due to iron reduction in the second 10 years of the simulation compared with 19.6 kg in the initial 10 years. Iron reduction is still resulting in significant mass losses after 20 years since the anaerobic region of the plume is continuing to spread. This spreading also results in a larger region of the plume reaching threshold concentrations of ferric iron. Consequently, iron reduction ceases in those areas leading to more sulfate reduction and methanogenesis. The net mass loss due to sulfate reduction (17.2

kg) approaches the loss that results from iron reduction (18.6 kg) between years 10 and 20. If the simulation was continued to a longer time, mass loss due to sulfate reduction would most likely surpass that due iron reduction as the majority of model cells reached threshold concentrations of ferric iron.

	Aerobic Biodegradation	Iron Reduction	Sulfate Reduction	Methanogenesis
6 Years				
Net Mass Loss	35878	11649	1780	665
Percent of net mass loss	71.8%	23.3%	3.6%	1.3%
Cumulative Mass Loss	35878	11649	1780	665
Percent of cumulative mass loss	71.8%	23.3%	3.6%	1.3%
10 Years				
Net Mass Loss	38594	8033	4958	1974
Percent of net mass loss	72.1%	15.0%	9.3%	3.7%
Cumulative Mass Loss	74472	19683	6737	2639
Percent of cumulative mass loss	71.9%	19.0%	6.5%	2.5%
20 Years				
Net Mass Loss	83215	18217	17291	5747
Percent of net mass loss	66.9%	14.6%	13.9%	4.6%
Cumulative Mass Loss	157687	37899	24029	8386
Percent of cumulative mass loss	69.2%	16.6%	10.5%	3.7%

Table 5.7 Long term total hydrocarbon mass loss by each TEAP (in grams)

The mass loss rates over time can be seen in Figure 5.3. Trends similar to those observed near the end of the first 6 years of the simulation (Table 5.5 and Figure 5.2) continue through the remaining 14 years. Rates of mass loss due to aerobic biodegradation remain relatively constant during that time. The mass loss rates due to iron reduction continue to decrease slightly over time as more of the grid cells reach threshold concentrations of ferric iron. Sulfate reduction and methanogenesis mass loss rates show slight increases from around the sixth year through the end of the simulation.

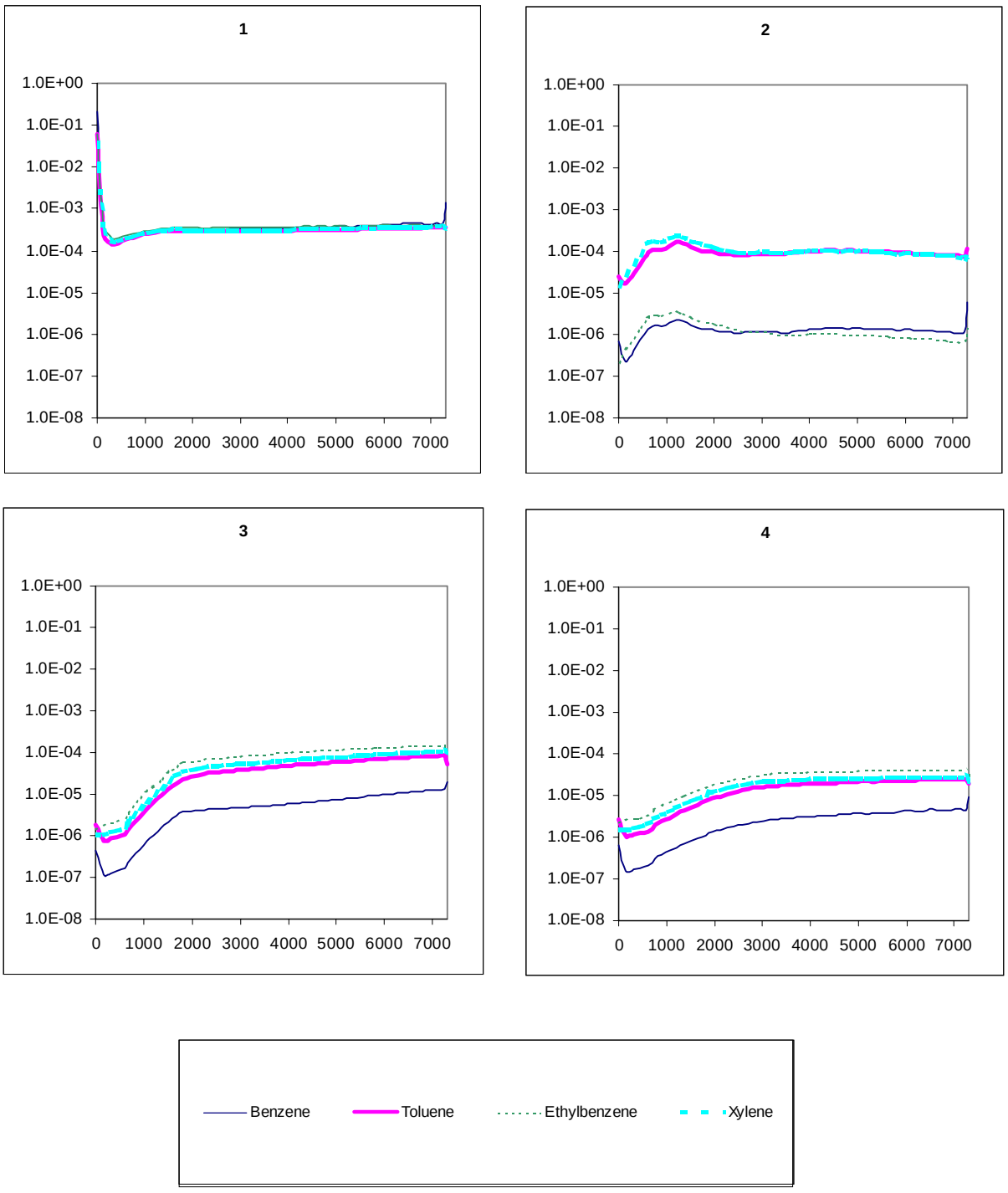

Figure 5.3 Long term rates of biodegradation (x 10^{6} day^{-1}) over time (in days). Plot 1 shows loss rates due to aerobic biodegradation and plots 2, 3, and 4 show loss rates due to iron reduction, sulfate reduction, and methanogenesis respectively.

	Aerobic Biodegradation	Iron Reduction	Sulfate Reduction	Methanogenesis	Total
6 Years					
Benzene	23.4%	0.1%	0.2%	0.1%	23.7%
Toluene	19.8%	8.2%	0.9%	0.4%	29.3%
Ethylbenzene	23.6%	0.2%	2.3%	0.8%	27.0%
Xylene	20.1%	11.3%	1.3%	0.5%	33.2%
10 Years					
Benzene	34.0%	0.2%	0.4%	0.2%	34.7%
Toluene	26.8%	9.3%	2.4%	1.0%	39.4%
Ethylbenzene	31.9%	0.2%	5.2%	2.0%	39.2%
Xylene	26.8%	11.4%	3.3%	1.3%	42.7%
20 Years					
Benzene	43.9%	0.2%	0.6%	0.3%	45.0%
Toluene	34.1%	10.9%	5.0%	1.8%	51.7%
Ethylbenzene	38.2%	0.1%	9.5%	3.2%	51.1%
Xylene	34.3%	11.5%	6.6%	2.2%	54.6%

Table 5.8 Percentage of mass biodegraded relative to the mass input into the aquifer

Table 5.8 depicts the percentage of each BTEX compound biodegraded by each TEAP relative to the amount of mass available for biodegradation. This available mass at a particular time step (1) is found using the following equation:

$$M_{in} = M_{out} + M_{bio} + M_{aqueous} + M_{adsorbed} \tag{5.3}$$

where

M_{in} is the cumulative mass dissolved from the NAPL plume (M);

M_{out} is the mass that leaves the system through the concrete swail (M);

M_{bio} is the cumulative mass biodegraded (M);

$M_{aqueous}$ is the contaminant mass in the aqueous phase at time step 1 (M); and

$M_{adsorbed}$ is the contaminant mass in the solid phase at time step 1 (M).

Over time, it can be seen that the biodegradation mechanisms become more efficient at degrading the contaminant mass put into the aquifer. Between year 6 and year 20, the efficiency of benzene biodegradation nearly doubles going from 23.4% to 43.9%. Similar significant increases are seen for the other three BTEX compounds with the efficiencies increasing from 19.8% to 34.1% for toluene, from 23.6% to 38.2% for ethylbenzene, and from 20.1% to 34.3% for xylene. It has been shown in Table 5.7 that each of the TEAPs aside from iron reduction is resulting in more contaminant mass loss in the second ten years of the simulation compared to the first 10 years.

Since each of the TEAPs is resulting in significant mass losses, the efficiency of the natural system is increasing.

This table shows that, given an adequate amount of time, the microbial populations have the ability to eliminate contamination introduced into the Laurel Bay aquifer. It should also be noted that a large percentage of mass is leaving the system through the concrete swail. The cumulative mass losses through the swail and due to biodegradation are compared in Table 5.9. For all of the compounds aside from benzene, the mass lost due to biodegradation is always larger than the mass lost through the swail. By twenty years, more benzene is leaving the system through the swail, 26.2 kg, than is lost due to biodegradation, 23.8 kg. Since benzene is the most soluble BTEX compound, it is the first to exit the system through the swail. That can help to explain the trend seen in Table 5.8 showing that the system is least efficient at removing benzene. If more of the compound leaves through the swail, less is available for biodegradation by the microbial populations.

	Benzene	Toluene	Ethylbenzene	Xylene
6 Years				
Swail	2415	4861	955	2508
Biodegradation	7508	22817	4295	15352
10 Years				
Swail	12769	25178	5517	13162
Biodegradation	14829	47032	10127	31543
20 Years				
Swail	26256	64914	15278	37253
Biodegradation	23781	104467	24933	74820

Table 5.9 Cumulative mass loss through swail and biodegradation (in grams)

The mass of each BTEX compound in the aqueous phase can be seen in Figure 5.4. A peak is reached for each of the compounds around year 6 or 7. Following the peak, the aqueous phase masses either decrease or remain at steady state levels. This indicates that a balance is achieved between the contaminant mass dissolving from the NAPL and the mass lost through the concrete swail and due to the biodegradation processes.

Noticeable decreases in the masses of benzene and toluene are exhibited following the peaks. By the end of the 20 year simulation, the mass of benzene in the aqueous phase is less than 2.5 kg compared to around 17.0 kg at the peak. The mass of toluene in the aqueous phase decreases but not as significantly. The mass drops from around 40.0 kg at the peak to less than 30.0 kg after 20 years. Since benzene and toluene are the more soluble compounds, more of their mass will be in the aqueous phase. Consequently, more mass will travel with the groundwater

flow to the swail where it will exit the system. Table 5.8 shows that there is a significant amount of benzene mass loss due to biodegradation after year 6.

Figure 5.4 shows that the masses of ethylbenzene and xylene exhibit slight decreases following the peaks, but for the most part, they show steady state conditions. It can be seen in Table 5.6 that they account for a large percentage of the mass still in the NAPL phase after 20 years due to their low solubilities. The mass still dissolving from the NAPL is balanced by the mass biodegraded and the mass lost through the swail to produce steady state conditions.

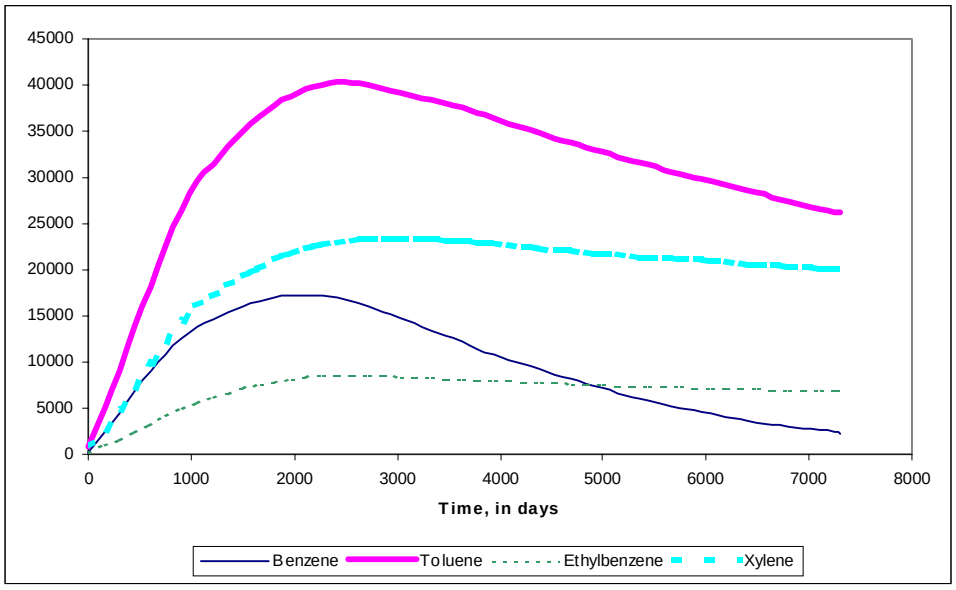

Figure 5.4 Mass in the aqueous phase (in grams)

6.0 Conclusions

6.1 Summary of Findings

This research has shown that SEAM3D is capable of simulating interconnected processes over time and space at the Laurel Bay site. A detailed site model was developed with the ability to simulate the transport and biodegradation of four BTEX compounds, three electron acceptors, and three end products at the site. The model is calibrated to field data from 1994 and verified using data from both 1996 and 1997. Results of the calibration and verification process show that simulated concentrations along a transect through the plume compare relatively well with observed concentrations in the field.

Differences between the measured concentrations and the model predicted concentrations and travel distances and flow paths of the BTEX contaminants have the potential to be significantly impacted by recharge events in the field. Due to the shallow, highly permeable nature of the aquifer, periods of high or low rainfall can alter the levels of DO and sulfate as well as the flow patterns of the groundwater which in turn affect contaminant transport. Since the SEAM3D contaminant transport model was coupled with a steady-state groundwater flow model, it does not reflect transient flow conditions that occur in the field. Another limitation of the model is its inability to simulate the reaction between sulfide and ferrous iron that yields pyrite. The concentrations of sulfide estimated by the model were higher than those measured in the field. Research has indicated that measuring the aqueous concentrations of sulfide underestimates the degree of sulfate reduction that is occurring (Kennedy et al., 1998).

Results of calibration and verification show that the SEAM3D model can be used to determine the feasibility of natural attenuation as a remediation alternative at the Laurel Bay site. Benzene transport at Laurel Bay is the major concern due to its classification as a possible human carcinogen and the 5 ppb drinking water MCL. Benzene is also the most mobile of the BTEX compounds, so it poses the largest threat of reaching a POC. This research has demonstrated the high mobility of benzene, as it is the first substrate simulated to reach the concrete swail. Benzene is also the most biodegradable of the four hydrocarbons simulated with aerobic biodegradation accounting for over 95 % of mass loss. The fact that benzene is the most mobile as well as the most biodegradable can be useful when monitoring and designing remedial alternatives for BTEX contaminated sites.

The model shows the BTEX plume reaching a steady-state condition 6 to 7 years into the simulation. For the remainder of the simulation, the concentrations of the BTEX compounds in

the aqueous phase decrease or remain at a constant level. Once steady-state is achieved, the amount of contaminants dissolved from the NAPL plume are balanced by the masses leaving through the swail combined with the masses biodegraded. This study has shown that the contaminant mass of benzene exiting the model domain through the swail exceeds the mass lost due to biodegradation over time. This indicates that the natural attenuation capacity of the aquifer was insufficient to stabilize the plume and prevent it from reaching the defined POC.

It is most often assumed that once a plume becomes anaerobic, the remainder of the attenuation is due solely to anaerobic processes. This research has shown evidence to the contrary. Aerobic biodegradation is the primary mass loss mechanism at all stages of the simulation even after anaerobic conditions are achieved in large areas of the plume. As the DO levels drop to zero in the most contaminated areas of the plume, aerobic biodegradation still continues along the plume edges. Dissolved oxygen is added to the system through recharge, groundwater inflow from upgradient, and mixing of the contaminant plume with the uncontaminated groundwater along the edges. The sum of the mass losses due to the three anaerobic processes, iron reduction, sulfate reduction, and methanogenesis, does not total the mass biodegraded aerobically. Aerobic biodegradation also occurs at the highest rate. If aerobic conditions could be maintained within the plume through the addition of dissolved oxygen, the model would predict more rapid remediation of the Laurel Bay site.

6.2 Future Research

Limitations of the model discussed in the previous section along with the knowledge that significant contamination is being lost through the concrete swail present several opportunities for further modeling work at the Laurel Bay site. A transient flow model could be developed using rainfall data available for Beaufort, South Carolina, so the model would more appropriately simulate the heavy and low rainfall periods when compared with the steady-state model used in this study. Water table elevations are available for multiple sampling events over a 6 year span, and they could be used to calibrate this model. A transient flow model could then be coupled with the SEAM3D contaminant transport model.

Modification of the SEAM3D computer code may be necessary to improve the model's simulation of end product concentrations. The code could be updated to simulate the reaction of sulfide with ferrous iron that has been observed in the field. The addition of the reaction between those two ions producing pyrite may eliminate the propensity for the model to underestimate the amount of sulfate reduction occurring at the Laurel Bay site.

Another future research opportunity at the Laurel Bay site would involve incorporating containment of the contaminants or source remediation into the model. Once the groundwater flow model is calibrated to the site water table levels and gradients, a barrier could be installed using the Horizontal Flow Barrier (HFB) package within GMS. This groundwater flow model could then be coupled with the contaminant transport model and used to determine the length of time necessary for complete biodegradation of the contamination if it is contained. The amount of source reduction necessary to prevent the contamination from reaching the swail could also be determined using the model. The mass scheduling feature of the NAPL package within SEAM3D can be used to simulate source removal. Contaminant mass can be excavated over time to determine the total amount of mass reduction necessary to prevent contamination from reaching the defined POC.

References

ABB Environmental Services, Inc. 1993. Contaminant assessment report: Marine Corps Exchange Service Station, Laurel Bay. GWPD#A-07-AA-13575, Knoxville, TN.

Acton, D.W. and J.F. Barker. 1992. In situ biodegradation potential of aromatic hydrocarbons in anaerobic groundwaters. *Journal of Contaminant Hydrology*, 9:325-352.

Anderson, M.P. and W.W. Woessner. 1992. *Applied Groundwater Modeling Simulation of Flow and Advective Transport*. San Diego, CA: Academic Press, Inc.

Atlas, R.M. 1988. Microbiology: Fundamentals and Applications. 2nd ed. MacMillan Publishing Co., New York.

Atlas, R.M. and C.E. Cerniglia. 1995. Bioremediation of petroleum pollutants: diversity and environmental aspects of hydrocarbon biodegradation. *Bioscience*, 45:332-338.

Baedecker, M.J., I.M. Cozzarelli, R.P. Eganhouse, D.I. Siegel, and P.C. Bedient. 1993. Crude oil in a shallow sand and gravel aquifer. III: Biogeochemical reactions and mass balance modeling in anoxic groundwater. *Applied Geochemistry*, 8:569-586.

Barker, J.F., G.C. Patrick and D. Major. 1987. Natural attenuation of aromatic hydrocarbons in a shallow sand aquifer. *Ground Water Monitoring Review*, 7:64-71.

Bedient, P.B. and H.S. Rifai. 1992. Ground water contaminant modeling for bioremediation: A review. *Journal of Hazardous Materials*, 32:225-243.

Borden, R.C., P.B. Bedient, M.D. Lee, C.H. Ward, and J.T. Wilson. 1986. Transport of dissolved hydrocarbons influenced by oxygen-limited biodegradation, 2, Field application. *Water Resources Research*, 22(13):1983-1990.

Borden, R.C., C.A. Gomez, and M.T. Becker. 1995. Geochemical indicators of intrinsic bioremediation. *Ground Water*, 33(2):180-189.

Brauner, J.S. 1995. Two-dimensional modeling of *in situ* bioremediation using sequential electron acceptors, *Master's Thesis*, VPI & SU.

Burmaster, D.E. and R.H. Harris. 1982. Groundwater contamination: an emerging threat. *Technology Review*, 84(7): 50-62.

Carsel, R.F. and R.S. Parrish. 1988. Developing joint probability distributions of soil water retention characteristics. *Water Resources Research*, 24:755-769.

Chapelle, F.H., P.M. Bradley, D.R. Lovley, and D.A. Vroblesky. 1996 Measuring rates of biodegradation in a contaminated aquifer using field and laboratory methods. *Ground Water,* 34(4):691-698.

Chapelle, F.H. and P.M. Bradley. 1998. Selecting remediation goals by assessing the natural attenuation capacity of groundwater systems. *Bioremediation Journal*, 2(3-4):227-238.

Chapelle, F.H. 1999. Bioremediation of petroleum hydrocarbon-contaminated ground water: the perspectives of history and hydrology. *Ground Water*, 37(1): 122-132.

Charbeneau, R.J. and J.W. Weaver. 1992. Modeling contaminant transport through subsurface systems. *Journal of Hazardous Materials,* 32:293-311.

Chen, Y.M., L.M. Abriola, P.J.J. Alvarez, P.J. Anid, and T.M. Vogel. 1992. Modeling transport and biodegradation of benzene and toluene in sandy aquifer material: comparisons with experimental measurements. *Water Resources Research*, 28:1833-1847.

Chiang, C.Y., J.P. Salanitro, E.Y. Chai, J.D. Colthart and C.L. Klein. 1989. Aerobic biodegradation of benzene, toluene, and xylene in a sandy aquifer—data analysis and computer modeling. *Ground Water*, 27(6):823-834.

Clement, T.P., Y. Sun, B.S. Hooker, and J.N. Peterson. 1998. Modeling multispecies reactive transport in groundwater. *Ground Water Monitoring & Review*, 18(2): 79-92.

Corapcioglu, M.Y. and A.L. Baehr. 1987. A compositional multiphase model for groundwater contamination by petroleum products: 1. Theoretical considerations. *Water Resources Research,* 23(1):191-200.

Davis, J.W., N.J. Klier, and C.L. Carpenter. 1994. Natural biological attenuation of benzene in ground water beneath a manufacturing facility. *Ground Water*, 32(2):215-226.

Edwards, E.A., L.E. Wills, D. Grbic-Galic, and M. Reinhard. 1991. Anaerobic degradation of toluene and xylene-evidence for sulfate as the terminal electron acceptor. *In-situ Biormediation Applications and Investigations for Hydrocarbon and Contaminated Site Remediation,* edited by R.E. Hinchee and R. Olfenbuttel, pp. 463-470, Battelle Memorial Institute, Columbus, Ohio.

Federal Register, vol. 54, no. 155, Monday, August 14, 1989, pp. 33449-33484.

Fetter, C.W. 1994. *Applied Hydrogeology. 3rd Edition.* Saddle River, NJ: Prentice-Hall, Inc.

Gibson, D.T., and V. Subramanian. 1984. Microbial degradation of aromatic hydrocarbons. In *Microbial Degradation of Organic Compounds,* ed. D.T. Gibson, 181-252. New York: Marcel Dekker.

Grbic-Galic, D. and T.M. Vogel. 1987. Transformation of toluene and benzene by mixed methanogenic cultures. *Applied Environmental Microbiology,* 53:254-260.

Haag, F.M., M. Reinhard, and P.L. McCarty. 1991. Degradation of toluene and p-xylene in anaerobic microcosms: Evidence for sulfate as a terminal electron acceptor. *Environmental Toxicology Chemistry*, 10:1379-1390.

Hall, C.W. and J.A. Johnson. 1992. Limiting factors in ground water remediation. *Journal of Hazardous Materials*,32:215-223.

Hutchins, S.R., G.W. Sewell, D.A. Kovacs and G.A. Smith. 1991. Biodegradation of aromatic hydrocarbons by aquifer microorganisms under denitrifying conditions. *Environmental Science & Technology*, 25:68-76.

Kao, C. and R.C. Borden. 1997. Site-specific variability in BTEX biodegradation under denitrifying conditions. *Ground Water*, 35(2):305-311.

Kennedy, L.G., J.W. Everett, K.J. Ware, R. Parsons, and V. Green. 1998. Iron and sulfur mineral analysis methods for natural attenuation assessments. *Bioremediation Journal*, 2(3-4): 259 276.

Klecka, G.M., J.W. Davis, D.R. Gray and S.S. Madsen. 1990. Natural bioremediation of organic compounds in ground water: Cliffs-Dow Superfund site. *Ground Water*, 28(4):534-543.

LaGrega, M.D., P.L. Buckingham, J.C. Evans, and The Environmental Resources Management Group. 1994. *Hazardous Waste Management*. New York, NY: McGraw-Hill, Inc.

Lahvis, M.A., A.L. Baehr, and R.J. Baker. 1999. Quantification of aerobic biodegradation and volatilization rates of gasoline hydrocarbons near the water table under natural attenuation conditions. *Water Resources Research*, 35(3): 753-765.

Landmeyer, J.E., F.H. Chapelle and P.M. Bradley. 1996. Evaluation of intrinsic bioremediation as an option to contain gasoline contamination, Laurel Bay Exchange, Marine Corps Air Station, Beaufort, South Carolina. *USGS Water Resources Investigations Report Number 96-4026*, Denver, CO.

Landmeyer, J.E., F.H. Chapelle, P.M. Bradley, J.F. Pankow, C.D. Church, and P.G. Tratnyek. 1998. Fate of MTBE relative to benzene in a gasoline-contaminated aquifer (1993-1998). *Ground Water Monitoring & Remediation*, Fall:93-102.

Lovley, D.R., M.J. Baedecker, D.J. Lonergan, I.M. Cozzarelli, E.J. Phillips, and D.I. Siegel. 1989. Oxidation of aromatic contaminants coupled to microbial iron reduction. *Nature*, 339: 297-299.

Lovley, D.R., J.C. Woodward and F.H. Chapelle. 1994. Stimulated anoxic-biodegradation of aromatic hydrocarbons using Fe(III) ligands. *Nature*, 370:128-131.

Lovley, D.R., J.C. Woodward and F.H. Chapelle. 1996. Rapid anaerobic benzene oxidation with

a variety of chelated Fe(III) forms. *Applied Environmental Microbiology*, 62:288-291.

McAllister, P.M. and C.Y. Chiang. 1994. A practical approach to evaluating natural attenuation of contaminants in ground water. *Ground Water Monitoring Review*, Spring:161-173.

Munoz, J.F., and M.J. Irarrazaval. 1998. A numerical model for simulation of bioremediation of hydrocarbons in aquifers. *Ground Water*, 36(2): 215-224.

Murarka, I., E. Neuhauser, M. Sherman, B.B. Taylor, D.M. Mauro, J.Ripp, and T.Taylor. 1992. Organic substances in the subsurface: Delineation, migration, and remediation. *Journal of Hazardous Materials*, 32:245-261.

Parker, J.C., D.W. Waddill and J.A. Johnson. 1994. *UST Corrective Action Technologies: Engineering Design of Free Product Recovery Systems*, US EPA. Risk Reduction Engineering Laboratory, Edison, N.J.

Ray, B.T. 1995. *Environmental Engineering*. New York, NY: PWS Publishing Company.

Rice, D.W., R.D. Grose, J.C. Michaelson, B.P Dooher, D.H. Mac Queen, S.J. Cullen, W.E. Kastenberg, L.E. Everett, and M.A. Marino. 1995. *California Leaking Underground Fuel Tank (LUFT) Historical Case Analysis*. UCRL AR-122207. Environmental Protection Department, Environmental Restoration Division, Lawrence Berkeley Laboratory, Berkeley, CA.

Small, M.C. 1998. Risk-Based corrective action, natural attenuation, and changing regulatory paradigms. *Bioremediation Journal*, 2(3-4):221-225.

Swett, G.H. and D. Rapaport. 1998. Natural attenuation: is the fit right? *Chemical Engineering Progress*, June:37-43.

Voss, C.I., 1984, A finite-element simulation model for saturated-unsaturated, fluid-density dependent ground-water flow with energy transport or chemically-reactive single-species solute transport: U.S. Geological Survey Water-Resources Investigations Report 84-4369, 409 p.

Vroblesky, D.A. and F.H. Chapelle. 1994. Temporal and spatial changes of terminal electron accepting processes in a petroleum-hydrocarbon contaminated aquifer and the significance for contaminant biodegradation. *Water Resources Research*, 30(5):1561-1570.

Waddill, D.W. and M.A. Widdowson. 1997. SEAM3D: A numerical model for three-dimensional solute transport and sequential electron acceptor-based bioremediation in groundwater. Technical Report.

Waddill, D.W., and M.A. Widdowson. 1998. A three-dimensional model for subsurface transport and biodegradation. *ASCE Journal of Environmental Engineering*, 124(4):336-344.

Weiner, J.M., T.S. Lauck, and D. R. Lovley. 1998. Enhanced anaerobic benzene degradation with the addition of sulfate. *Bioremediation Journal*, 2(3-4):159-173.

Widdowson, M.A. Spring 1998. Unpublished. *Dynamics of Groundwater Class Notes*.

Wiedemeier, T.H., J.T. Wilson, D.H. Kampbell, R.N. Miller, and J. Hansen. 1995. Technical protocol for implementing intrinsic bioremediation with long-term monitoring for natural attenuation of fuel contamination dissolved in groundwater. Volume 1 & 2. San Antonio, Texas: Air Force Center for Environmental Excellence, Technology Transfer Division, Brooks AFB.

Wiedemeier, T.H., M.A. Swanson, J.T. Wilson, D.H. Kampbell, R.N. Miller, and J.E. Hansen. 1996. Approximation of biodegradation rate constants for monoaromatic hydrocarbons (BTEX) in groundwater. *Ground Water Monitoring and Remediation*, 16(3):186-194.

Wilson, B.H., G.B. Smith, and J.F. Rees. 1986. Biotransformations of selected alkylbenzenes and halogenated aliphatic hydrocarbons in methanogeneic aquifer material: a microcosm study. *Environmental Science & Technology*, 20:997-1002.

Zheng, C. and G.D. Bennett. 1995. *Applied Contaminant Transport Modeling*. New York, NY: Van Nostrand Reinhold.